POLITECNICO DI TORINO

Master's Degree in Aerospace Engineering

Politecnico
di Torino

Master's Degree Thesis

Propulsive and Combustion Modeling of M=2 Aircraft Using Biofuels in Conceptual Design

Supervisors

Prof. Nicole VIOLA

Prof. Roberta FUSARO

Ing. Guido SACCONE

Dott.sa Grazia PICCIRILLO

Candidate

Cataldo MOSCHETTI

December 2025

Abstract

The recent surge in **environmental concerns** and a revived interest in **supersonic flight** have spurred intensive scientific efforts aimed at realizing a new generation of **Sustainable Supersonic Aircraft**. Simultaneously, the International Civil Aviation Organization (ICAO) Assembly Resolution Act A39-1 directs the Council to review its Annexes, ensuring they adequately address the challenges that the operation of supersonic aircraft may pose to the public. This thesis discusses a methodology and tools designed to anticipate, at the conceptual design stage, the emissions of a supersonic aircraft. The methodology is applied to analyze emissions for a supersonic aircraft with a flight speed of M=2, akin to the **Concorde**. The adoption of a modeling approach demonstrates the applicability of the methodology for estimating emissions resulting from the combustion of various types of fuels, particularly **Alternative Aviation Fuels**.
The intention of this work is to use the **Olympus 593 turbojet**, reference test case for validation as well as to eventually assess the impact of biofuels on an already existing supersonic aircraft. The work starts with research on the aircraft and its propulsion system. In parallel, research was also carried out on the state of the art of aviation fuels and their characteristics, data useful later for estimating emissions. Through the analysis of the propulsive system, it is possible to obtain the performances for various operating conditions, thanks to a propulsive system design code written in Matlab environment and its subroutines, above all the extremely accurate gas model function, based on **CEA Model** developed by NASA and **CANTERA**, an open-source suite of tools integrated in Pyhton and Matlab for problems involving chemical kinetics, thermodynamics, and transport processes. Subsequently, through an in-depth design of the combustion chamber, in combination with the accurate gas model, it is possible to estimate emissions of NOx, UHC and CO for the considered engine and various types of fuel. The design of the combustor is necessary for the chosen method for the evaluation of emission indexes: the semi-empirical Lefebvre and Murthy relations. In fact, Lefebvre and Murthy have been expressed that $NO_x x$, CO and UHC formation is proportional to the product of three terms which are the mean residence time in the combustion zone, chemical reaction rates and mixing rates. Each of these terms

is related to quantities in the combustion chamber such as T_{pz}, the temperature in the primary zone of the combustion chamber, V_c, the Combustion Volume, or V_e, the Evaporation Volume. The last in turn related to the flow rate in the primary zone and the effective evaporation constant λ_{eff}, defined as the ratio of square of the initial droplet diameter to the evaporation time.

Dedication

To my cousin Massimiliano, who passed away too soon. A person of great intelligence and creativity, crushed by the weight of life. A person I feel I understand deeply now, and who was my most vivid thought in the darkest moments, preventing life from destroying me too to the point of no return.

Acknowledgements

I want to thank my parents, who have provided constant financial and emotional support during these very troubled years, for their patience and for always allowing me to have broad perspectives.
Thanks to all my friends for making my life bearable so far and for the endless moments of joy and support without expecting anything in return. Special thanks to Maki and Giuseppe, who are always there for me on any occasion.
I would like to thank my psychologist, Michela Roccello, for her tremendous professional support, without which it would have been impossible to complete this work and learn to cope with my daily life.
Thanks to my teachers Roberta Fusaro and Nicole Viola, the engineer Guido Saccone and dr. Grazia Piccirillo for their extreme patience and support in this thesis project.
Thanks to my dog Polly for all the happiness she brings into my life.

Table of Contents

List of Figures

List of Tables

Chapter 1

Introduction

Recent rise in environmental concern and renewed interest in supersonic flight involved an intense scientific activity aimed to realize a new generation of **Sustainable Supersonic Aircraft**. The motivation of this thesis is to investigate the use of alternative fuels on the **Olympus 593** (the Concorde engine), try to understand how these fuels work on a typical mission and above all to evaluate the emissions of the engine and the products of these emissions.

1.1 The environmental concern

The usage of fossil fuels started at the beginning of the industrial revolution and played a fundamental role in supplying energy demands all over the globe. This, in combination with a great industrialization, an exponential increase of population and a rapid urbanization, lead to a global energy crisis.
82% of the global primary energy consumption in the last years was supplied by **Fossil Fuels**, including petrol, diesel, coal and natural gas, making them the main source of energy worldwide.
Energy-rich petroleum has fueled many of the undeniable advances of the modern, globalized society, including global connectivity through land and air transportation. However, such boons are balanced by the deleterious effects of the massive reliance on chemical propulsion. The result was a severe degradation of air quality and climate change because of toxic and **Greenhouse Gas (GHG) emissions**. Recently the world has faced the challenge of decarbonizing transportation. Because the vast majority of jet fuels are derived from petroleum, the U.S. Government in 2015 set the ambitious goal of carbon-neutral U.S. jet aviation growth by 2020 [1]. The growth of air traffic is having an increasing environmental impact Fig.1.1.

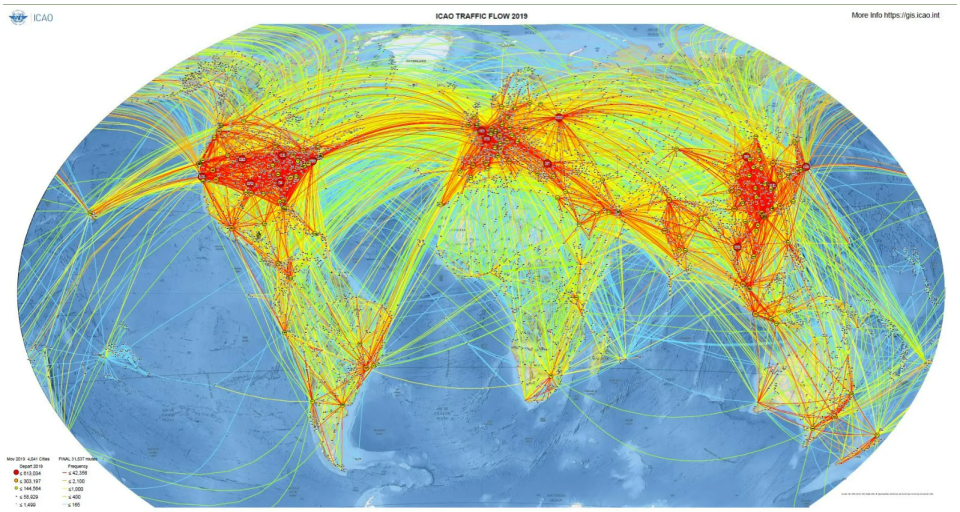

Figure 1.1: Global Air Traffic

There is a rising awareness and apprehension about climate change, prompting the aviation industry to play a role in curbing its carbon footprint as part of global initiatives to reduce CO_2 emissions. The aviation sector, encompassing both international and domestic flights, contributes to approximately 2% of global CO_2 emissions. Despite this, concerns persist regarding aircraft noise, particularly in proximity to airports worldwide. Additionally, there is a growing focus on local air quality (LAQ), with increasing attention directed towards small particles emitted during engine combustion, commonly known as **Nonvolatile Particulate Matter (nvPM)**[2].
In 2021, the European Union (EU) embraced the Zero Pollution Action Plan, outlining a vision to diminish air, water, and soil pollution to levels that no longer pose harm to health and natural ecosystems by the year 2050. Intermediate targets for the year 2030, in comparison to 2017 levels, were established, aiming to reduce pollution at its source. These targets include a 30% reduction in the share of individuals chronically disturbed by transport noise and an improvement in air quality to lower the number of premature deaths resulting from air pollution by 55%. To enforce EU air pollution regulations, a combination of air quality standards and source-based mitigation controls is implemented. This involves measures such as regulating engine emissions and setting standards for fuel quality. The overarching goal is to advance environmental quality and public health by curbing pollution across various domains.[3].
In this context, there is a growing global interest in **Sustainable Aviation Fuels (SAFs)** as a reliable alternative, offering a renewable and sustainable solution to the reliance on fossil fuels in aviation. SAFs are anticipated to play a crucial role alongside hydrogen and electric propulsion in the overall effort

to decarbonize aviation. Given the current limitations in battery density and hydrogen fuel storage, SAFs are essential for achieving net-zero emissions in long-haul aviation, particularly in the short term. They are expected to contribute to the sustainability of large commercial aircraft in the medium term, bridging the gap until hydrogen and electric planes become both technically and commercially viable. SAFs are considered key in meeting short-term sustainability targets in aviation due to their scalability, which allows for quicker implementation compared to other emerging technological solutions. In the long term, SAFs are expected to remain a viable option for sustainable long-haul flights, potentially complementing liquid hydrogen technologies. Notably, SAFs exhibit a somewhat reduced non-CO_2 footprint compared to conventional jet fuels. Additionally, they often emit lower levels of nitrogen oxides (NO_x) than traditional kerosene, thanks to lower combustion temperatures, further reducing their radiative forcing impact. [4].

1.2 The Supersonic Flight

As already mentioned, in addition to interest in environmental issues, interest in supersonic transport has also been revived in recent times. A **Supersonic Transport (SST)** is a civilian supersonic aircraft designed to transport passengers beyond the speed of sound. The first supersonic aircraft was the **Bell X-1** developed in 1940. The sound barrier was break for the first time in 1947 by the Air Force pilot Chuck Yeager. After this first case other military aircraft were designed and diveloped, but the civilian supersonic programs started only in 1960. In a period from 1960 and 1971, when the programs of civilian supersonic transport were terminated for economic and environmental issues, two major projects have been launched: the soviet **TU-144** and the most successful British/French **Concorde**, opertaive from 1976 to 2003. For the latter, aircraft chosen for this work, studies began in 1954. After a phase of study and design, six prototypes began operations in 1965, with the first flight in 1969.
Concorde is an aircraft design with a narrow fuselage, an ogival delta wing, and a droop nose for landing visibility. It is powered by four Rolls-Royce/Snecma Olympus 593 turbojets with variable engine intake ramps, and reheat for take-off and acceleration to supersonic speed. Constructed from aluminium, it was the first airliner to have analogue fly-by-wire flight controls. The airliner had transatlantic range while supercruising $M = 2$ for 75% of the distance.
On 25 July 2000, Air France Flight 4590 crashed shortly after take-off with all 109 occupants and four on the ground killed. This was the only fatal incident involving Concorde; commercial service was suspended until November 2001. The remaining aircraft were retired in 2003, 27 years after commercial operations had begun. Eighteen of the 20 aircraft built are preserved and are on display in Europe

Figure 1.2: The Concorde

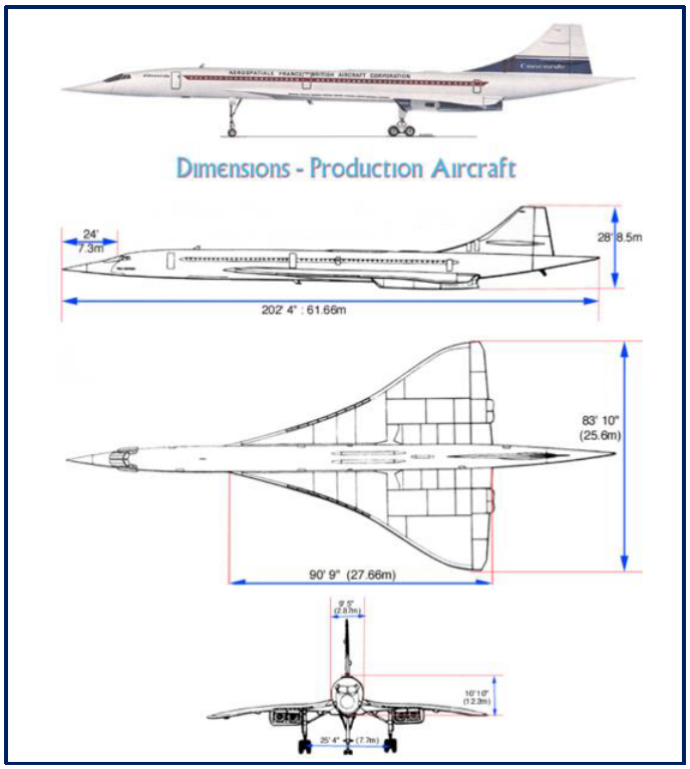

Figure 1.3: Concorde dimensions

and North America.
Today different programs are developing for the future of SST, programs like the **Boom Overture**, the largest project under development and very similar to the

Concorde, or the **Exosonic**, only 70 passengers and operating at $M = 1.7$. Than others smaller projects (aircraft that can carry fewer than 20 passengers) like **Spike Aerospace S-512** or the **Aerion AS-2**.
The supersonic flight presents various challenges for all these projects, challenges like: the **Sonic Boom** and the impossibility of allowing supersonic flights over populated areas due to the impact this has on people, animals, and buildings (this is why the Concorde operated over the ocean); the **Wave Drag** issue near the Mach 1 flight; the **Propulsion System**, very complex to guarantee best perfomances in a vast range of conditions, from low subsonic to supersonic; **Noise**; and, of coure, **Environmental Impact**.

1.3 Case Study and Purpose

As already mentioned the case study for this work is the analysis of the Concorde propulsive system, as the most important representative of supersonic civil aviation and the basis for future projects like Boom Overture. In this context the study of the Concorde has the great potential for development of high-speed civil aircraft from a technical, environmental and economic point of view.
With the case study in mind, the main purposes of this thesis work are two:

- to generate a **propulsive database** for the Concorde mission in order to evaluate all the operative conditions of its propulsive system, the **Rolls-Royce/Snecma Olympus 593 MK610**
- to evaluate pollutant emissions of this propulsive system with conventional fuels and **Sustainable Aviation Fuels (SAFs)**(in particular C1 and C5 described in Sec.2.2), to to evaluate the differences, in terms of NO_x, CO and UHC emissions, with the use of these fuels

The firts objective consist in various steps, starting from the list of requirements related to the propulsion systems. These requirements and all the values that satisfy them are derived from literature and the previous analysis of the aircraft design. The mission profile is derived by using the ASTOS software and, hence, it was possible to evaluate the required thrust of the aircraft during all phases of the reference mission. In order to design the engine from requirements, a mathematical model is adopted. Therefore all parameters are selected in order to properly match the requirements. The development of the propulsive database is performed by running several Off-design simulations, in which the three main independent varaibles are varied (flight Mach, Altitude and throttle).
The second part of the study aim to compare three type of fuels to evaluate if there are benefits, in term of performances and emissions, using alternative fuels. The steps in this part consist of finding all the variables needed to calculate emissions

using the semi-empirical relationships of Lefebvre and Murthy, calculating emissions for certain particularly representative flight phases, and finally validating the results. The values sought are obtained from literature, the engine model, and the kinetic schemes of the various fuels involved.
The formulation adopted for the emissions calculation is adapted to another case study, and only partially fit this one: the semi-empirical correlations are case by case solutions and need to be adapted based on a large set of experimental data not available for this case study. There's no ad hoc procedure or legislation for emission evaluation for civil supersonic transport. Considering the absence of accompanying documentation, the **MORE&LESS** research project is conceived, with its ultimate goal being to facilitate the development of future legislation by analysing and developing different case study operating in the supersonic regime. Hopefully this work will provide support to the MORE&LESS project, providing useful information on supersonic propulsion systems and their emissions, including when using alternative fuels.

1.4 MORE&LESS

Figure 1.4: MORE&LESS

MORE&LESS(**MDO** and **RE**gulations for **L**ow boom and **E**nvironmentally **S**ustainable **S**upersonic aviation) addresses the challenge of contributing to help Europe shape, together with the international community, high environmental standards in line with ICAO Assembly Resolution A39-1, by a thorough and holistic analysis of the environmental impact of supersonic aviation. MORE&LESS

aims at maintaining a high level of citizens and environmental protection at local, regional and global levels, and supports the consequent establishment of regulations and procedures for the future supersonic aviation through solid technical bases. The scientific findings in the fields of aerodynamics, jet-noise, sonic-boom, propulsion, pollutant emissions and environmental impact are in fact transposed into guidelines for the Regulatory Community. Through low and high-fidelity modelling activities and test campaigns, already accepted and validated software tools are enhanced and extended to cover supersonic aviation, to be eventually integrated into the multidisciplinary holistic framework. The application of this framework to the case-studies is the proving ground to verify that the enabling technologies of supersonic aircraft, trajectories and operations comply with the environmental requirements.

Chapter 2

Alternative Jet Fuels

2.1 Sustainable Aviations Fuels

Sustainable Aviation Fuels are recognized to be possible clean substitutes for fossil jet fuels. According to ATAG [1], Sustainable Aviation Fuel is a more generic term than biofuels, and it is preferred by the aviation sector because of the wider scope of its meaning. "Biofuels", instead, generally refers to specific SAF fuels produced from biological resources (plant or animal). However, current technology allows fuel to be produced from other alternative sources, including non-biological resources.
The American Society for Testing and Materials develops standard specifications to define kerosene-type fuels for aviation engines:

- **ASTM D1655**: presents specifications for Jet A-1 fuel setting the requirements for the fuel chemical and physical properties, but also for any additives such as antioxidants and so on.
- **ASTM D4054**: standard practices for qualification and approval of new aviation turbine fuels and fuel additives (Fig 2.1).
- **ASTM D7566**: standard specification for aviation turbine fuels containing synthesized hydrocarbons.

Currently, seven different technology pathways plus two co-processing pathways [1] to produce bio-jet fuels have been certified, together with 5 types of **Synthetized Paraffinic Kerosene (SPK)** as blending components for conventional jet fuel to make up bio-jet fuels. The main production pathways of certified SPKs are listed in the Table 2.1. Due to stringent quality control measures for fuels, any fuels obtained from various sources must be entirely "**drop-in**". This indicates that the new fuel or fuel blend serves as a substitute for traditional jet fuel, seamlessly interchangeable

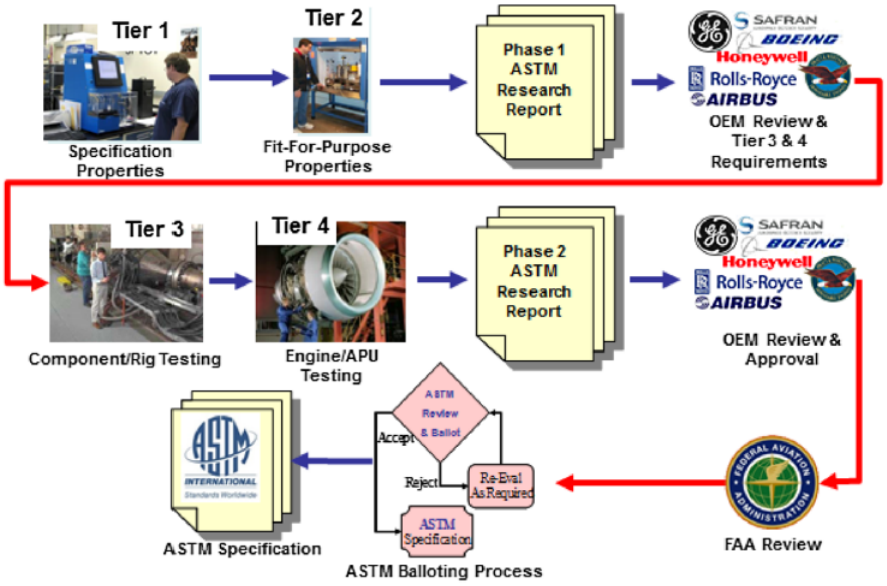

Figure 2.1: D4054 qualification process [5]

and compatible with conventional jet fuel when mixed. Additionally, a drop-in fuel blend doesn't necessitate modifications to the aircraft/engine fuel system or the fuel distribution network, and it can be utilized without adjustments on currently operational turbine-powered aircraft. To ensure adherence to technical and safety standards, Sustainable Aviation Fuel (SAF) must undergo rigorous laboratory, ground, and flight tests following an internationally recognized standard led by **ASTM International**. This organization unites numerous researchers, technical experts, and scientists to establish the technical prerequisites ensuring fuel safety. The aviation industry places the utmost importance on safety. In light of this and the specific criteria for fuels utilized in aircraft, the evaluation process for potential new fuels is exceptionally stringent. This involves thorough testing in laboratories, utilizing ground-based equipment, and subjecting the fuel to the extreme conditions encountered during in-flight operations. An exhaustive process is employed to assess and qualify the suitability of each type of Sustainable Aviation Fuel (SAF) before its deployment.

For approval of usage, Sustainable Aviation Fuel (SAF) must adhere to specific standards established by numerous aviation and fuels experts convening at ASTM. Once it demonstrates compliance with these requirements, it is blended with conventional jet fuel, not exceeding 50% by volume according to current standards. The blended fuel undergoes re-testing to ensure continued compliance. The existing blend limits are in place to guarantee an appropriate level of safety and compatibility with aircraft fueling systems, primarily due to the aromatic compounds present

Sustainable Aviation Fuels		
Pathways	**Certification Name**	**Feedstock**
Fischer-Tropsch	FT-SPK	Energy crops, lignocellulosic biomass, solid waste
Fischer-Tropsch with Aromatics	FT-SPK/A	Energy crops, lignocellulosic biomass, solid waste
Hydroprocessed Esters and Fatty Acids (HEFA)	HEFA-SPK	Waste fats, oils, greases (FOGs) from vegetable and animal sources
HEFA from algae	HC-HEFA-SPK	Micro-algae oils
Alcohol-to-Jet	ATJ-SPK	Sugar, starch crops, lignocellulosic biomass
Direct Sugars to Hydrocarbons (DSHC)	HFS-SIP	Conventional sugars, lignocellulosic sugars
Catalytic Hydrothermolysis Jet (CHJ)	CHJ or CH-SK	Waste fats, oils, greases (FOGs) from vegetable and animal sources
FOG Co-Processing	FOG-CP	Waste fats, oils, greases (FOGs) from vegetable and animal sources
FT Co-Processing	FT-CP	Fischer-Tropsch biocrude

Table 2.1: The certified production pathways of SPK [1] [6] [7]

in conventional fossil-based fuels, crucial for systems utilizing nitrile rubber seals. There is a likelihood of higher blend limits being sanctioned in the future as synthetic aromatic compounds gain approval and major aircraft manufacturers strive to ensure compatibility with 100% SAF by around 2030. Upon full qualification, a SAF is recognized as jet fuel and can be utilized without restrictions, aligning with other international standards. Certified aviation biofuels must meet physicochemical properties outlined in the ASTM D7566 standard, essential for proper combustion in aircraft engines, among other factors. Some of the properties have been shown in Figure 2.2 [8].

Property	Value
Density	from 0.775 to 0.840 g/cm^3
Viscosity at −40 °C	max. 8.0 mm^2/s
Viscosity at −20 °C	max 12.0 mm^2/s
Flash Point	min. 38 °C
Freezing Point	max -40 °C
Calorific value	min 42.8 MJ/kg
Lubricity	0.85 mm
Aroma content	min 8, max 25%
Naphthalene content	max 3.0%
Distillation residue	1.5%
Distillation loss	1.5%

Figure 2.2: Physicochemical properties to meet by SAFs

In addition to the aforementioned considerations, it's crucial to highlight a key distinction when dealing with SAFs compared to traditional kerosene fuels. The primary difference lies in the emission lifecycles, which are linear for conventional fuels but become circular for biofuels. For instance, in the case of biofuels, a significant contribution to net CO_2 emissions occurs at the outset of the circular path. The CO_2 absorbed by plants during biomass growth is nearly equivalent to the carbon emitted when the fuel is burned. This circular phenomenon allows for the potential to achieve carbon neutrality over the life cycle, excluding emissions generated during production processes and distribution. This stands in contrast to the linear nature of traditional fuel emissions. It emphasizes the transformative potential of biofuels in creating a circular and more environmentally sustainable lifecycle.

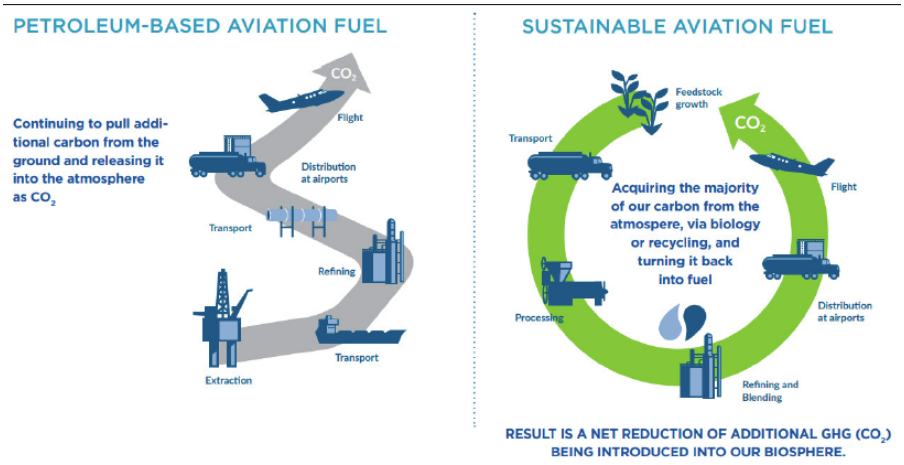

Figure 2.3: Life Cycle comparison in terms of carbon dioxide emission of fossil fuel and Sustainable Aviation Fuel [8]

2.2 Category "C" fuels

For our study, we selected two fuels labeled as **C-1** and **C-5**, aiming to compare their emissions with **Jet-A**, which represents conventional aviation fuel. The properties of Jet-A are detailed in Appendix A. In the United States, the **National Jet Fuel Combustion Program (NJFCP)** has developed a range of conventional jet fuels and "test fuels" specifically designed to characterize the fuel sensitivity and response of combustion devices. These fuels were created to cover a spectrum of jet fuel composition and properties, encompassing both conventional and alternative jet fuels. It's important to note that the test fuels and alternative fuels may not meet all jet fuel specifications, such as density. Test fuels were formulated to explore specific aspects of fuel property or composition space, such as boiling range or viscosity, while many alternative fuels have obtained approval in fuel specifications like ASTM D7566, permitting their use as 50% blends (or less) with conventional fuels. The "**Rules and Tools**" [5] program had defined several categories of fuels to be used to characterize fuel effects on combustion, some of which are being carried forward by NJFCP [9]:

- **Category A** - conventional fuels derived from petroleum, encompassing the range of properties typically encountered (viscosity, flash point, aromatic content, etc.).

- **Category B** - alternative jet fuels found to have unacceptable combustion properties (not used in NJFCP).

- **Category C** - test fuels designed to explore the "edges" of the jet fuel composition property space, such as fuels being at the viscosity limit of the specification or fuels whose composition is outside of typical experience (such as cycloparaffin content).

C-1 and C-5 are fuels of category C and, as indicated previously, the main objective of the Category C "test fuels" was to identify hydrocarbon blends that had "unusual" (outside of experience) properties. The NJFCP selected five "test fuels" based on properties and availability. It was decided that these test fuels were to be tested in their neat form without blending with petroleum jet fuels to increase the likelihood of observing differences. The characteristics of this five fuels are compared in Figure 2.4. In the 2015 mid-year meeting of the NJFCP team, results for tests of the Category C test fuels were reviewed and it was decided to focus on the C-1 and C-5 test fuels in the near-term, since the various tests seemed to be the most sensitive to those fuels, and each represented extremes in chemical and physical properties (Figure 2.5).

	NJFCP Test Fuels				
NJFCP Fuel ID	C-1	C-2	C-3	C-4	C-5
POSF numbers	11498, 12368, 12384	11813, 12223	12341, 12363	12344, 12489	12345, 12713, 12789, 12816
Composition	Gevo ATJ; C12/C16 highly-branched iso-paraffins	84% C14 iso-paraffins; 16% 1,3,5 trimethyl benzene from Swift*	64% A-3; 36% Amyris farnesane (C15 iso-paraffin)	60% Sasol* IPK (C10-C13 highly branched iso-paraffins)/40% C-1	74% C10 iso-paraffins, 26% 1,3,5 trimethyl benzene
Notable characteristics	Very low cetane, unusual boiling range	On-spec fuel, extremely chemically-asymmetric boiling range	High viscosity fuel, at -20 C viscosity limit for jet fuel	Low cetane, conventional, wide-boiling range	Very flat boiling range (fuel boils at one temperature)

Figure 2.4: Category C Fuel Types [9]

		C-1	C-2	C-3	C-4	C-5
Property	Test method					
Density	D4052	0.760	0.781	0.808	0.760	0.769
Flash point, C	D93	50	58	66	46	44
Viscosity, -20 C (cSt)	D445	4.9	5.2	8.0, 8.3	3.9	1.9
Aromatics, vol%	D1319	1	17.6	11.2	2.3	26.2
Heat of Combustion, MJ/kg	D4809 AF, SwRI	43.88±0.09 (15 meas.)	43.6, 43.4	43.3, 43.3	43.8, 43.8	42.8, 43.0
H content, mass% (meas)	D3701 SwRI	15.28, 15.43	14.42	14.18	15.33	13.96
H content, mass % (meas)	D7171 AF	15.2	14.1	14.1	15.5	14.1
H content, mass % (meas)	D5291 SwRI	15.34	14.31	14.05	15.33	13.93
H content, mass%	GCxGC	15.3	14.4	14.2	15.4	13.9
H/C ratio (based on D3701)	calculation	2.17	2.00	1.97	2.15	1.94
Molecular formula	GCxGC	$C_{12.6}H_{27.2}$	$C_{12.4}H_{24.8}$	$C_{12.8}H_{25.3}$	$C_{11.4}H_{24.8}$	$C_{9.7}H_{18.7}$
Derived cetane #	D6890	17.1 (range 15.1-18.1)	50.4	47	28	39.6
Smoke pt, mm	D1322	29.0	30.0	26.0	26.0	25.0
Freeze pt, C	D5972	<-61	-45	-54	<-61	-56
Distillation, C	D86					
IBP		173	172	183	161	156
10%		178	190	204	169	161
20%		179	198	212	170	162
50%		182	224	230	179	162
90%		228	233	245	206	164
FBP		263	236	256	239	174

Figure 2.5: Category C Fuel Properties [9]

In Fig.2.6 there are the compositions of varios fuels, included the ones object of this work (A-2 fuel is the Jet-A)

Name	POSF#	Composition	Average Formula
A1	10264	16.40% 1,2,4-trimethylbenzene (C_9H_{12}) + 37.33% *iso*-undecane ($iC_{11}H_{24}$) + 25.22% *n*-undecane ($nC_{11}H_{24}$) + 21.05% butyl-cyclohexane ($MC_{10}H_{20}$)	$C_{10.5}H_{21.2}$
A2	10325	23.42% 1,2,4-trimethylbenzene (C_9H_{12}) + 26.09% *iso*-dodecane ($iC_{12}H_{26}$) + 19.33% *n*-undecane ($nC_{11}H_{24}$) + 31.16% pentyl-cyclohexane ($MC_{11}H_{22}$)	$C_{10.8}H_{21.1}$
A3	10289	27.35% 1,2,4-trimethylbenzene (C_9H_{12}) + 15.71% *iso*-tridecane ($iC_{13}H_{28}$) + 13.02% *n*-dodecane ($nC_{12}H_{26}$) + 29.72% hexyl-cyclohexane ($MC_{12}H_{24}$) + 14.21% methyl-dicyclohexane ($DC_{13}H_{24}$)	$C_{11.5}$ $H_{21.6}$
C1	11498	86.49% *iso*-dodecane ($iC_{12}H_{26}$) + 13.51% *iso*-hexadecane ($iC_{16}H_{34}$)	$C_{12.5}$ $H_{27.1}$
C2	12223	28.45% 1,2,4-trimethylbenzene (C_9H_{12}) + 71.55% *iso*-tetradecane ($iC_{14}H_{30}$)	$C_{12.6}$ $H_{24.9}$
C3	12341	19.85% 1,2,4-trimethylbenzene (C_9H_{12}) + 37.56% *iso*-pentadecane ($iC_{15}H_{32}$) + 9.44% *n*-dodecane ($nC_{12}H_{26}$) + 22.43% hexyl-cyclohexane ($MC_{12}H_{24}$) + 10.72% dicyclohexane ($DC_{12}H_{22}$)	$C_{12.5}$ $H_{24.6}$
C4	12344	8.72% *iso*-nonane (iC_9H_{20}) + 17.85% *iso*-denane ($iC_{10}H_{22}$) + 24.70% *iso*-undecane ($iC_{11}H_{24}$) + 43.85% *iso*-dodecane ($iC_{12}H_{26}$) + 4.88% *iso*-hexadecane ($iC_{16}H_{34}$)	$C_{11.3}$ $H_{24.7}$
C5	12345	34.38% 1,2,4-trimethylbenzene (C_9H_{12}) + 48.90% *iso*-denane ($iC_{10}H_{22}$) + 16.72% *n*-denane ($iC_{10}H_{22}$)	$C_{9.7}$ $H_{18.6}$
C6	10279-2	16.18% *iso*-dodecane ($iC_{12}H_{26}$) + 60.73% hexyl-cyclohexane ($MC_{12}H_{24}$) + 23.09% dicyclohexane ($DC_{12}H_{22}$)	$C_{12.0}H_{23.9}$

Figure 2.6: Fuels composition and average molecular formula [10]

It is also shown **Adiabatic Flame Temperature** behaviour with all differnt fuels (Fig.2.7). It is possible to see that C1 and C5 have higher T_{ad} compared to Jet-A and this result will come in handy in Sec.7.2.1.

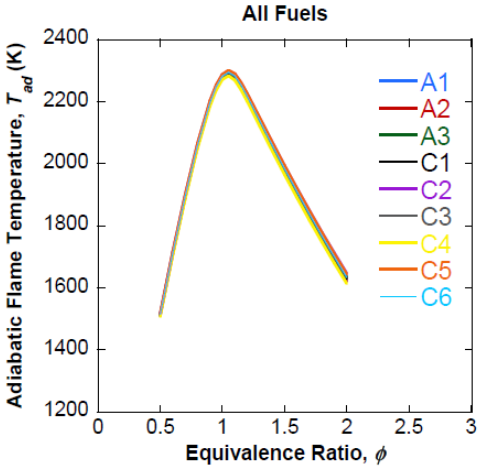

Figure 2.7: Fuels Adiabatic Flame Temperature vs Equivalence Ratio [10]

2.2.1 C-1

C-1 is usually an **Alcohol to Jet (ATJ)** SAF. This process uses a series of catalytic steps to dehydratate alcohols like ethanol or isubutalnol oligomerize them into longer hydrocarbons, and then refine them into a synthetic jet fuel blend. In fact, as shown in Fig.2.8, there are two main steps in the ATJ production process: an alcohol synthesis from feedstock to alcohol and than a process of Dehydratation, Oligomerisation, Hydrogenation and Fractionation Typical feedstock for ATJ are

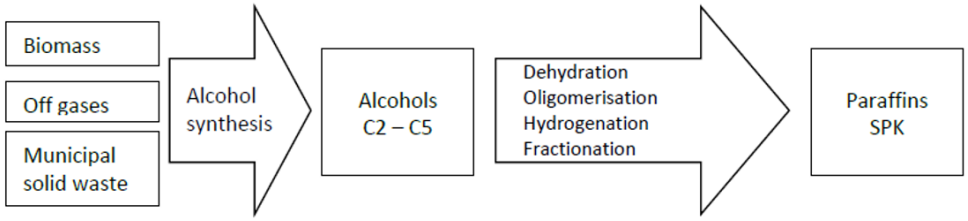

Figure 2.8: ATJ production process

usually agricultural waste (corn shoots, grass, straw) and cellulosic biomass.
In other cases C-1 can be an **Iso-Paraffinic Kerosene (IPK)**, a synthetic aviation fuel derived from sources like coal or natural gas through the Fischer-Tropsch process (Fig.2.9).

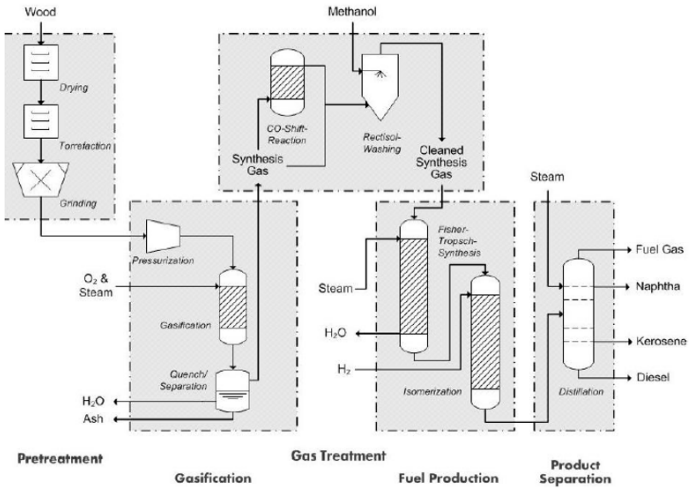

Figure 2.9: FT production process

IPK is an iso-paraffinic kerosene, meaning it is a mix of iso-paraffins (branched alkanes). A key feature is its low aromatic content, which differs significantly from conventional jet fuels like Jet A and has a lower **Derived Cetane Number** (DCN)

than some conventional fuels, which affects its ignition properties. It has a longer chemical ignition delay and can exhibit multiple negative temperature coefficient (NTC) regions during combustion.
Abuot the Derived Cetane Number, C-1 was designed to be the lowest Cetane fuel available. Cetane number (cetane rating) (CN) is an indicator of the combustion speed of fuels and compression needed for ignition. The CN is an important factor in determining the quality of a fuel, but not the only one. So have a low CN means that C-1 has a slower burning process than conventional fuels and this greatly influences the combustion process, which usually takes place in a very limited time, and emissions emitted.

2.2.2 C-5

C-5 is a **Synthetic Jet Fuel**. Synthetic jet fuel is a type of Sustainable Aviation Fuel (SAF) produced using non-biological, synthetic processes, most commonly by combining hydrogen from water electrolysis and carbon dioxide to create a hydrocarbon fuel. Also called e-kerosene, this type of fuels are designed to be completely "drop-in" fuels. The main advantage is, of course, a significant reduction in net carbon emissions, as the carbon comes from captured CO_2 rather than fossil fuels. The production process is again the Fischer-Tropsch syntesis already mentioned. In Fig.2.10 there's the complete production process of a synthetic aviation fuel

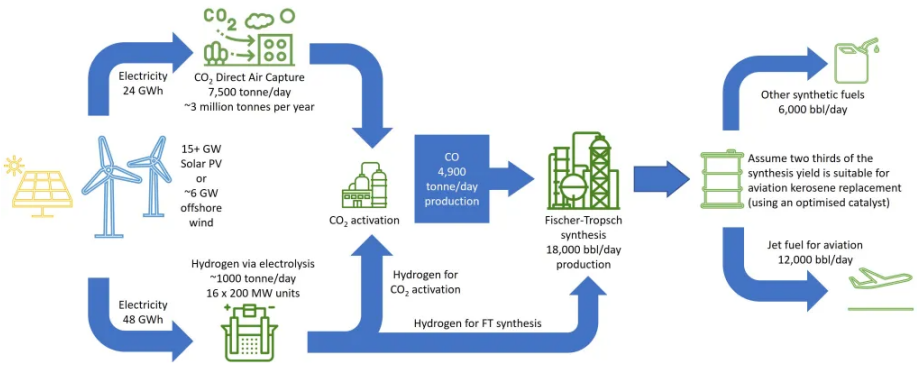

Figure 2.10: Synthetic Fuels production process [11]

The C-5 was designed to be a fully-formated fuel that meets all of the jet fuel specification requirements, but with a very "flat" boiling range. This means that the fuel evaporate around one temperature and not across an entire range, and as before for C-1, this results in less efficient combustion and higher emissions, especially of CO and unburned hydrocarbons, due to the poorer combustion process.

Chapter 3

Methodology

Aircraft engine design and Emissions evaluation are highly complex processes that often require years of study and development. The emissions evaluation, in particular, is not a subject that is well known or fully understood by the scientific community. There are a lot of metodologies to solve the problem, but only for restricted and specific cases, without a general approach.
Of course there's no universal pathway for the entire process of this work of thesis, but it is possible to summarise the main steps used in the flowchart in Fig.3.1.
The process exposed is iterative. Generally the starting point is the **Request for Proposal (RFP)**, which is a requirements document describing the desidered performance of the aircraft/engine system. In this work this stage is skipped because the aircraft and the engine covered in this thesis are well known. Instead the work start from a literature search for all necessary information about propulsive system on-design and fuels, conventional and alternative ones.
Once all the information are obtained it is possible to study the mission type, which will provide information about flight conditions and the performances required to complete the mission. It is thus possible to proceed with the on-design study of the propulsion system. This step, and the next ones concerning the propulsion system, are carried out using an updated version of Francesco Piccionello's code [12] to obtain a conceptual design engine model. Within the on-design study and subsequently also in the off-design study, it is necessary to have an accurate gas model in order to define the state and properties of the gas at each station of the engine, to obtain a good model of the internal flows within the engine, which is essential for calculating the performance of the engine itself. The code includes a routine that does just that, called **FAIR**, based on **CEA model**, which is used exactly as it is for conventional fuels but updated for alternative fuels through the use of **CANTERA**. All the work done on the Gas Model is well explained in the next section.

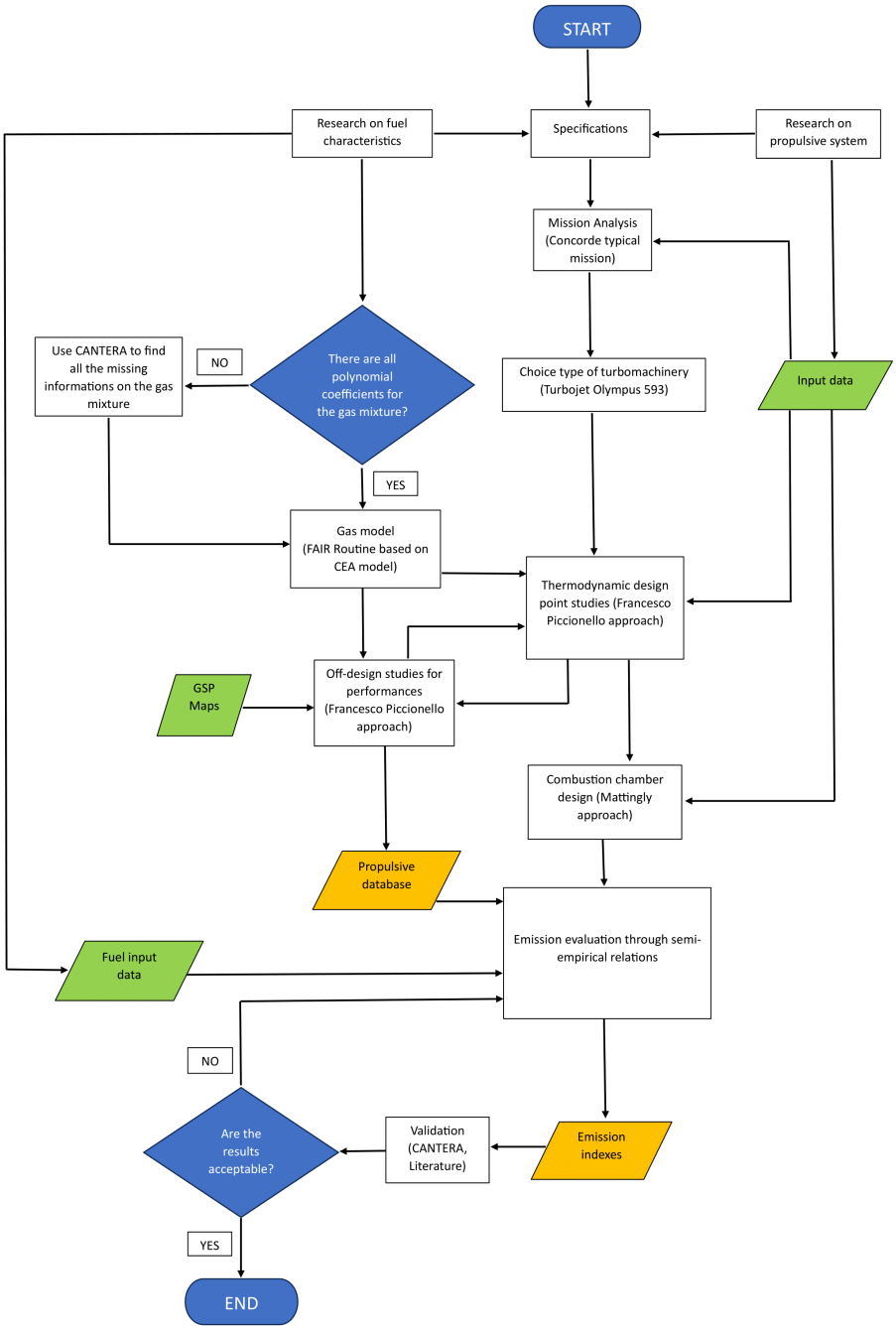

Figure 3.1: Flowchart methodology used in this thesis work

After the On-design simulations and with a fully upgraded FAIR routine, it is possible to proceed to the Off-Design analysis. The approach implemented for this part is the **Matrix Iteration Method** analized in two thesis work, the one already mentioned by Francesco Piccionello and the one by Gregorio Stiuso [13]. This analysis involves solving the thermodynamic cycle problem using the **Newton-Raphson method** and scaling existing maps of some components to find efficiencies, pressures and corrected mass flow rates. The main limitation of this method is related to the assumption that the specific component of the new engine has a "similar" and "proportional" map to an existing one. After the all the iterations varying flight Mach, Altitude and Throttle it is possible to generate a **Propulsive Database** with the performances in all the operative conditions of the engine during the mission. In addittion it is possible to compare the conditions obtained with the required ones. All these processes repeted for all fuels.
After the engine design is complete, it is possible to merge the engine parameters with those related to fuels to start the emissions evaluation. For this final step a lot of data are required because the Lefebvre and Murthy semi-empirical correlations are based on parameters relative to the geometry of the combustion chamber, the thermodynamic cycle, the thermochemical properties of the fuels and the combustion process. The results obtained are the **Emission Indexes** in $[g/kg\ fuel]$ of three pollutant emission: **Carbon Monoxide** (CO), **Unburnt Hydrocarbons** (UHC) and **Nitrogen Oxides** (NO_x). The flight conditions chose for the emissions evaluation are the **Supercruise** at $M = 2$, the **Take-Off** and the **Idle** condition. The results are then validated through CANTERA and literature.

Chapter 4

Gas Model

It is necessary, to reach a satisfying accuracy in the calculation of engine properties, to introduce a well structured gas model. For this reason we need to consider the variation of the constant pressure coefficient with the variation of pressure and temperature. This section will discuss the methodology used to model the thermodynamic state of the gas. The formulation exposed is used by Francesco Piccionello in his Master Thesis [12] and also by different engine programs, such as GasTurb [14] and GSP 11 [15], to obtain an accurate gas model.
This model is deeply developed for conventional aviation fuel, but not for alternative fuel, so in the following work an adaptation of the model is proposed (Sec. 4.2.4).

4.1 Half-Ideal Gas model

A thermodynamic system is described by two state variables. If we consider the entalphy (J/Kg), we can express it in function of temperature and pressure

$$h = f(T, p) \tag{4.1}$$

And in diferential form

$$dh = \left(\frac{\partial h}{\partial T}\right)_{P=cost} dT + \left(\frac{\partial h}{\partial p}\right)_{T=cost} dp \tag{4.2}$$

For Mattingly [16] [17], the working fluid in a gas turbine can be modeled as a **half-ideal perfect gas**, which implies that the gas obeys the following properties

$$C_p = f(T) \tag{4.3}$$

$$C_p \neq f(p) \tag{4.4}$$

$$\left(\frac{\partial h}{\partial p}\right)_{T=cost} = 0 \tag{4.5}$$

In fact C_p represents the Constant Pressure Heat, defined as

$$C_p = \left(\frac{\partial h}{\partial T}\right)_{p=cost} \tag{4.6}$$

An half-ideal gas model is valid for temperatures between 200K and 2220K for air and air-fuel mixtures. The final enthalpy formulation can be obtained from Eq. 4.6

$$dh = \left(\frac{\partial h}{\partial T}\right)_{P=cost} dT = C_p(T)dT \tag{4.7}$$

$$h(T) = \int_{T_{ref}}^{T} C_p(T)dT \tag{4.8}$$

T_{ref} is the reference temperature, which can be selected arbitrarily but must be consistent with reference temperature of the **fuel heating value (FVH)**. The Eq. 4.8 demonstrates that the enthalpy function dependes on the variation of C_p. The problem at this point is to find an appropriate expression for it.

4.2 The Variable Specific Heat Model

4.2.1 Chemical Equilibrium

The constant pressure coefficient expression can be derived from Chemical Equilibrium data, which relies on the Chemical Equilibrium assumption. Considering the following reaction

$$N_A A + N_B B \rightleftharpoons N_C C + N_D D \tag{4.9}$$

the chemical equilibrium, essentially, is a condition in which the forward rate of reaction of reactants A and B equals the backward rate of reaction of products C and D. It corresponds to the minimum value of the **Gibbs function** ($G = H - TS$) for the entire mixture as shown in Fig. 4.1 This condition has a significant limitation: the results do not account for the rate of changes in mole numbers or the integrated values that may occur at specific moments due to the brief residence of fluid in certain engine components. Consequently, the assumption of small residence time does not facilitate the attainment of chemical equilibrium. To address this, more intricate models can be developed and implemented to accurately replicate these conditions. Typically, such models are employed for the detailed design of the chamber, especially during the conceptual design phase.

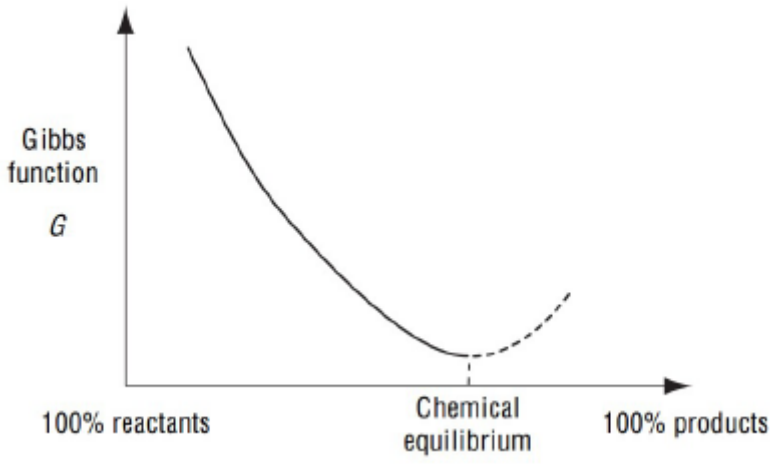

Figure 4.1: Chemical equilibrium: Gibbs function

4.2.2 Chemical Equilibrium Algorithm

The most commonly used method for the determination of specific heat and other thermodynamic quantities is the **Chemical Equilibrium Algorithm (CEA)**. From the NASA Glenn thermochemical database [18] and by using the CEA run, a free computer program, it is possible to calculate, for a generic hydrocarbon ($C_{12}H_{23}$) with a give fuel-to-air ratio f the specific heat of the fuel and air mixture as

$$C_p = \frac{C_{p,air} + f \cdot C_{p,prod}}{1+f} \tag{4.10}$$

Both specific heat coefficients are given by a seven-order polynomial

$$C_p = A_0 + A_1 T + A_2 T^2 + A_3 T^3 + A_4 T^4 + A_5 T^5 + A_6 T^6 + A_7 T^7 \tag{4.11}$$

So the polynomial coefficients are calculated through the polynomial fitting of CEA data. They are listed in Tab.4.1

Using Eq. 4.8, it is possible to calculate the enthalpy for the pure air or for the products as

$$h = h_{ref} + A_0 T + \frac{A_1}{2}T^2 + \frac{A_2}{3}T^3 + \frac{A_3}{4}T^4 + \frac{A_4}{5}T^5 + \frac{A_5}{6}T^6 + \frac{A_6}{7}T^7 + \frac{A_7}{8}T^8 \tag{4.12}$$

And for the gas mixture

$$h = \frac{h_{air} + f \cdot h_{prod}}{1+f} \tag{4.13}$$

Other important parameters are pressure and entropy in the case of half-ideal gas model. Considering the differential equation for Gibbs entropy [16], they are

Air Alone		Air and Fuel	
A_0	1.5020051 x10^{-1}	A_0	7.3816638 x10^{-2}
A_1	-5.15366879 $\times 10^{-5}$	A_1	1.2258630 $\times 10^{-3}$
A_2	6.5519486 $\times 10^{-8}$	A_2	-1.3771901 $\times$10−6
A_3	-6.7178376 $\times 10^{-12}$	A_3	9.96886793 $\times 10^{-10}$
A_4	-1.5128259 $\times 10^{-14}$	A_4	-4.2051104 $\times 10^{-13}$
A_5	7.6215767 $\times 10^{-18}$	A_5	1.0212913 $\times 10^{-16}$
A_6	-1.4526770 $\times 10^{-21}$	A_6	-1.3335668 $\times 10^{-20}$
A_7	1.0115540 $\times 10^{-25}$	A_7	7.2678710 $\times 10^{-25}$
h_{ref}	-1.7558886 Btu/lbm	h_{ref}	30.58153 Btu/lbm
Φ_{ref}	0.0454323 Btu/lbm	Φ_{ref}	0.6483398 Btu/lbm

Table 4.1: Polynomial coefficients for pure air and products [12] [18] [17]

evaluated considering

$$Tds = dh - RT \cdot \frac{dP}{P} \tag{4.14}$$

where R represents the gas constant of the mixture. It is possible to rewrite Eq. 4.14 to relate the change in entropy with pressure as follow

$$ds = \frac{dh}{T} - R\frac{dP}{P} \Rightarrow$$

$$\Delta s = s_2 - s_1 = \int_1^2 \frac{dh}{T} - R\, ln\left(\frac{P_2}{P_1}\right) \Rightarrow$$

$$\Delta s = s_2 - s_1 = \int_1^2 \frac{C_p(T)}{T} dT - R\, ln\left(\frac{P_2}{P_1}\right)$$

Therefore, the entropy variation is given by

$$s_2 - s_1 = \phi_2 - \phi_1 - R\, \left(\frac{P_2}{P_1}\right) \tag{4.15}$$

now, ϕ, the entropy function, is defined as

$$\phi \doteq \int_{T_{ref}}^{T} \frac{C_p}{T} dT \tag{4.16}$$

and it becomes

$$\phi = \phi_{ref} + A_0 ln(T) + \frac{A_1}{2}T^2 + \frac{A_2}{3}T^3 + \frac{A_3}{4}T^4 + \frac{A_4}{5}T^5 + \frac{A_5}{6}T^6 + \frac{A_6}{7}T^7 + \frac{A_7}{8}T^8 \tag{4.17}$$

For a gas mixture

$$\phi = \frac{\phi_{air} + f\ \phi_{prod}}{1+f} \tag{4.18}$$

For convenience, it si possible to define reduced pressure as

$$P_r \doteq exp\left(\frac{\phi - \phi_{ref}}{R}\right) \tag{4.19}$$

The reduced pressure is a useful parameter for modeling engine components. For example, during the compressor's On-design analysis, the polytropic efficiency is considered constant, allowing to relate the overall pressure ratio as follows

$$\phi_{t3} - \phi_{t2} = \frac{R}{e_c} ln\left(\frac{P_{t3}}{P_{t2}}\right)$$

$$\pi_c \doteq \frac{P_{t3}}{P_{t2}} = exp\left(\frac{\phi_{t3} - \phi_{t2}}{R}\right)$$

Which can be rewritten in terms of reduced pressure

$$\pi_c = \left(\frac{P_{rt3}}{P_{rt2}}\right)^{e_c} \tag{4.20}$$

4.2.3 The FAIR Routine

The mathematical equations of the half-ideal gas model have been presented in the section above, which are implemented in a function called **FAIR**, in MATLAB Envinronment. This subroutine is fundamental to predict the engine performances of the engine model. Particularly, it allows the evaluation of the entire gas state with one of the following inputs: **temperature** (T), **enthalpy** (h), or **reduced pressure** (P_r). Also, the fuel-to-air ratio (f) of the mixture must be given, or otherwise, if the gas is air alone, it is possible to set it equal to zero. The outputs include:

- R: the universal gas constant of the mixture.
- C_p: the constant pressure specific heat of the mixture.
- γ: the ratio of the constant specific heat at constant pressure over the constant specific heat at constant volume of the mixture.
- a: the speed of sound of the mixture.
- T: the temperature of the mixture (if unknown).
- h: the enthalpy of the mixture (if unknown).

- ϕ: the entropy function.
- s: the entropy of the mixture.
- P_r: the reduced pressure of the mixture (if unknown).

In cases where enthalpy or pressure is the input, a nonlinear system must be solved to obtain the temperature and other quantities. The solution of the system can be obtained using the $fzero$ function in MATLAB with a selected tolerance of 10^{-14}. The routine has been validated using the table in Appendix D of "Elements of Gas Turbine Propulsion" [17]. The results obtained using MATLAB match those in the table, both in the International System Unit and the Imperial Unit System.
The Fig. 4.2 and Fig. 4.3 illustrate the variation of the constant pressure heat C_p and the ratio of specific heats γ, respectively. These results are computed using "FAIR" for fuel-to-air ratio ranging from 0 (pure air mixture) to the stoichiometric value $f_{st} = 0.0685$ for a generic hydrocarbon fuel $C_{12}H_{23}$. The temperature range considered is from 220 K to 2000 K. As observed, both parameters change significantly with temperature and air mixture, especially when the temperature rises above 500 K. It is possible to observe that an increase in the C_p variation

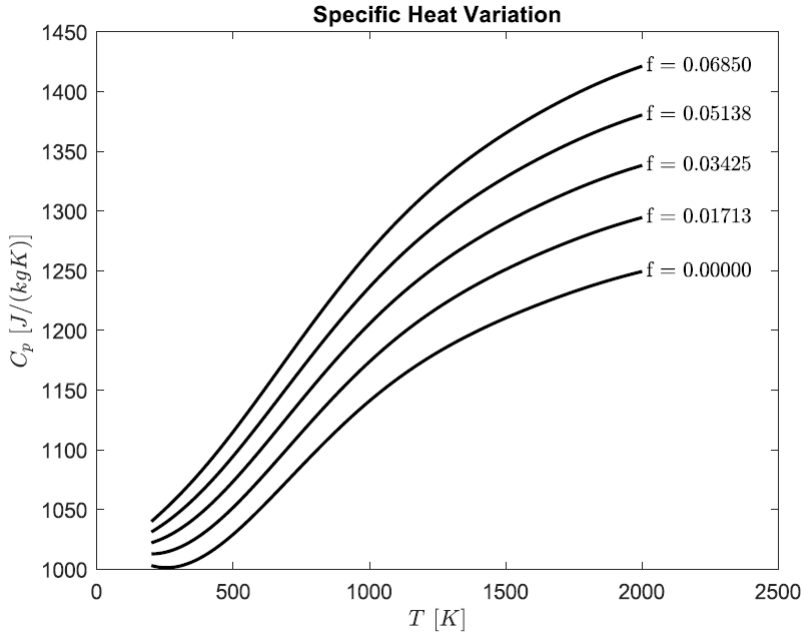

Figure 4.2: Specific heat C_p vs. temperature for a generic $C_{12}H_{23}$ hydrocarbon and air combustion products [12]

leads to a variation of enthalpy, which means the related thermodynamic work and power will be affected by an error. Another important consideration is the

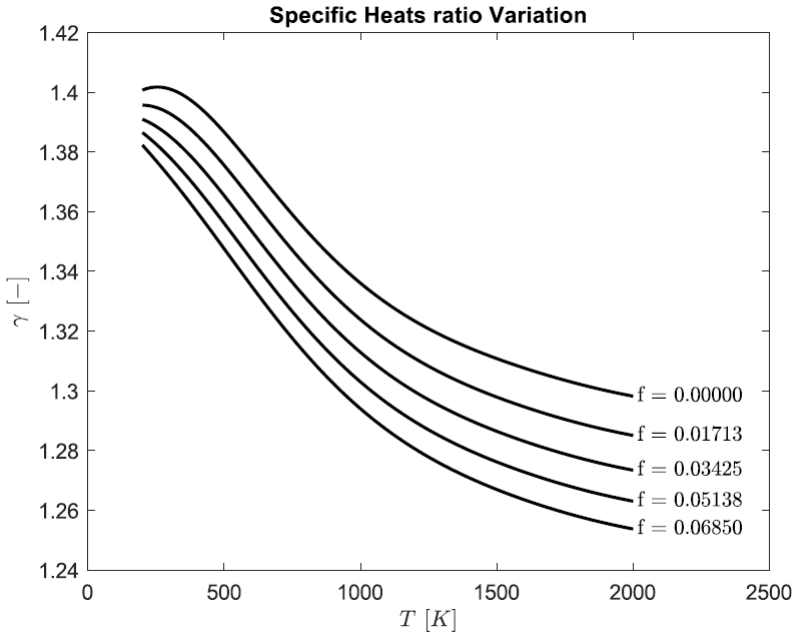

Figure 4.3: Ratio of specific heat γ vs. temperature for a generic $C_{12}H_{23}$ hydrocarbon and air combustion products [12]

chosen fuel for the analysis. Generally, typical propellants used in aeronautical propulsion do not vary from each other in terms of specific heat, so it is possible to justify the use of a generic hydrocarbon composition to simulate the performances of a jet engine, neglecting the real chemical composition. The case is different if alternative fuels such as bio-fuel or hydrogen mixture are considered. According to the references, the procedure to obtain polynomial coefficient does not differ from the exposed one and the equations are still valid in the proposed range.

4.2.4 MATLAB routines for C1 and C5

For C1 and C5 we have a different situation because we don't have the polynomial values for the CEA model so we need to evaluate them. To do so we need to use **CANTERA** in combination with MATLAB routines already mentioned. These values are obtained approximately with respect to experimental measurements. However, the results obtained are encouraging.
CANTERA is an open-source suite of tools for problems involving chemical kinetics, thermodynamics, and transport processes. This software automates the chemical kinetic, thermodynamic, and transport calculations so that the users can efficiently incorporate detailed chemical thermo-kinetics and transport models into their calculations, utilizes object-oriented concepts for robust yet flexible phase

models, and algorithms are generalized so that users can explore different phase models with minimal changes to their overall code. Is currently used for applications including combustion, detonations, electrochemical energy conversion and storage, fuel cells, batteries, aqueous electrolyte solutions, plasmas, and thin film deposition. Furthermore, CANTERA, has a lot a different interfaces among which is MATLAB. Proceeding step by step, air and fuel have been set in a stoichiometric ratio to ensure perfect combustion. To do this, some reactions need to be balanced for C1

$$C_{13}H_{28} + x\, O_2 + y\, 3{,}762 \cdot N_2 \rightleftharpoons i\, CO_2 + j\, H_2O + k\, 3{,}762 \cdot N_2 \tag{4.21}$$

$$C_{13}H_{28} + \left(13 + \frac{28}{4}\right)\, O_2 + 20\, 3{,}762 \cdot N_2 \rightleftharpoons 13\, CO_2 + 14\, H_2O + 20\, 3{,}762 \cdot N_2 \tag{4.22}$$

and C5

$$C_{10}H_{19} + x\, O_2 + y\, 3{,}762 \cdot N_2 \rightleftharpoons i\, CO_2 + j\, H_2O + k\, 3{,}762 \cdot N_2 \tag{4.23}$$

$$C_{10}H_{19} + \frac{59}{4}\, O_2 + \frac{59}{4}\, 3{,}762 \cdot N_2 \rightleftharpoons 10\, CO_2 + \frac{19}{2}\, H_2O + \frac{59}{4}\, 3{,}762 \cdot N_2 \tag{4.24}$$

Simplified relationships were used for the balances, assuming that the only combustion products are CO, H_2O, and N_2, as these are the products present in the greatest quantities under equilibrium conditions.If air is used as an oxidizer it has to be taken into account that dry air contains only about 21% oxygen (78% nitrogen, 1% noble gases). Thus, for air $x_{N_2} = 3{,}762\, x_{O_2}$, where "x" is the mole fraction.
So, for both cases, has been found υ ($\upsilon_{C1} = 20$ and $\upsilon_{C5} = 14{,}75$), that denotes the number of moles of O_2 in the reaction equation for a complete reaction to CO_2 and H_2O.
Thanks to these results, we can calculate the mole fractions and mass fractions of air and fuels, and using the latter we can calculate the stoichiometric fuel-to-air ratio for CANTERA.

$$x_{fuel,st} = \frac{1}{1 + \upsilon \cdot (1 + 3{,}762)} \tag{4.25}$$

$$x_{air,st} = 1 - x_{fuel,st} \tag{4.26}$$

$$w_{fuel,st} = \frac{x_{fuel,st}\ M_{fuel}}{\sum_i x_i M_i} \tag{4.27}$$

$$w_{air,st} = \frac{x_{air,st}\ M_{air}}{\sum_i x_i M_i} \tag{4.28}$$

$$f_{st} = \frac{w_{fuel,st}}{w_{air,st}} \tag{4.29}$$

where M is the molar mass.
We obtain $f_{C1,st} \cong 0{,}0667$ and $f_{C5,st} \cong 0{,}0683$ (for conventional jet fuels we have

$f_{st} \cong 0{,}0685$).
Once these values have been obtained, we can proceed with the calculations in cantera. The latter allows us to calculate characteristic gas values in various situations. For our case study, we want to obtain the polynomial coefficients for C_p, h and ϕ for C1 and C5 so that we can enter them into the FAIR routine and calculate the performance of our engine using the new fuels.
To do this, the first step is the solution of the **Reaction Mechanism**, which contains all the information relating to the combustion process: species involved, characteristics of these species, and all the elementary reactions involved in the process. By entering the Reaction Mechanisms in the "**Solution**" function, it is possible to collect all objects needed to describe a chemically-reacting solution. Instances can be created to represent any type of solution: a mixture of gases, a liquid solution, or a solid solution, for example. For more information on the Reaction Mechanisms, see the Appendix B.
Then the gas conditions are set using the "**Set**" function (Fig. 4.4 and Fig. 4.5). It is possible to enter various variables to define the state of the gas mix during calculations: in this work, the initial conditions of temperature and pressure and the mass fractions of air and fuel are imposed.
Finally the chemical equilibrium is calculated as the composition of the gas mixture varies (Fig. 4.6). In particular, the fuel/air ratio is varied from zero to the previously calculated stoichiometric condition. The standard atmosphere (ISA) is considered the reference condition.

```
40  gas = Solution('c1.yaml');
41  set(gas,'T',T_ref,'P',P_ref,'Y',['O2:',num2str(yo2),',POSF11498:',num2str(yf),',N2:',num2str(yn2)]);
42  equilibrate(gas,'UV');
43  gas()
```

Figure 4.4: Set function for C1 in reference conditions

```
100 gas = Solution('Z79_C5.yaml');
101 set(gas,'T',T_ref, 'P',P_ref,'Y',['O2:',num2str(yo2),',POSF12345:',num2str(yf),',N2:',num2str(yn2)]);
102 equilibrate(gas,'UV');
103 gas()
```

Figure 4.5: Set function for C1 in reference conditions

```
34  yo2 = 1/(4.76*(1+f(j)));
35  yf  = f(j)/(1+f(j));
36  yn2 = (1/(1+f(j)))/(1+(1/3.76));
```

Figure 4.6: Mass fractions to modify composition

Once the chemical equilibrium has been calculated, CANTERA allows the

calculation of various gas-related quantities using specific functions (Fig. 4.7).

```
45
46
47
48
49
50
51
52
53
54
55
```

```
Cp_ref(j) = cp_mass(gas);
Cv_ref(j) = cv_mass(gas);
R_ref(j) = Cp_ref(j)-Cv_ref(j);
gam_ref(j) = Cp_ref(j)/(Cp_ref(j)-R_ref(j));

h_ref(j) = enthalpy_mass(gas);

s_ref(j) = entropy_mass(gas);

phi_ref(j) = s_ref(j)+R_ref(j)*log(P_ref);
```

Figure 4.7: Cantera functions

To calculate the coefficients of CEA method, using a nested for loop, the temperature is also varied in addition to the composition. Once all the results have been obtained for different temperatures and mass fractions, the average values are calculated for all mass fractions, obtaining all the values necessary for using the FAIR routine, like the conventional jet-fuel case (Tab. 4.2).

Air and C1		**Air and C5**	
A_0	7.95514172 x10^{-1}	A_0	8.48734076 x10^{-1}
A_1	3.98493 $\times 10^{-5}$	A_1	-4.04348 $\times 10^{-4}$
A_2	8.81228 $\times 10^{-8}$	A_2	1.39319 $\times$10−6
A_3	-1.32523 $\times 10^{-10}$	A_3	-1.36699 $\times 10^{-10}$
A_4	-9.45689 $\times 10^{-13}$	A_4	6.61756 $\times 10^{-13}$
A_5	5.84839 $\times 10^{-16}$	A_5	-1.46868 $\times 10^{-16}$
A_6	6.74778 $\times 10^{-21}$	A_6	8.27418 $\times 10^{-21}$
A_7	-5,70069 $\times 10^{-25}$	A_7	-7.42804 $\times 10^{-25}$
h_{ref}	15.428655 Btu/lbm	h_{ref}	16.006024 Btu/lbm
Φ_{ref}	0.797612 Btu/lbm	Φ_{ref}	0.697622122 Btu/lbm

Table 4.2: Polynomial coefficients for Air mixed with C1 and C5

Just as with conventional fuels, the behavior of Cp and Gamma can be evaluated with temperature and fuel-to-air ratio changes (Fig. 4.8, Fig. 4.9, Fig. 4.10 and Fig. 4.11). The temperature range considered is from 298 K to 2500 K. As observed, both parameters change significantly with temperature and air mixture, especially when the temperature rises above 500 K.

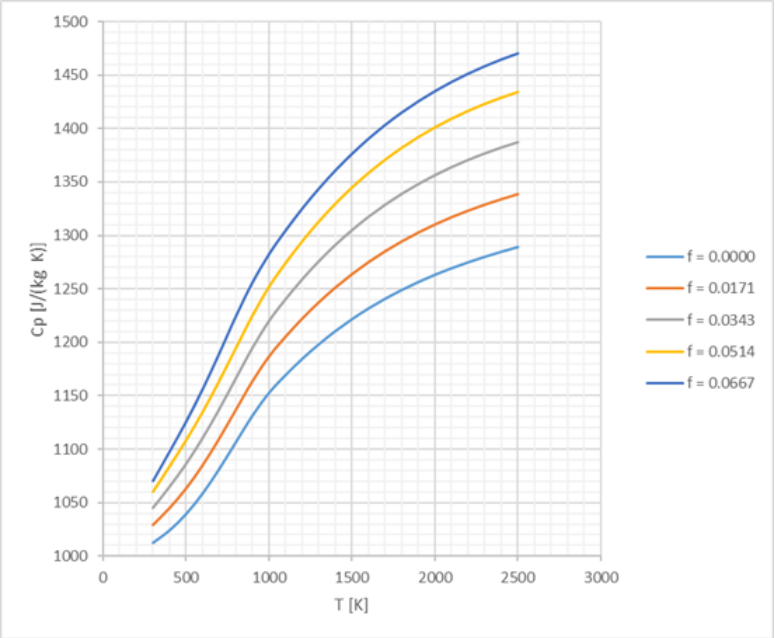

Figure 4.8: Specific heat C_p vs. temperature for a generic C1 and air combustion products

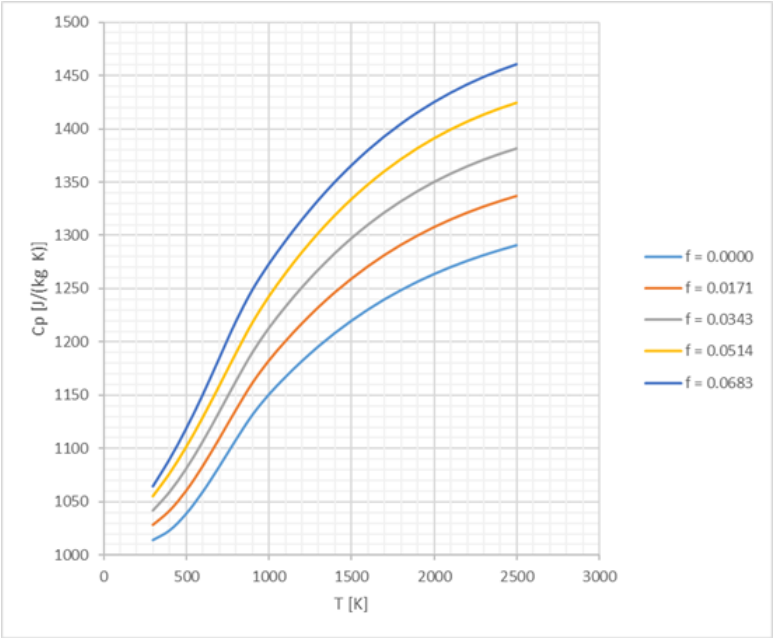

Figure 4.9: Specific heat C_p vs. temperature for a generic C5 and air combustion products

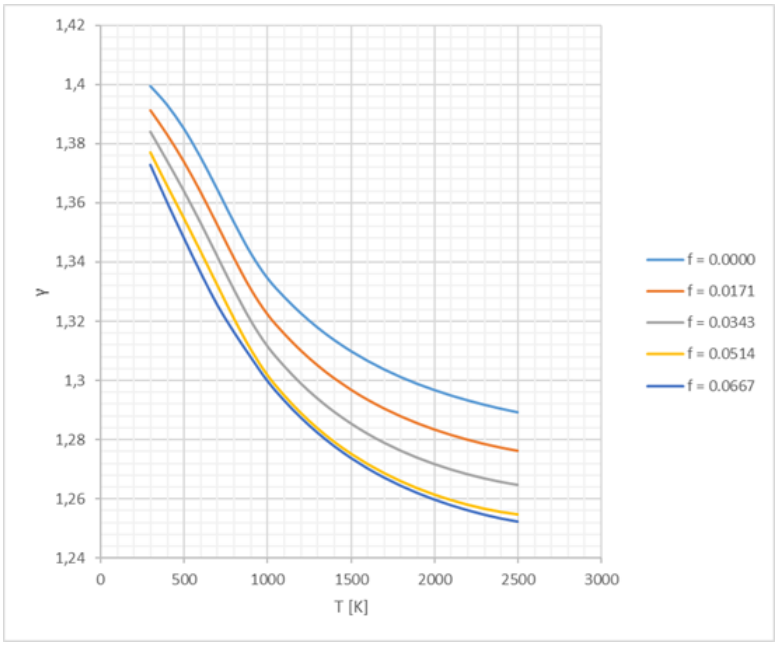

Figure 4.10: Ratio of specific heat γ vs. temperature for C1 and air combustion products

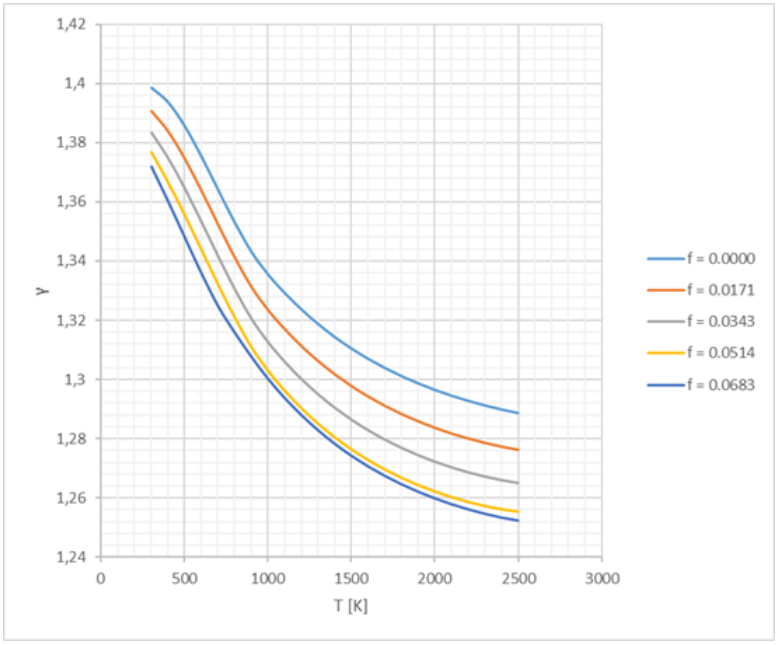

Figure 4.11: Ratio of specific heat γ vs. temperature for C5 and air combustion products

4.3 The Modified Specific Heat Model

Another model used for the calculation of the gas characteristics is the **Modified Specific Heat**. This assumes that the values of cp and gamma are constant, average values of all those available. In this model the gas is assumed calorically perfect, which means:

$$C_p(T) = C_p \tag{4.30}$$

$$C_v(T) = C_v \tag{4.31}$$

$$\gamma(T) = \gamma \tag{4.32}$$

With obvious consequences in other formulas

$$h_2 - h_1 = C_p \cdot (T_2 - T_1) \tag{4.33}$$

$$s_2 - s_1 = C_p \cdot ln\left(\frac{T_2}{T_1}\right) - R \cdot ln\left(\frac{P_2}{P_1}\right) \tag{4.34}$$

So

$$\frac{T_2}{T_1} = \left(\frac{P_2}{P_1}\right)^{(\gamma-1)/\gamma} \cdot exp\left(\frac{s_2 - s_1}{C_p}\right) \tag{4.35}$$

In addition, the process is considered isentropic.

$$\frac{T_2}{T_1} = \left(\frac{P_2}{P_1}\right)^{(\gamma-1)/\gamma} \tag{4.36}$$

With these assumptions, we can evaluate the error that arises when taking a constant C_p. If we consider $C_p = 1002$ for a constant $f = 0.0000$, we see that the error increases as T increases Tab. 4.3. Same behavior for $\gamma = cost = 1.4$ Tab. 4.4.
After combustion the temperature will increase significantly, in today system can

T	220 K	500 K	800 K
C_p	1002 $J/(kg \cdot K)$	1029 $J/(kg \cdot K)$	1098 $J/(kg \cdot K)$
ϵ	0.00%	+2.69%	+9.58%

Table 4.3: Specific Heat Variation for pure air

reach above 2000 K. Assigning an average value for C_p and γ is very challenging and, in some cases, a bad approximation. According to the literature (Ref. [16], Ref. [17]), the general assigne values are

$$C_p' = 1184 \ J/(kg \cdot K) \tag{4.37}$$

$$\gamma' = 1.33 \tag{4.38}$$

T	220 K	500 K	800 K
γ	1.40	1.39	1.35
ϵ	0.00%	-0.71%	-3.57%

Table 4.4: Specific Heat ratio Variation for pure air

T	600 K	1000 K	1300 K	1800 K
$f = 0.0171$ $C_p[J/(kg \cdot K)]$	1075	1173	1226	1280
$\epsilon[\%]$	-9.20	-0.93	$+3.55$	$+8.11$
$f = 0.0343$ $C_p[J/(kg \cdot K)]$	1099	1205	1263	1322
$\epsilon[\%]$	-7.18	$+1.77$	$+6.67$	$+11.7$
$f = 0.0685$ $C_p[J/(kg \cdot K)]$	1145	1266	1332	1403
$\epsilon[\%]$	-3.29	$+6.93$	$+12.5$	$+18.5$

Table 4.5: Specific Heat ratio Variation for pure air

It is possible to compare these new values with those of the Variable Specific Heat Model(4.5). We can see that the error becomes too large as the temperature increases. The gas model needs to be as accurate as possible since the related error will affect the enthalpy and, as a consequence, the engine performance. A significant impact of the C_p variation is on the Unistalled TSFC, which strongly depends upon the fuel/air ratio and so the enthaply calculations related to the TIT (Temperature Inlet Turbine). The Modified Specific Heat Gas model has the vantage of a very low computational cost, but at the price of a significant error in performance predictions.

Chapter 5

Engine Model

In this chapter, a numerical model of the **Olympus-593** engine is presented. The work unfolds through a systematic process, focusing on different sections of the cycle and scrutinizing the impact of each variable, followed by a comparison of results with the available propulsive database. The approach start with outlining the typical mission profile of the Concorde to derive all relevant environmental conditions. These conditions are then employed to study the air intake comprehensively, and the outcomes serve as the baseline for the propulsion cycle analysis. Subsequently, the engine data are utilized to approximate performance metrics, which are then juxtaposed with data found in existing literature. This comprehensive methodology ensures a complete exploration of the engine's behavior under various conditions, offering valuable insights and enabling comparisons with established propulsive benchmarks.
All this steps are deeply explained in the further sections.

5.1 Olympus-593 model

The first purpose of this thesis work consists in analyzing, as deep as possible, the engine model through using the typical thermodynamic and balance equations.
Certain flight conditions are important in the preliminary design phase of the Olympus 593 analysis. A "**Supersonic Engine**" is never just that, since it also must perform well over a wide range of subsonic speeds before and after cruise conditions. Multiple design points must be considered. Each design point has its own demands but severe compromises must always be made to ensure operational compatibility.

- Engine performance during cruise conditions is crucial, as a significant portion of the fuel is consumed during this phase. Unlike subsonic aircraft, supersonic aircraft engines cannot be throttled back during cruise because sustaining

supersonic flight requires substantial thrust. In many cases, the performance at the top-of-climb stage determines the sizing requirements for the propulsion system. This emphasizes the importance of optimizing engine efficiency and performance during the cruise phase to enhance overall fuel efficiency and mission effectiveness for supersonic aircraft.

- The take-off phase is a critical consideration because it demands the maximum absolute thrust to accelerate the aircraft from brake-release and enable it to take off within a specified distance. However, once the landing gear is retracted, and drag is reduced, the engine can be throttled back. This is advantageous since, as mentioned earlier, take-off noise is a significant concern, and it is directly influenced by jet speed. Therefore, the objective during take-off is to maximize airflow to maintain the required momentum of the exhaust jet at a lower velocity, contributing to a reduction in take-off noise levels.
- For certain aircraft, a "pinch point" emerges between the net thrust an engine can provide and the thrust required by the airplane during transonic situations. Consequently, this specific mission segment may play a crucial role in determining the optimal size for the engine. Addressing the challenges posed during the transition through the sound barrier becomes imperative in optimizing engine performance and ensuring the aircraft's efficient and effective operation during transonic conditions.

Some values of relevant parameters are shown in Figure 5.1.

	Cruise	End of Runway T. O.	Max Climb
Mach Number	2.0	0.302	1.2
Altitude (ft)	53,000	0	40,000
Conditions	ISA + 5°C	ISA + 10°C	ISA + 5°C
Inlet Pressure Recovery	0.937	0.986	0.986
After burner	Off	On	On
Net Thrust (lbf)	10,030	33,620	13,610
Specific Fuel Consumption (lbm/lbf/hr	1.19	1.39	1.41

Figure 5.1: Performance data Engine at Critical Flight Conditions [19]

Two points were chosen for the preliminary analysis of the engine and starting from these two an analysis of the sizes and performances was carried out in all the other selected flight conditions.

- The primary design point for the engine should be **Supersonic Cruise** conditions at 53000 feet/Mach 2. The net thrust must be approximately 10000

lbf.

- The second “off-design” point should be **Rolling Take-off** at sea level/Mach 0.35. The net thrust must be approximately 33600 lbf with reheat.

For the other off-design points, the mission profile of the following section is considered.

5.2 Mission profile

The **Mission Profile** proves to be a valuable tool for the project as it identifies key points in terms of altitude and duration, providing crucial information for the overall calculation of mission duration. The air parameters, heavily utilized later in the project, are altitude-dependent, making their accurate definition essential for evaluating engine data and performances. The definition of the mission profile is contingent on the type of aircraft under development, specifically, in this case, a supersonic passenger transport aircraft. The phases are delineated chronologically, with some classified as "on-ground" while others are categorized as "in-flight" phases. Each phase contributes unique considerations and challenges to be addressed in the development process. (Table 5.1).

Phase	**Dur.**	**Start**		**End**	
	[min]	**[m]**	**[FL]**	**[m]**	**[FL]**
Warm-Up & Taxi-out	10	0	0	0	0
Take-Off	10	0	0	0	0
Subsonic Climb	10	0	0	4572	150
Subsonic Cruise	15	4572	150	8815	289
Supersonic Climb	20	8815	289	14784	485
Supersonic Cruise	150	14784	485	16859	553
Supersonic Descent	20	16859	553	7315	240
Subsonic Cruise (Descent)	10	7315	240	3000	100
Subsonic Descent	10	3000	100	1524	50
Approach & Touchdown	5	1524	50	0	0
Taxi-in	10	0	0	0	0

Table 5.1: Duration and Altitudes Mission Profile

The cruise phases at varying altitudes consider the fact that these segments are frequently overseen by mechanisms, such as autopilots. These mechanisms optimize specific parameters to achieve trajectories with reduced fuel consumption, unlike scenarios where the objective is to minimize surface temperature (as seen in the

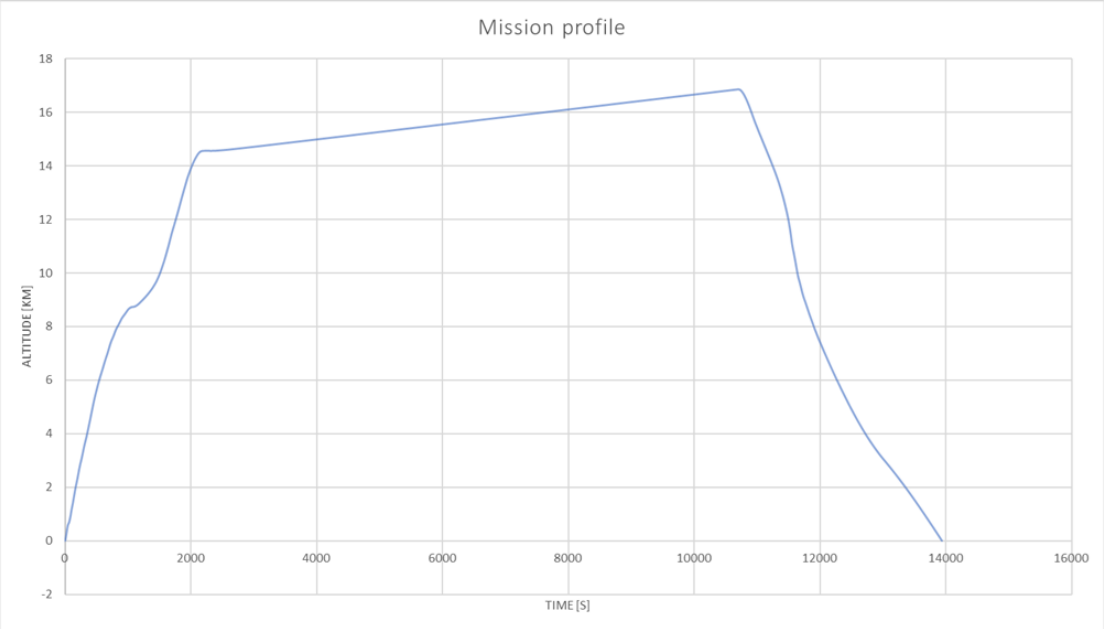

Figure 5.2: Mission Profile

supersonic cruise of the Concorde, for instance). Another essential point to note is the definition of the landing phase: its start is defined by a predetermined obstacle stipulated by regulations and concludes when the aircraft comes to a complete stop.(Figure 5.2).

5.3 Main component

The following description gives an overview of the stations that constitute the engine model. All components and stations of the model are represented in Figure 5.3.

- STATION 0: Undisturbed condition upstream;
- STATION 1: Air Intake inlet;
- STATION 2: Air Intake exit, Low Pressure Compressor inlet;
- STATION 24: Bleed system inlet;
- STATION 25: Low Pressure Compressor exit, High Pressure Compressor inlet;
- STATION 3: High Pressure Compressor exit, Combustor inlet;

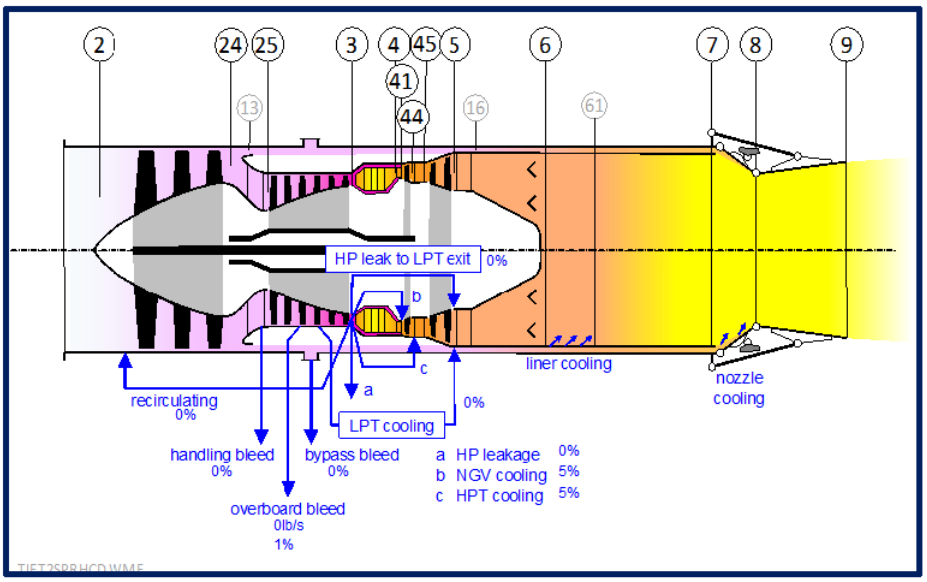

Figure 5.3: Schematic Engine with Reheat [19]

- STATION 4: Combustor exit, High Pressure Turbine inlet;
- STATION 41/44: Air Cooling system exit;
- STATION 45: High Pressure Turbine exit, Low Pressure Turbine inlet;
- STATION 5: Low Pressure Turbine exit, Exhaust Cone inlet;
- STATION 6: Exhaust Cone exit, Afterburner inlet;
- STATION 7: Afterburner exit, Nozzle inlet;
- STATION 8: Nozzle Throat;
- STATION 9: Exhaust (Engine exit);

5.4 Atmosphere model

The Concorde profile mission involves a variation in altitude between 0 and 55300 ft (16859 m), so the first step for evaluate the Engine cycle data is the definition of an **Atmosphere Model** in order to define the environmental conditions in term of flight level. The variables (temperature, pressure and density) are computed through the following model, taken from [20] and based on **International Standard Atmosphere (ISA)**. The model is implemented in MATLAB environment,

Standard Conditions	
Temperature T_{st} [K]	288.15
Pressure p_{st} [Pa]	101325
Density ρ_{st} [Kg/m^3]	1.225

Table 5.2: Initial condition of the atmosphere model, referred to standard conditions

developing a function called "ISA". The atmosphere model involves two sets of formulas to evaluate environment conditions between 0 and 11000 m and between 11000 and 20000 m.

- $\mathbf{0 < z < 11000m}$

$$T_0 = T_{st} - 0.0065z \tag{5.1}$$

$$p_0 = p_{st}\left(1 - 0.0065\frac{z}{T_{st}}\right)^{5.2561} \tag{5.2}$$

$$\rho_0 = \rho_{st}\left(1 - 0.0065\frac{z}{T_{st}}\right)^{4.2561} \tag{5.3}$$

The conditions at $z_{11} = 11000m$ are reported in table 5.3:

Conditions at $z_{11} = 11000m$	
Temperature T_{11} [K]	216.65
Pressure p_{11} [Pa]	22630
Density ρ_{11} [Kg/m^3]	0.3639

Table 5.3: Conditions at z=11000m

- $\mathbf{11000 < z < 20000m}$

$$T_0 = T_{11} \tag{5.4}$$

$$p_0 = p_{11}exp\left(\frac{-g\left(z - z_{11}\right)}{RT_{11}}\right) \tag{5.5}$$

$$\rho_0 = \rho_{11}exp\left(\frac{-g\left(z - z_{11}\right)}{RT_{11}}\right) \tag{5.6}$$

The conditions at $z_{11} = 20000m$ are reported in table 5.4:

Conditions at $z_{20} = 20000m$	
Temperature T_{20} [K]	216.65
Pressure p_{20} [Pa]	5471.65
Density ρ_{20} [Kg/m^3]	0.089

Table 5.4: Conditions at z=20000m

The atmosphere model allows to calculate the speed of sound "**a**", useful to compute flight speed:

$$a_0 = \sqrt{\gamma \bar{R} T_0}$$

where γ is the adiabatic expansion coefficient of the air (equal to 1.4) and $\bar{R}$ is the specific universal gas constant (with a value of 287.05 $\left[\frac{J}{Kg\ K}\right]$).In Fig. 5.4 5.5 and 5.6 are reported temperature, pressure and density along with the altitude.
Considering the **Variable Specific Heat (VHS)** as the gas model, the static

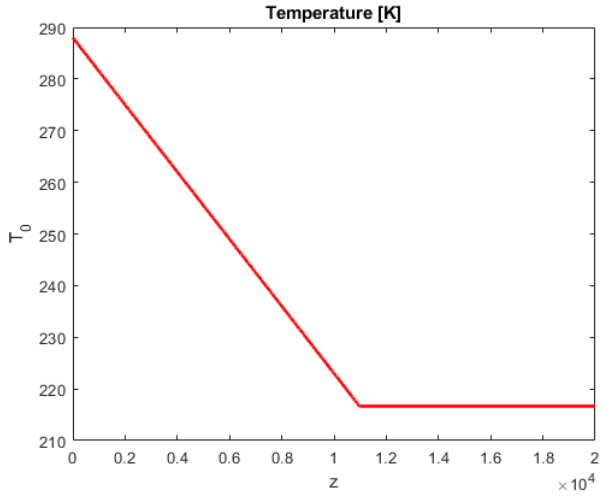

Figure 5.4: ISA Temperature

environment enthalpy (h_0) is evaluated using the "FAIR" routine, having the external static temperature T_0 evaluated from ISA model as input. Then, the total enthalpy of the airflow environment h_{t0} is calculated by

$$h_{t0} = h_0 + \frac{1}{2}(M_0 \cdot a_0)^2 \tag{5.7}$$

where M_0 is the flight Mach number and a_0 is the speed of sound calculated by "FAIR" too. Next, it is possible to determine the gas state of the environment using

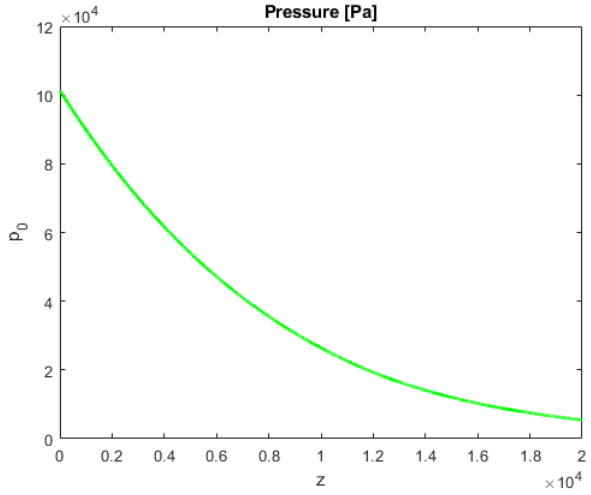

Figure 5.5: ISA pressure

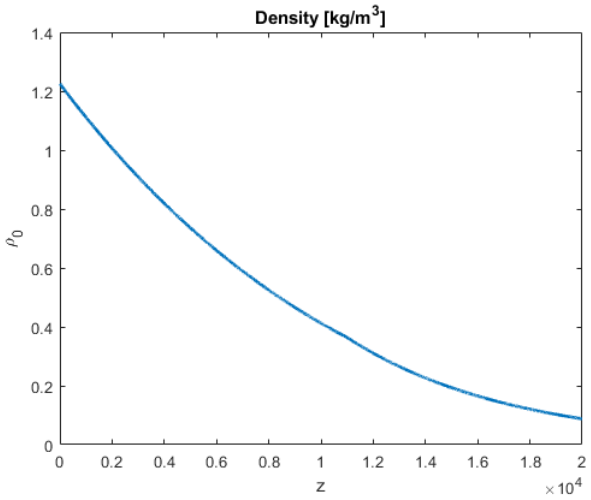

Figure 5.6: ISA density

h_{t0} as the input. Besides some negligible terms, the computation provides outputs such as P_rt0 and T_{t0}, then the ratios τ_r and π_r are evaluated as follows

$$\tau_r = \frac{h_{t0}}{h_0} \tag{5.8}$$

$$\pi_r = \frac{P_{rt0}}{P_{r0}} \tag{5.9}$$

The transformation of the environment is nearly isentropic, so the total pressure P_{t0} can be determined using the following equation

$$P_{t0} = \frac{P_{rt0}}{P_{r0}} \cdot P_0 \tag{5.10}$$

By using the **Modified Specific Heat (MSH)** model teh calculation of the gas state of the environment is straightforward. Given the average values of γ and C_p which are typically assumed to be 1.400 and 1004 $\frac{J}{kg \cdot K}$ respectively, the exposed equations can be rewritten as follows

$$T_{t0} = T_0 \left(1 + \frac{\gamma - 1}{2} M_0^2\right) \tag{5.11}$$

$$P_{t0} = P_0 \left(1 + \frac{\gamma - 1}{2} M_0^2\right)^{\frac{\gamma}{\gamma - 1}} \tag{5.12}$$

$$\tau_r = \frac{T_{t0}}{T_0} \tag{5.13}$$

$$\pi_r = \frac{P_{t0}}{P_0} \tag{5.14}$$

In summary, the two different gas models are implemented in the MATLAB environment in order to solve the gas state of the environment air stream. Firstly, knowing the flight altitude, given by the user as an independent variable, the ISA function is executed, then with the external temperature T_0 and the pressure P_0, the total enthalpy h_{t0} and pressure P_{t0} are evaluated using equations from Eq. 5.11 to Eq. 5.14 in the case of MSH as the gas model or from Eq. 5.7 to Eq. 5.10.

5.5 On design

To obtain a complete propulsion database, the first step is to define the mathematical model of all the engine components for on-design operation, and then expand the case studies by varying altitude, Mach number, and throttle in off-design conditions.

5.5.1 Inlet

The **Olympus Inlet** is a two-dimensional arrangement, both the external/internal and all external compression systems merit consideration for a Mach number of 2. Initially, Mach 2 might seem an unconventional speed; it is certainly too low to firmly advocate for partial internal compression. However, concerns were initially raised about the cowl drag associated with a conventional external compression geometry. The decision to choose for external compression was influenced by

the inherent stability of the associated shock pattern and the simplicity of the bleed arrangements and control systems. With the development of the external-compression design, significant progress was made in refining the external/internal compression system. The selection of external compression has been well-justified due to the ease of intake control during flight. For instance, there is no "unstart" mode, and there is a substantial margin between any operating condition and buzz. Achieving optimal performance across a wide range of flight conditions is facilitated by allowing bleed flow to naturally compensate for changes in engine air flow demand, without the need for intervention from any artificial control system. Additionally, favorable engine-face velocity distributions are achieved with a straightforward throat bleed geometry. These attributes permit the use of a low-gain control system that remains mostly dormant during the majority of supersonic flight. Inlets are installed in the engines, aiming to bring the free stream

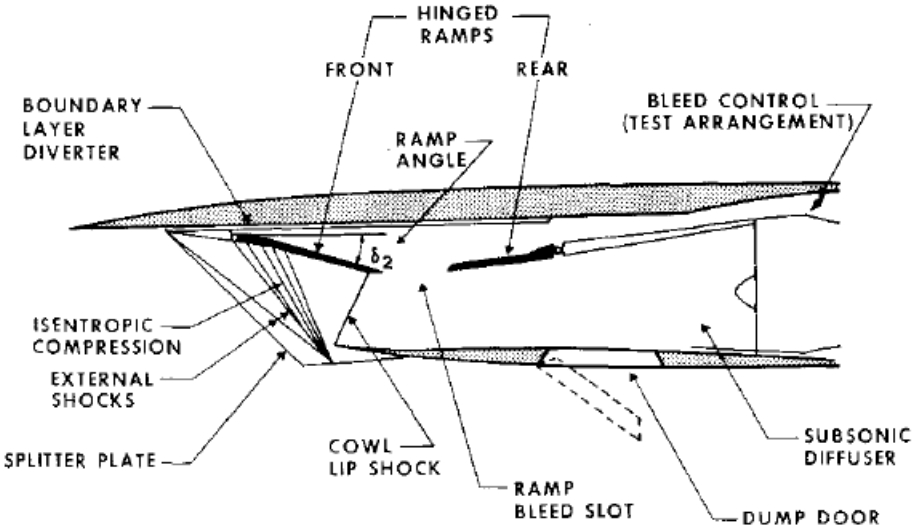

Figure 5.7: Architecture of Olympus-593 Inlet [21]

air into the compressor working in concert with compressors to give the overall pressure ratio of the engine cycle

$$\frac{P_{t3}}{P_0} = \frac{P_{t0}}{P_0}\frac{P_{t2}}{P_{t0}}\frac{P_{t3}}{P_{t2}} = \pi_r \pi_d \pi_c \tag{5.15}$$

π_r π_d is the inlet's pressure ratio and π_c represents the engine's **Overall Pressure Ratio (OPR)**.
For the analysis of the Inlet characteristics it is necessary a deep study of the flow entering the intake. Through this study it is possible to see that the total pressure

ratios obtained for various flight conditions are similar to those obtained through MIL-E-5008B. So, for simplicity, we're gonna use this formulation. The **Military specification MIL-E-5008B** has been adopted to estimate the inlet's adiabatic efficiency η_R and total pressure ratio π_d variation with the flight Mach number M_0 as follow

$$\pi_d = \pi_{d,max} \cdot \eta_R \tag{5.16}$$

$$\eta_R = \begin{cases} 1 & M \leq 1 \\ 1 - 0.075(M_0 - 1)^{1.35} & 1 < M_0 \leq 5 \\ \frac{800}{M_0^4 + 935} & M_0 > 5 \end{cases} \tag{5.17}$$

Thus, it is possible to compute the inlet's output state

$$\tau_d = \frac{h_{t2}}{h_{t0}} = 1 \Rightarrow h_{t2} = h_{t0} \tag{5.18}$$

$$\pi_d = \frac{P_{t2}}{P_{t1}} \Rightarrow P_{t2} = \pi_d \cdot P_{t1} \tag{5.19}$$

The term η_R is related to shock waves, $\pi_{d,max}$ to the inlet's wall friction, this second term is selected considering the **Engine Level of Technology** and engine's category shown

			Level of technology			
Component	Figure of merit	Type	1	2	3	4
Diffuser	$\pi_{d\,\max}$	A[a]	0.90	0.95	0.98	0.995
		B[b]	0.88	0.93	0.96	0.97
		C[c]	0.85	0.90	0.94	0.96

Figure 5.8: Table of level of technology for different aircraft configurations [16]

5.5.2 Compressor

In this chapter we will discuss the equations describing the operation of an **axial compressor**, typical of engines used in aviation and particularly for supersonic transport. We will be dealing with a very complex design because of the interactions with other components, particularly the turbines. As for the Olympus, we are dealing with 2 compressors, one low-pressure (the first one) and the other high-pressure. For the generation of propulsive database we need only the thermodynamic analysis of the components, using the gas model (for conventional fuels and alternative fuels) and the on-design and off-design analysis.

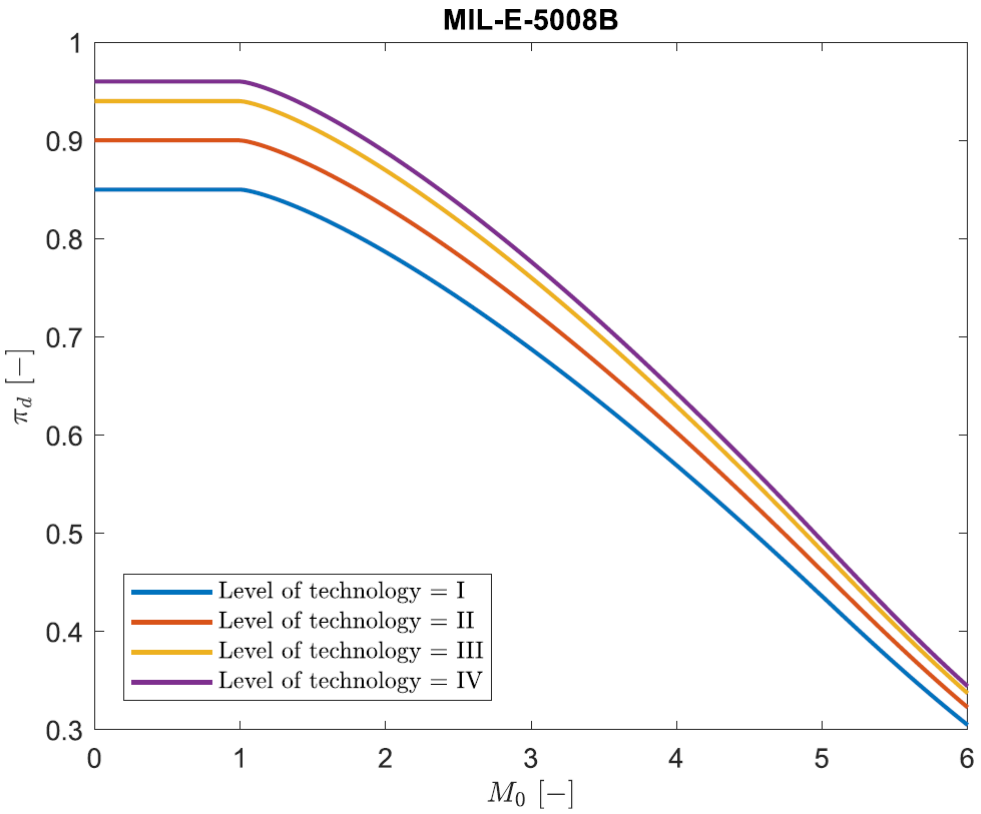

Figure 5.9: Inlet's pressure ratios vs M_0 for different technology levels [12]

5.5.2.1 Compressor mathematical model

Based on the Mattingly model [16], in this section we will elaborate the mathematical model of the compressor (applicable in both low and high pressure cases). We will start by considering the compressor adiabatic and go on to define the **Isentropic Efficiency** η_c as the fundamental parameter. The latter defined as

$$\eta_c \doteq \frac{ideal\ \ work\ \ of\ \ compression\ \ for\ \ given\ \ \pi_c}{actual\ \ work\ \ of\ \ compression\ \ for\ \ given\ \ \pi_c} \tag{5.20}$$

With the hypothesis of an adiabatic compressor we can consider Q_e, in the first law of thermodynamic, equal to zero. So the first law of thermodynamic is transformed as follow, to obtain the compression work as function of total enthalpy

$$W_i + Q_e = \Delta h_t \Rightarrow W_i = \Delta h_t \Rightarrow W_c = h_{t3} - h_{t2} \tag{5.21}$$

After these considerations we can define the ideal work of the compressor as an isentropic work, considering the ideal total enthalpy at the compressor exit

$$W_{c,ideal} = h_{t3i} - h_{t2} \tag{5.22}$$

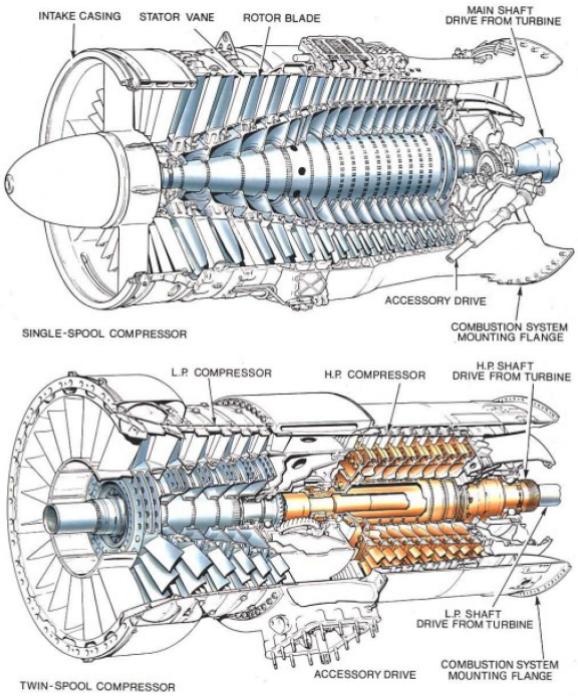

Figure 5.10: Typical axial compressors configurations [22]

With a combination of Eq. 5.21 and 5.22 it is possible to define the isentropic efficiency of the compressor as follow

$$\eta_c = \frac{h_{t3i} - h_{t2}}{h_{t3} - h_{t2}} \tag{5.23}$$

For the parametric analysis, that we will see later, it is necessary to know the total pressure ratio π_s for each component (in our case the LP and HP compressors). The product of these pressure ratios returns the **Overall Pressure Ratio (OPR or π_c)** of the engine, that represents the total pressure ratio of all compression stages. Based on this, we can write

$$\pi_c \doteq \frac{P_{t3}}{P_{t2}} \tag{5.24}$$

We can consider at first a simplified case, i.e. a model with C_p, C_v and γ constant with respect to temperature variation, and then adapt the considerations to our model (The Half-Ideal Gas model). In the former model it is possible to relate the total temperature to the total pressure in ideal condition by using isentropic

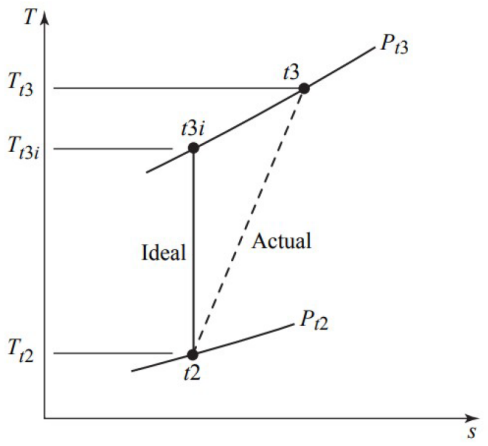

Figure 5.11: Actual and Ideal compression process [12]

equations

$$\tau_{ci} = \frac{T_{t3i}}{T_{t2}} = \left(\frac{P_{t3}}{P_{t2}}\right)^{\frac{\gamma-1}{\gamma}} = \pi_c^{\frac{\gamma-1}{\gamma}} \tag{5.25}$$

So the isentropic efficiency

$$\eta_c = \frac{\pi_c^{\frac{\gamma-1}{\gamma}} - 1}{\tau_c - 1} \tag{5.26}$$

Now we can consider an engine with more compression stages (two stages for the Olympus). The equations from 5.24 to 5.26 are still valid, but now we need to consider more pressure ratios through the equation

$$\pi_s \doteq \frac{Total\ \ Pressure\ \ Output}{Total\ \ Pressure\ \ Input} = \frac{P_{t,f}}{P_{t,i}} \tag{5.27}$$

And the OPR can be calculated as

$$OPR = \pi_c = \prod_{j=1}^{N} \pi_{s,j} \tag{5.28}$$

Where N is the total number of stages (two for the Olympus).
After this considerations we can see how to solve the compressor equations on-design. To do so it is necessary to know η_c or τ_c (that implies the knowledge of T_{t3}). Since T_{t3} is an output of the compressor analysis it is possible to use another parameter: the **Compressor Polytropic Efficiency** e_c. This parameter allows to find directly τ_c and is defined as

$$e_c = \frac{ideal\ \ work\ \ of\ \ compression\ \ for\ \ differential\ \ pressure\ \ change}{actual\ \ work\ \ of\ \ compression\ \ for\ \ differential\ \ pressure\ \ change} \tag{5.29}$$

So for the simplified model previously described (calorically perfect gas) it is possible to rewrite e_c equation (5.29) as

$$e_c \doteq \frac{dw_i}{dw} = \frac{dh_{ti}}{dh_t} = \frac{dT_{ti}}{dT_t} \tag{5.30}$$

For ideal compression, $T_{ti} = P_{ti}^{\frac{\gamma-1}{\gamma}}$, so we can write

$$\frac{dT_t}{T_t} = \frac{\gamma-1}{\gamma}\frac{dP_t}{P_t} \tag{5.31}$$

$$e_c = \frac{dTi}{dTt} = \frac{dT_{ti}/T_t}{dT_t/T_t} = \frac{\gamma-1}{\gamma}\frac{dP_t/P_t}{dT_t/T_t} \tag{5.32}$$

Now we can assume e_c as a constant and integrating between t2 and t3, we can finally calculate adiabatic efficiency as

$$\eta_c = \frac{\pi_c^{\frac{\gamma-1}{\gamma}} - 1}{\tau_c - 1} = \frac{\pi_c^{\frac{\gamma-1}{\gamma}} - 1}{\pi_c^{\frac{\gamma-1}{\gamma\, e_c}} - 1} \tag{5.33}$$

This equation is very accurate to predict the relationship between η_c and π_c (for e_c given). It is possible to observe that the adiabatic efficiency decreases with π_c increase.
In the case of Variable specific heat 5.29 can be rewritten as

$$e_c = \frac{dh_{ti}}{dh_t} = \frac{dh_{ti}/T_t}{dh_t/T_t} \tag{5.34}$$

Using Gibbs

$$\frac{dh_{ti}}{T_t} = R\frac{dP_t}{P_t} \tag{5.35}$$

$$\frac{dh_{ti}}{T_t} = R\frac{dP_t}{P_t} \tag{5.36}$$

Considering constant polytropic specific heat and integrating from t2 and t3

$$\phi_{t3} - \phi_{t2} = \int_{t2}^{t3} \frac{dh_{ti}}{T_t} = \frac{R}{e_c} ln\left(\frac{P_{t3}}{P_{t2}}\right) \tag{5.37}$$

Where ϕ_t is the entrophy function already defined in the Gas Model. So compressor pressure ratio π_c become

$$\pi_c = \frac{P_{t3}}{P_{t2}} = exp\left(e_c\frac{\phi_{t3} - \phi_{t2}}{R}\right) = \left(\frac{P_{rt3}}{P_{rt2}}\right)^{e_c} \tag{5.38}$$

Knowing P_{rt2}, π_c and e_c, the compressor state is given by

$$P_{rt3} = \pi_c^{1/e_c} \cdot P_{rt2} \tag{5.39}$$

$$P_{rt3i} = \pi_c \cdot P_{rt2} \tag{5.40}$$

Now it is possible to call "FAIR" twice by using P_{rt3} as the entrnce to calculate h_{t3}, P_{rt3i} and than η_c as

$$\eta_c = \frac{h_{t3i} - h_{t2}}{h_{t3} - h_{t2}} \tag{5.41}$$

Concluding, the compressor On-design, the corrected mass flow rate $\dot{m}_c$ is calculated by using the definition

$$\dot{m}_c = \frac{\dot{m}\sqrt{T_{t2}/T_{ref}}}{P_{t2}/P_{ref}} = \frac{\dot{m}\sqrt{\theta_2}}{\delta_2} \tag{5.42}$$

The corrected mass flow rate is used, in the next steps, for scaling map procedure usefull for off design calculation as described in Sec.5.7.

5.5.3 Combustion Chamber

The **Main Chamber** plays a critical role in increasing thermal energy through the exothermic combustion process, where fuel reacts with oxygen from the ingested air stream.
As described in Ref.[23], for the Olympus 593, the combustion chamber at first contained eight flame tubes like in Fig.5.12, but this configuration did not allow to achieve the necessary performance. Post-modification, there was but one large **annulus** like in Fig.5.13, and inside sixteen twin-armed vaporisers spraying upstream against the gas flow. Rather than simply providing a highly atomised spray, the vaporisers sat far enough into the combustion chamber to be raised in temperature sufficiently to vaporise the fuel, providing highly efficient, smoke-free combustion. The annulus was mounted between the compressors delivery casing and the first stage high pressure stator ring.

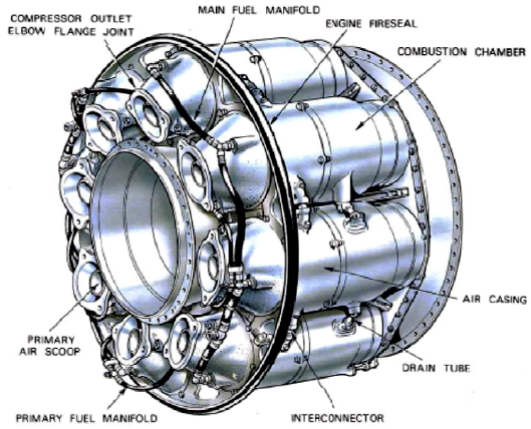

Figure 5.12: Example of tubo-annular combustor with 8 chambers [22]

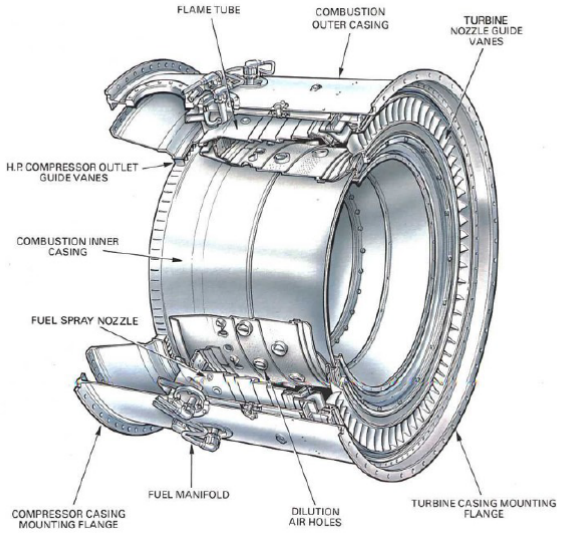

Figure 5.13: Example of annular combustor [22]

The latter, which has to withstand temperatures of up to 1148°C, is cooled by air trapped from the high pressure compressor at up to 560°C and allowed to escape into the gas stream through slots machined in the trailing edge of the blades, as explained in Sec.5.5.5.

5.5.3.1 Combustor mathematical model

By knowing P_{t3}, h_{t3}, or T_{t3}, typically representing the gas state results at the exit of the compressor stage, and considering the **LHV (Lower Heating Value)** of the fuel, it is possible to evaluate the combustion efficiency

$$\eta_b = \frac{\dot{m}_4 h_{t4} - \dot{m}_3 h_{t3}}{\dot{m}_f h_{PR}} \leq 1 \tag{5.43}$$

Where $\dot{m}_f$ is the fuel mass flow rate, $\dot{m}_3$ is the air mass flow upstream of the chamber and $\dot{m}_4$ is the sum of these rates. Typically, during on-design simulations, η_b is specified as a design parameter and is related to the engine level of technology. From the combustion efficiency equation, it is possible to find the **fuel/air ratio (f)**

$$f = \frac{\dot{m}_f}{\dot{m}_3} \tag{5.44}$$

This represents the fuel fraction in relation to air, foundamental for performance, emissions and the C_p as seen in Sec.4.2.2. By using Eq.5.43, Eq.5.44 is rewritten

$$f = \frac{h_{t4} - h_{t3}}{\eta_b h_{PR} - h_{t3}} \tag{5.45}$$

If the gas is modelled as calorically perfect

$$f = \frac{C_{pt} T_{t4} - C_{pt} T_{t3}}{\eta_b h_{PR} - C_{pt} T_{t3}} \tag{5.46}$$

where T_{t4} is the **Inlet Temperature of the Turbine (TIT)** and is typically specified by the designer.
For a more general Variable Specific Heat gas model, Eq.5.45 may not be used directly. In such cases, an iterative algorithm is employed to calculate the fuel/air ratio of the mixture until convergence is reached
Give η_b, P_{t3} and $\Delta T = T_{t4} - T_{t3}$, it is possible to scale a generic combustor map for off design simulation, as described in Sec.5.7. The pressure losses are considered constant, with the parameter π_b chosen from Fig.5.14 and defined as

$$\pi_b = \frac{P_{t4}}{P_{t3}} \tag{5.47}$$

Component	Figure of merit	Type[a]	Level of technology[b] 1	2	3	4
Diffuser	$\pi_{d\,max}$	A	0.90	0.95	0.98	0.995
		B	0.88	0.93	0.96	0.98
		C	0.85	0.90	0.94	0.96
Compressor	e_c		0.80	0.84	0.88	0.90
Fan	e_f		0.78	0.82	0.86	0.89
Burner	π_b		0.90	0.92	0.94	0.95
	η_b		0.88	0.94	0.99	0.999
Turbine	e_t	Uncooled	0.80	0.85	0.89	0.90
		Cooled		0.83	0.87	0.89
Afterburner	π_{AB}		0.90	0.92	0.94	0.95
	η_{AB}		0.85	0.91	0.96	0.99
Nozzle		D	0.95	0.97	0.98	0.995
	π_n	E	0.93	0.96	0.97	0.98
		F	0.90	0.93	0.95	0.97
Mechanical shaft	η_m	Shaft only	0.95	0.97	0.99	0.995
		With power takeoff	0.90	0.92	0.95	0.97
Maximum T_{t4}		(K)	1110	1390	1780	2000
		(R)	2000	2500	3200	3600
Maximum T_{t7}		(K)	1390	1670	2000	2220
		(R)	2500	3000	3600	4000

[a]A = subsonic aircraft with engines in nacelles D = fixed-area convergent nozzle
B = subsonic aircraft with engine(s) in airframe E = variable-area convergent nozzle
C = supersonic aircraft with engine(s) in airframe F = variable-area convergent-divergent nozzle
[b]Notes: Stealth may reduce π_{dmax}, π_{AB}, and π_n. The levels of technology can be thought of as representing the technical capability for 20-yr increments in time beginning in 1945. Thus level 3 of technology presents typical component design values for the time period 1985–2005.

Figure 5.14: Aircraft level of technology [16]

5.5.4 Turbine

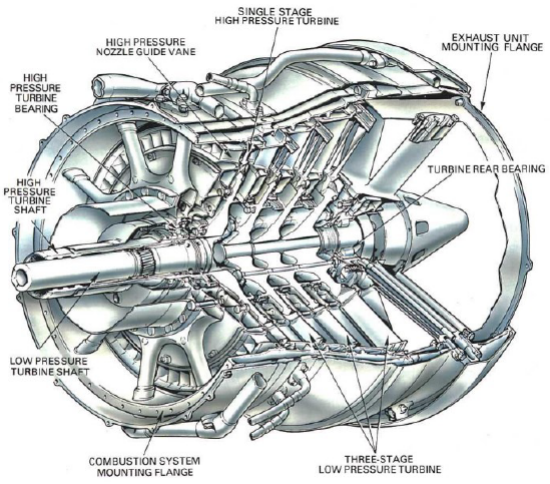

Figure 5.15: Turbine shaft arrangement [22]

The turbine's primary function is to provide power to drive the compressor and accessories by extracting energy from the hot gases released from the combustion

system. As hot gases expand to lower pressure and temperature, they drive the turbine at high rotational speeds.
The **TIT** is a foundamental parameter for the project of a good turbine and has always been dependent upon metallurgy, this because too high temperature can lead to to the malfunction and breakdown of the turbine itself. Only the very best of super-alloys can withstand the continuous battering from the 1000 °C plus, sonic velocity gas stream with the addition of a good cooling system. HP turbine blades of Olympus engine have eighteen cooling holes drilled top and bottom, this is a technique developed to provide cooling passages for guild vanes and blades alike, using air bled from HP compressor fifth stages as the cooling medium as discussed in Sec.5.5.5.

5.5.4.1 Turbine mathematical model

The first factor considered is the **Isentropic Efficiency** η_t

$$\eta_t = \frac{actual\ \ turbine\ \ work\ \ for\ \ a\ \ given\ \ \pi_t}{ideal\ \ turbine\ \ work\ \ for\ \ a\ \ given\ \ \pi_t} \tag{5.48}$$

Turbines are cooled, so the assumption of adiabatic flow is not entirely accurate. Howevere for preliminary design purposes, adiabatic flow represents a reasonable approximation, so

$$W_i + Q_e = \Delta h_t \Rightarrow -W_t = h_{t5} - h_{t4} \tag{5.49}$$

Where $Q_e = 0$

$$W_t = h_{t4} - h_{t5} \tag{5.50}$$

The adiabatic turbine efficiency can be expressed as

$$\eta_t = \frac{h_{t4} - h_{t5}}{h_{t4} - h_{t5i}} \tag{5.51}$$

For a calorically perfect gas

$$\eta_t = \frac{T_{t4} - T_{t5}}{T_{t4} - T_{t5i}} \tag{5.52}$$

The ratios τ_t and π_t are defined as

$$\tau_t = \frac{T_{t5}}{T_{t4}} \tag{5.53}$$

$$\pi_t = \frac{P_{t5}}{P_{t4}} \tag{5.54}$$

The **Polytropic Turbine Efficiency** e_t is defined similarly to the polytropic compressor efficiency

$$e_t = \frac{actual\ \ turbine\ \ work\ \ for\ \ a\ \ differential\ \ pressure\ \ change}{ideal\ \ turbine\ \ work\ \ for\ \ a\ \ differential\ \ pressure\ \ change} \tag{5.55}$$

Mathematically, the relationship between isentropic efficiency and polytropic efficiency is

$$\eta_t = \frac{1 - \tau_t}{1 - \tau_t^{1/e_t}} \tag{5.56}$$

The input parameter is e_t, which is related to the engine's level of technology. The pressure and enthalpy ratio can be evaluated based on the power balance of the shaft.

5.5.4.2 Shaft Power Balancing

The **Mechanical Efficiency of Power Shaft** is defined as

$$\eta_m = \frac{\dot{W}_c}{\dot{W}_t} \tag{5.57}$$

So, usign the definition of $\dot{W}$

$$\dot{W}_c = \dot{W}_t \cdot \eta_m \tag{5.58}$$

$$\dot{m}_3(h_{t3} - h_{t2}) = \dot{m}_4(h_{t4} - h_{t5}) \cdot \eta_m \tag{5.59}$$

In the balancing equation, the entalphy h_{t5} is calculated, instead, the h_{t4} is determined by the throttle ratio and fuel/air mixture ratio. The compressor power is computed based on the **OPR**, and the Mechanical Shaft Efficiency is generally set to reflect the engine's level of technology, accounting for power losses due to accessories driving, fuel pumps and oil leakages, which are often close to one.
To calculate the mass flow raates at stations 4 and 5, **Mass Conservation** is used

$$\sum \dot{m}_i = 0 \tag{5.60}$$

The results depend on engine architecture. With the hypotesis of a single-spool turbojet for simplicity the calculation is easier and it is possible to write

$$\dot{m}_4 = \dot{m}_3 + \dot{m}_b \tag{5.61}$$

$$\dot{m}_4 = \dot{m}_3 \cdot (1 + f) = \dot{m}_0 \cdot (1 + f) \tag{5.62}$$

Applying this semplification we can write

$$h_{t5} = h_{t4} - \frac{\eta_m}{(1 + f)}(h_{t3} - h_{t2}) \tag{5.63}$$

For calorically perfect gas

$$T_{t5} = T_{t4} - \frac{\eta_m \cdot C_{pt}}{C_p \cdot (1 + f)}(T_{t3} - T_{t2}) \tag{5.64}$$

In order to increase the accuracy of the model, the power extrction of accessories P_T at each present shaft with the related efficiency η_{mP} may be included, which will modify the balance

$$\dot{W}_c = \dot{W}_t \cdot \eta_m + P_T/\eta_{mP} \tag{5.65}$$

The shaft gives another important equation related to the number of speed congruence between compressor and turbines installed

$$N_c = N_t \tag{5.66}$$

5.5.5 Turbine Air Cooling System

Turbine Air Cooling Systems are an integral part of the engine, because they are used to maintain the temperatures within safe limits. In particular this system ensure that the turbine blades and vanes remain within the design limits and safe from the too high temperatures generated during combustion.

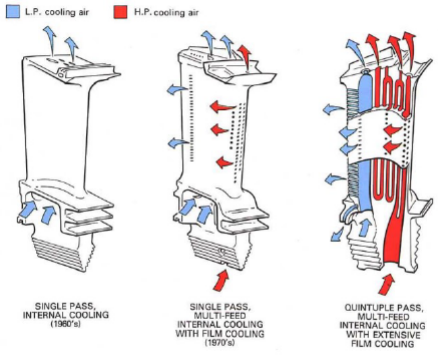

(a) Development of high-pressure turbine blade cooling

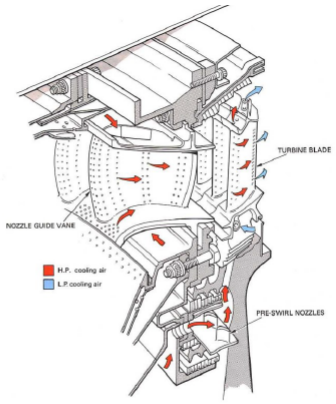

(b) Nozzle guide vane and turbine blade cooling arrangement

Figure 5.16: Turbine air cooling system [22]

A common method of cooling is the use of the **Compressor Bleed Air**, which consist in extracting a small quantity of air from the compressor and routing it through internal passages within the engine to cool various components.
The fraction of cooling air depends on the engine design, tipically indicated with ϵ, and in a range of 1% and 6% of total airflow. The exact amount is based on engine type, power settings and environmental conditions. A possible way to estimate the cooling fraction is given by Ref.[16]

$$\epsilon = \frac{1.8 \cdot T_{t4,max} - 2400}{16000} \qquad if \quad T_{t4,max} \geq 1332 \tag{5.67}$$

$$\epsilon = 0 \qquad if \quad T_{t4,max} < 1332 \tag{5.68}$$

The proposed model is derived from the power balance and mass flow rate conservation.
It is possible to define comprssor bleed as

$$\epsilon = \frac{\dot{m_{cool}}}{\dot{m}_c} \tag{5.69}$$

This fraction is subtracted fromthe compressor's outlet and added to the nozzle vanes of coolant mixer. By applying the mass flow conservation

$$\sum \dot{m} = 0 \Rightarrow \tag{5.70}$$

$$\dot{m_{4.1}} = \dot{m}_4 + \epsilon \dot{m}_3 \Rightarrow \tag{5.71}$$

$$\dot{m_{4.1}} = \dot{m}_3 \cdot [(1-\epsilon)(1+f) + \epsilon] \tag{5.72}$$

The stagnation enthalpy at the outlet of the coolant mixer is given by the power balance equation.

$$\dot{m_{4.1}} h_{t4.1} = \dot{m}_4 h_{t4} + \epsilon \dot{m}_3 h_{t3} \tag{5.73}$$

No pressure losses are teken into account in this model.

5.5.6 Exhaust Nozzle

The **Exhaust Nozzle** plays a crucial role in incresing the velocity of exhaust gases before dischrge. For simplicity purpose we don't consider the reheat.
In Concorde the exhaust assembly comprises of a **variable exhaust**, which consists of a primary nozzle and a secondary nozzle, the secondary being an arrangement of hinged "buckets" or "clamshells" whose position can be varied to control the exhaust in the most efficient way during all stages of flight.

Figure 5.17: Concorde exhaust nozzle [23]

There are two elements that form the variable exhaust system for the powerplant of Concorde. These are separated yet integrated to a common purpose. The two elements are firstly the Primary Nozzle and then the Secondary Nozzle. The primary nozzle sits at the end of the jet-pipe, and is a ring of petals, each one being operated by its own extending air-jacks. These operate all together to vary the diameter. The secondary nozzle assembly surrounds the primary nozzle, it has eyelid-like doors which are called "buckets". These buckets extend further after of the jet-pipe. Together they make up another form of convergent/divergent duct.

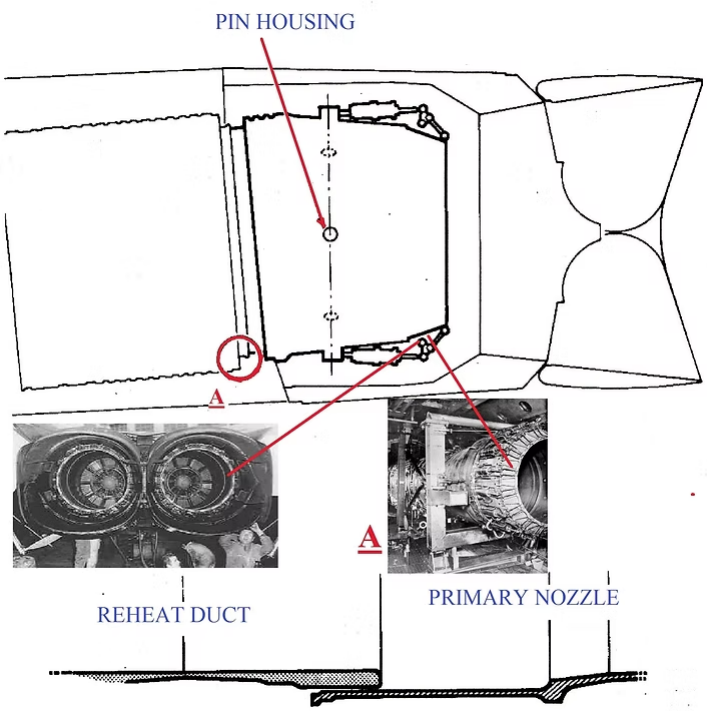

Figure 5.18: Concorde exhaust nozzle section [23]

For the mathematical model, at first, the unistalled thrust equation is considered 5.74

$$F = \dot{m}_9 V_9 + A_9 \cdot (P_9 - P_0) - \dot{m}_0 V0 \tag{5.74}$$

The maximum thrust is achieved when the exit pressure equals the external pressure ($P_9 = P_0$).
The configurations of nozzle for aeronautical applications are two: the simple convergent and the convergent-divergent (C-D).

5.5.6.1 Simple Convergent Nozzle mathematical model

The **Simple Convergent Nozzle** is employed when the pressure ratio between the upstream total pressure of the nozzle (P_{t9}) and the static external pressure (P_0) is less than 4.

$$\frac{P_{t9}}{P_0} < 4 \tag{5.75}$$

This configuration is ideal for subsonic applications due to its simplicity, as it lacks of moving parts. The first assumption of the nozzle model is that the flow is one-dimensional and adiabatic, meaning there is no thrust loss due to the non-axial exit of exhaust gases. In mathematical terms means that the **Angularity Coefficient** of the stream is equal to 1

$$C_A = \frac{1}{\dot{m}} \cdot \int cos\alpha_j \, d\dot{m} = 1 \tag{5.76}$$

In addition the pressure losses of the duct (π_n) are considered constant

$$\pi_n = \frac{P_{t9}}{P_{t8}} = cost \tag{5.77}$$

The third assumption concerns the preliminary sizing of the nozzle, specifically the exit Mach number M_9, which is set to satisfy the condition $P_9 = P_0$. With all these it is possible to calculate the exit nozzle area with the mass flow rate parameter.

$$A_9 = \frac{\dot{m}_9\sqrt{T_{t9}}}{P_{t9} \cdot MFP(M_9, T_{t9}, f_9)} \tag{5.78}$$

To evaluate nozzle performance, two cases must be distinguished: On-design analysis, where the M_9 is arbitrarily set to 1 to achive chocked flow and Off-design analysis, where the exit conditions depend on upstream flow and external pressure. In Off-design, the calculations are the same, but the critical pressure ratio is computed and compared to

$$\frac{P_{t9}}{P_0} \leq \left(\frac{P_t}{P}\right)_{M=1} \tag{5.79}$$

If condition 5.79 is met, the flow is unchoked, so $P_9 = P_0$ and the M_9 is obtained from compressible flow routine.
If the flow is choked

$$\frac{P_{t9}}{P_0} \geq \left(\frac{P_t}{P}\right)_{M=1} \tag{5.80}$$

in this case $M_9 = 1$ and the ratio

$$\frac{P_{t9}}{P_0} = \left(\frac{P_t}{P}\right)_{M=1} \tag{5.81}$$

With this it is possible to calculate static pressure, this time different from external pressure

$$P_9 = \frac{P_{t9}}{(P_t/P)_{M=1}} \tag{5.82}$$

Where $(P_t/P)_{M=1}$ can be calculated using compressible routine (RGCCOMPR) for the real gas model (VSH) or isentropic relations for modified gas model as follow

$$\left(\frac{P_t}{P}\right)_{M=1} = \left(1 + \frac{\gamma' - 1}{2} \cdot M^2\right)^{\frac{\gamma'}{\gamma'-1}} = \left(\frac{\gamma' - 1}{2}\right)^{\frac{\gamma'}{\gamma'-1}} \tag{5.83}$$

To prevent flow separation it is important to limit over-expansion in the nozzle. A simple estimate for the maximum allowable ratio of the pressure preceding the shock wave (P_s) to the external pressure is suggested in Ref.[16]

$$\frac{P_s}{P_0} \approx 0.37 \tag{5.84}$$

To conclude it is possible to evaluate the exit gas static temperature T_9 and speed V_9.
The corrected mass flow rate, instead, is defined as

$$\dot{m_{c8}} = \frac{\dot{m}_8 \sqrt{T_{t8}/T_{ref}}}{P_{t8}/P_{ref}} \tag{5.85}$$

Eq.5.85 is used only with On-design calculations. During Off-design the corrected mass flow rate is calculated using nozzle map.

5.5.6.2 Convergent-Divergent Nozzle mathematical model

A more complex configuration is the **Convergent-Divergent (C-D) Nozzle**, which is generally used in supersonic applications like Concorde, where the pressure ratio (Eq.5.75) is significantly higher. As already said for Concorde nozzle, this type of nozzle is characterized by moving parts, which can change the throat and exit areas affecting engine thrust.
Until now we considered all engine areas constant. In C-D nozzle throat area (A_8) and exit area (A_9) are an exeption. The exit area can be changed to automatically achieve $P_9 = P_0$. In some cases, the throat area will be manually adjusted from its reference value to avoid surging. These conditions appear especially when the throttle ratio is near the minimum and the flight Mach number and altitude are low as well. The first and second assumptions made for the simple convergent nozzle are still valid.
Firstly, M_9 is determined from $P_{t9}/P_{9=0}$ by usign RGCOMPR for the real gas

model or isentropic relations for the calorically perfect gas. By knowing M_9, it is possible to calculate the **Mass Flow Parameter** (MFP_9) and the ratio T_{t9}/T_9. For the area A_9 Eq.5.78 is used (in $P_9 = P_0$ condition). From T_{t9}/T_9 it is possible to find T_9 and subsequently V_9 using the FAIR routine.
For On-design analysis, it is beneficial to have the throat choked, particularly if M_8 is set to 1. If the Mach number (M_9) is greater than one (choke conditions), M_8 is set equal to M_9 (M8 = M9). The throat area is then computed using the Mass Flow Parameter definition

$$A_8 = \frac{\dot{m}_8\sqrt{T_{t8}}}{P_{t8} \cdot MFP(M_8, T_{t8}, f_8)} \tag{5.86}$$

The entire procedure remains the same for both On-design and Off-design calculations. The only difference is in the interpolation of the corrected mass flow rate ($\dot{m}_{c8}$).

5.6 Station Numbering and Formulas

As already said the engine is a Dual-spool Turbojet. A high-pressure spool, where a high-pressure compressor and a high-pressure turbine are mounted, as it is possible to see in Fig.5.19. The turbines are both cooled with bleed air fractions extracted from the high-pressure compressor outlet. The exhaust nozzle is a convergent-divergent with a variable exit area. Finally, a bleed air fraction is extracted from the high-pressure compressor.

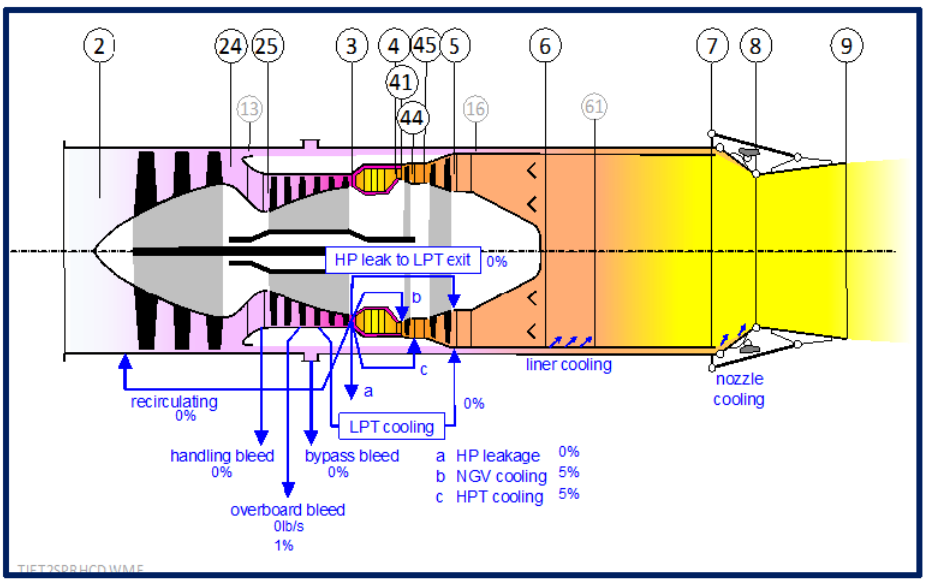

Figure 5.19: Schematic Engine with Reheat [19]

All the stations are already listed in Sec.5.3. Here is listed the Engine Parts with their subscript, usefull for the following formulas (Tab.5.5).

Subscript	**Component**	**Station**
b	Burner	$3 \rightarrow 4$
c	Compressor	$2 \rightarrow 3$
cH	HP Compressor	$2.5 \rightarrow 3$
cL	LP Compressor	$2 \rightarrow 2.5$
d	Inlet	$0 \rightarrow 2$
m1	Coolant Mixer 1	$4 \rightarrow 4.1$
m2	Coolant Mixer 2	$4.4 \rightarrow 4..5$
n	Exhaust Nozzle	$7 \rightarrow 9$
t	Turbine	$4 \rightarrow 5$
tH	HP Turbine	$4 \rightarrow 4.5$
tL	LP Turbine	$4.5 \rightarrow 5$

Table 5.5: Duration and Altitudes Mission Profile

For simplicity purpose the Afterburner is not considered in the model.
Now we can list the equations for pressure and enthalpy ratio, usefull for the Engine Model definition in On-design and Off-design calculations. The free stream is considered adiabatic and isentropic, so

$$\tau_r = \frac{h_{t0}}{h_0} \qquad \pi_r = \frac{P_{t0}}{P_0} = \frac{P_{rt0}}{P_{r0}} \tag{5.87}$$

For the inlet

$$\pi_d = \frac{P_{t2}}{P_{t0}} \qquad \tau_d = \frac{h_{t2}}{h_{t0}} = 1 \tag{5.88}$$

For the low-pressure compressor

$$\pi_{cL} = \frac{P_{t2.5}}{P_{t2}} \qquad \tau_{cL} = \frac{h_{t2.5}}{h_{t2}} \tag{5.89}$$

For the high-pressure compressor

$$\pi_{cH} = \frac{P_{t3}}{P_{t2.5}} \qquad \tau_{cH} = \frac{h_{t3}}{h_{t2.5}} \tag{5.90}$$

The OPR and related pressure and temperature ratios

$$\pi_c = \frac{P_{t3}}{P_{t2}} \qquad \tau_c = \frac{h_{t3}}{h_{t2}} \tag{5.91}$$

For the burner

$$\pi_b = \frac{P_{t4}}{P_{t3}} \qquad \tau_b = \frac{h_{t4}}{h_{t3}} \tag{5.92}$$

For the coolant mixer 1

$$\pi_{m1} = \frac{P_{t4.1}}{P_{t4}} = 1 \qquad \tau_{m1} = \frac{h_{t4.1}}{h_{t4}} \tag{5.93}$$

For the high-pressure turbine

$$\pi_{tH} = \frac{P_{t4.4}}{P_{t4}} \qquad \tau_{tH} = \frac{h_{t4.4}}{h_{t4}} \tag{5.94}$$

For the coolant mixer 2

$$\pi_{m2} = \frac{P_{t4.5}}{P_{t4.4}} = 1 \qquad \tau_{m2} = \frac{h_{t4.5}}{h_{t4.4}} \tag{5.95}$$

For the low-pressure turbine

$$\pi_{tL} = \frac{P_{t5}}{P_{t4.5}} \qquad \tau_{tL} = \frac{h_{t5}}{h_{t4.5}} \tag{5.96}$$

For the exhaust nozzle

$$\pi_n = \frac{P_{t9}}{P_{t8}} \qquad \tau_n = \frac{h_{t9}}{h_{t8}} \tag{5.97}$$

Conditions 5 and 8 are considered identical.
For the mass flow rate, it is convenient to introduce dimensionless parameters. A leakage of air mass flow from the HP compressor, fraction of the core flow

$$\beta = \frac{bleed\ \ flow}{core\ \ flow} = \frac{\dot{m}_{bl}}{\dot{m}_0} \tag{5.98}$$

Cooling fraction are given by

$$\epsilon_1 = \frac{\dot{m_{cool1}}}{\dot{m}_0} \tag{5.99}$$

$$\epsilon_2 = \frac{\dot{m_{cool2}}}{\dot{m}_0} \tag{5.100}$$

Other important parameters are related to the fuel/air ratios across the stations since these will be one of the primary inputs of the FAIR function. For the burner

$$f = \frac{burner\ \ fuel\ \ flow}{burner\ \ inlet\ \ air\ \ flow} = \frac{\dot{m}_b}{\dot{m}_3} \tag{5.101}$$

The fuel-to-air ratio at station 4.1 is given considering

$$f_{4.1} = \frac{f}{1 + f + \epsilon_1/(1 - \beta - \epsilon_1 - \epsilon_2)} \tag{5.102}$$

The fuel-to-air ratio at station 4.5 is given considering

$$f_{4.5} = \frac{f}{1 + f + (\epsilon_1 + \epsilon_2)/(1 - \beta - \epsilon_1 - \epsilon_2)} \tag{5.103}$$

The station numbers and formulas are assigned following Ref.[16].
Finally it is possible to relate the core mass flow rate to one of each station

$$\dot{m}_0 = \dot{m}_1 = \dot{m}_2 \tag{5.104}$$

$$\dot{m}_3 = \dot{m}_4 = \dot{m}_0(1 - \beta - \epsilon_1 - \epsilon_2) \tag{5.105}$$

$$\dot{m}_{4.1} = \dot{m}_{4.4} = \dot{m}_0[(1 - \beta - \epsilon_1 - \epsilon_2)(1 + f) + \epsilon_1] \tag{5.106}$$

$$\dot{m}_{4.5} = \dot{m}_5 = \dot{m}_0[(1 - \beta - \epsilon_1 - \epsilon_2)(1 + f) + \epsilon_1 + \epsilon_2] \tag{5.107}$$

5.7 Off Design

During **Off-design** operation, the engine sees its operating point change across the various component maps. In particular, there is a variation in the values on the compressor and turbine maps. The variation in the operating point, for example our Dual-spool Turbojet engine, may be due to the modification of various parameters: by changing the flight conditions (varying the flight Mach number or flight altitude); by changing the throttle, thus determining a total temperature at the turbine inlet (T_{4t}) that is different from the design temperature; or, even, by varying the geometry of the nozzle area.
There are two types of approaches for determining the various off-design operating points: **Serial Nested Loop (SNL)** and **Matrix Iteration (MI)**.
The **Serial Nested Loop** incorporates the equations that guarantee the matching of certain components and the constraints on them, thus ensuring that everything is solved in a nested sequence.
In **Matrix Iteration**, all the equations that characterize the engine are set and these are solved simultaneously. This approach involves a partial derivative methodology. The approach used for this work is the matrix iteration, specifically through the tangent method, or **Newton-Raphson** method.
The first step for the Off-design study is to rescale the component maps.

5.7.1 Component Maps Rescaling

Each component has its own **map**, through which it is possible to evaluate the behavior simply by selecting a point on it.
The maps provide the compression ratio values, or expansion in the case of the turbine, the correct flow rate, the adiabatic efficiency, and the corrected RPM for each point.
Since the component maps for the simulated engine were not available, in the following chapters it was necessary to adapt the generic maps. The component maps used in the code are those from GSP aircraft engine simulation program. There's a database of generic maps used and rescaled case by case.
Once the operating conditions data for the On-design have been obtained, the maps of each component that make up the engine are calculated by translating the points of the known maps (GSP maps). Based on the above, three basic equations are used to rescale the component maps. These allow the compression or expansion ratio π, the adiabatic efficiency η, and the correct flow rate $\dot{m}_c$, to be rescaled.
The rescaling equations mentioned above are shown here:

$$\pi = \frac{\pi - 1}{\pi^* - 1} \cdot (\pi_r - 1) + 1 \tag{5.108}$$

$$\eta = \frac{\eta}{\eta^*} \cdot \eta_r \tag{5.109}$$

$$\dot{m} = \frac{\dot{m}\sqrt{\theta}}{\delta} = \frac{\frac{\dot{m}\sqrt{\theta}}{\delta}}{\left(\frac{\dot{m}\sqrt{\theta}}{\delta}\right)^*} \cdot \left(\frac{\dot{m}\sqrt{\theta}}{\delta}\right)_r \tag{5.110}$$

Where

$$\theta = \frac{T}{T_{ref}} \tag{5.111}$$

$$\delta = \frac{P}{P_{ref}} \tag{5.112}$$

In addition, the subscript "r" denotes the reference conditions of the On-design calculation, the asterisk "*" denotes the reference point of the original map.

5.7.1.1 Compressor Map Scaling

A compressor map typically consists of a contour plot with lines of pressure ratio versus corrected mass flow over a range of corrected spool speeds. Additionally, it includes constant efficiency contour lines and corrected speed numbers, usually scaled to a reference point. Realistic compressor maps are essential for accurately

predicting engine performance, as emphasized in Ref.[24].
The scaled new map is generated from the scaling factors. For the compressor

$$\pi_c = \frac{\pi_c - 1}{\pi_c^* - 1} \cdot (\pi_{c,r} - 1) + 1 \tag{5.113}$$

$$\eta_c = \frac{\eta_c}{\eta_c^*} \cdot \eta_{c,r} \tag{5.114}$$

$$\dot{m}_c = \frac{\dot{m}_c\sqrt{\theta}}{\delta} = \frac{\frac{\dot{m}_c\sqrt{\theta}}{\delta}}{\left(\frac{\dot{m}_c\sqrt{\theta}}{\delta}\right)^*} \cdot \left(\frac{\dot{m}_c\sqrt{\theta}}{\delta}\right)_r \tag{5.115}$$

Below are the scaled maps for low and high pressure compressors, with indication of surge line and reference point.

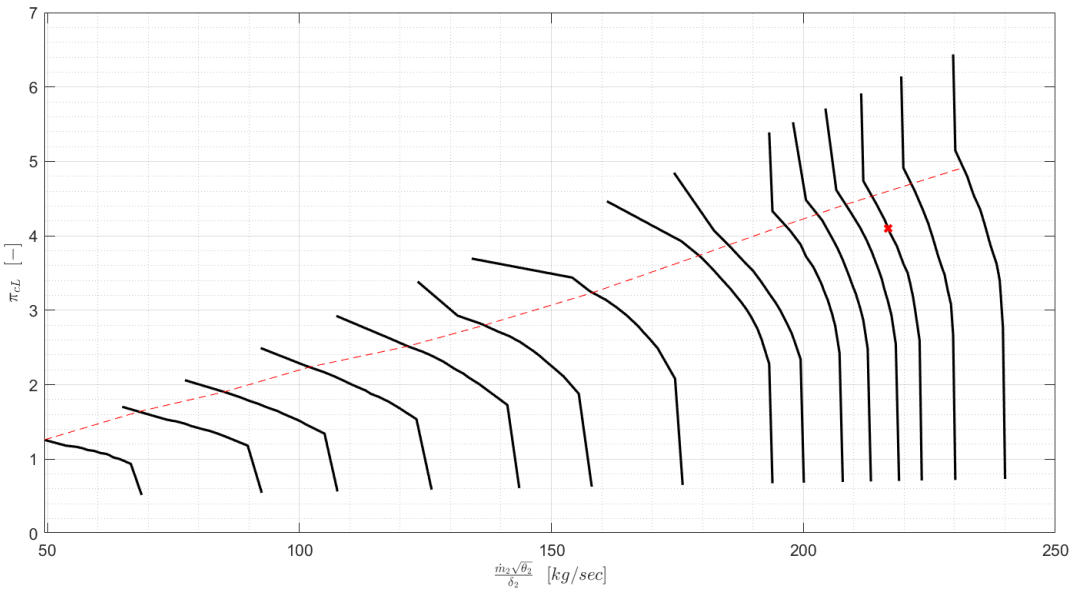

Figure 5.20: Scaled LP Compressor map

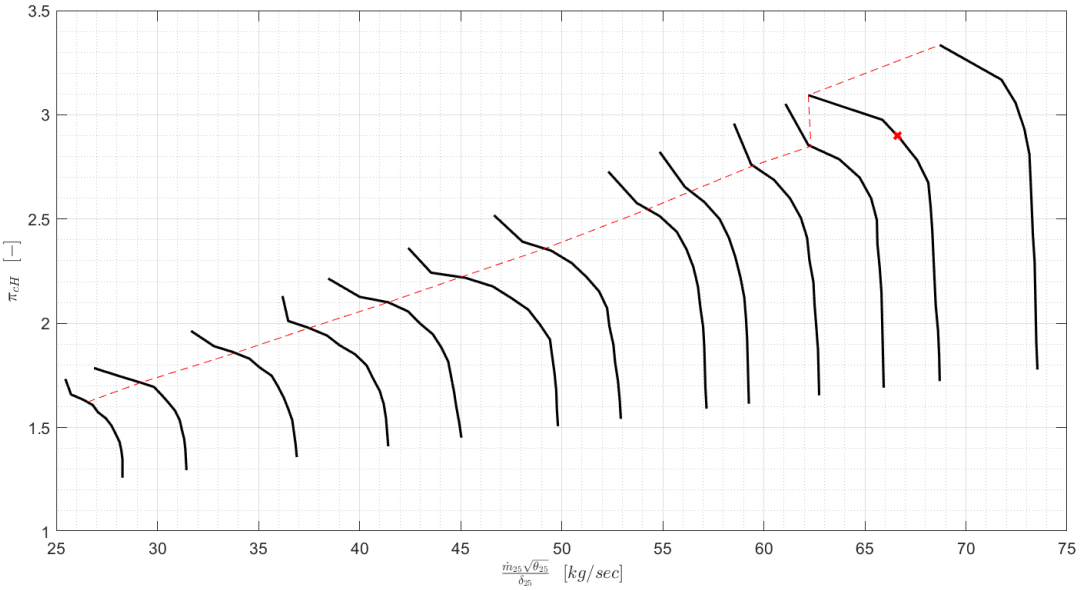

Figure 5.21: Scaled HP Compressor map

After this step we need to interpolate. The compressor map interpolation is articulated into three main steps having the compressor ratio π_c and the ratio of corrected number of speeds $\%N_c$ in input, the adiabatic efficiency η_c and corrected mass flow rate $\dot{m}_c$ as outputs. The first step of data interpolation is the increment number of speeds evaluation, obtained as follows

$$\Delta N_c = \frac{N_{c,guess} - N_c(i)}{N_c(i+1) - N_c(i)} \tag{5.116}$$

the index i is the result of

$$N_{c,guess} \geq N_c(i) \quad \wedge \quad N_{c,guess} < N_c(i+1) \tag{5.117}$$

So the routine will vary until the Eq.5.117 is satisfied.
The second step is to add the ΔN_c increment to the pressure ratio vector, corrected mass flow rate vector and the adiabatic efficiency vector.

$$\pi_{inter} = \pi(i) + \Delta N_c \cdot [\pi(i+1) - \pi(i)] \tag{5.118}$$

$$\eta_{inter} = \eta(i) + \Delta N_c \cdot [\eta(i+1) - \eta(i)] \tag{5.119}$$

$$\dot{m}_{c,inter} = \dot{m}_c(i) + \Delta N_c \cdot [\dot{m}_c(i+1) - \dot{m}_c(i)] \tag{5.120}$$

where π_{inter}, η_{inter} and $\dot{m}_{c,inter}$ are values given by the maps.
Then, for the third step, it is necessary to interpolate the pressure π_{guess}. In order

to do that, the pressure increment $\Delta\pi$ is calculated as

$$\Delta\pi = \frac{\pi_{guess} - \pi(j)}{\pi(j+1) - \pi(j)} \tag{5.121}$$

the index j is the result of

$$\pi_{guess} > \pi(j+1) \quad \wedge \quad \pi_{guess} \leq \pi(j) \tag{5.122}$$

Now it is possible to conclude the process by interpolating the given series

$$\dot{m}_c = \dot{m}_c(j) + \Delta\pi \cdot [\dot{m}_c(j+1) - \dot{m}_c(j)] \tag{5.123}$$

$$\eta = \eta(j) + \Delta\pi \cdot [\eta(j+1) - \eta(j)] \tag{5.124}$$

5.7.1.2 Combustor Map Scaling

The generic combustor map has the temperature variation across the chamber ($\Delta T = T_{t4} - T_{t3}$) on the x-axis and the curves represent efficiencies (η_b) for different P_{t3}/P_{ref} values on y-axis, as shown in scaled maps in Fig.5.22.
The scaling procedure is straightforward. Knowing the reference value of the combustion efficiency ($\eta_{b,OD}$) and the one from the map ($\eta_{b,map}$), the scaling factor is given as

$$f_{eta} = \frac{\eta_{b,OD}}{\eta_{b,map}} \tag{5.125}$$

The result in following figure

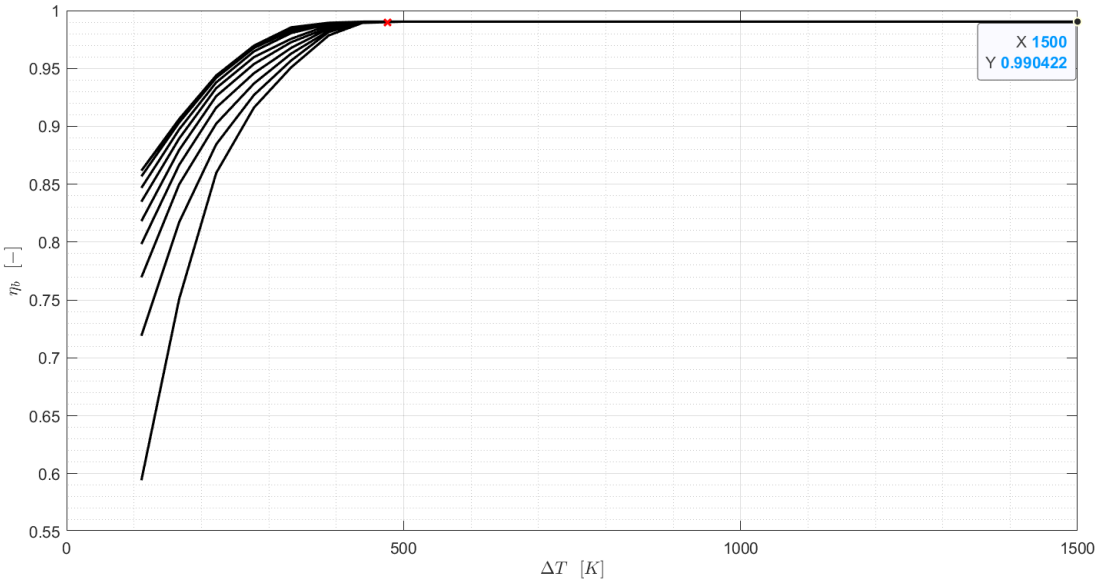

Figure 5.22: Scaled Combustor map

5.7.1.3 Turbine Map Scaling

Turbine map scaling is very similar to the compressor's one, with the necessary differences in the formulas

$$\pi_t = \frac{\pi_t - 1}{\pi_t^* - 1} \cdot (\pi_{t,r} - 1) + 1 \tag{5.126}$$

$$\eta_t = \frac{\eta_t}{\eta_t^*} \cdot \eta_{t,r} \tag{5.127}$$

$$\dot{m}_t = \frac{\dot{m}_t\sqrt{\theta}}{\delta} = \frac{\frac{\dot{m}_t\sqrt{\theta}}{\delta}}{\left(\frac{\dot{m}_t\sqrt{\theta}}{\delta}\right)^*} \cdot \left(\frac{\dot{m}_t\sqrt{\theta}}{\delta}\right)_r \tag{5.128}$$

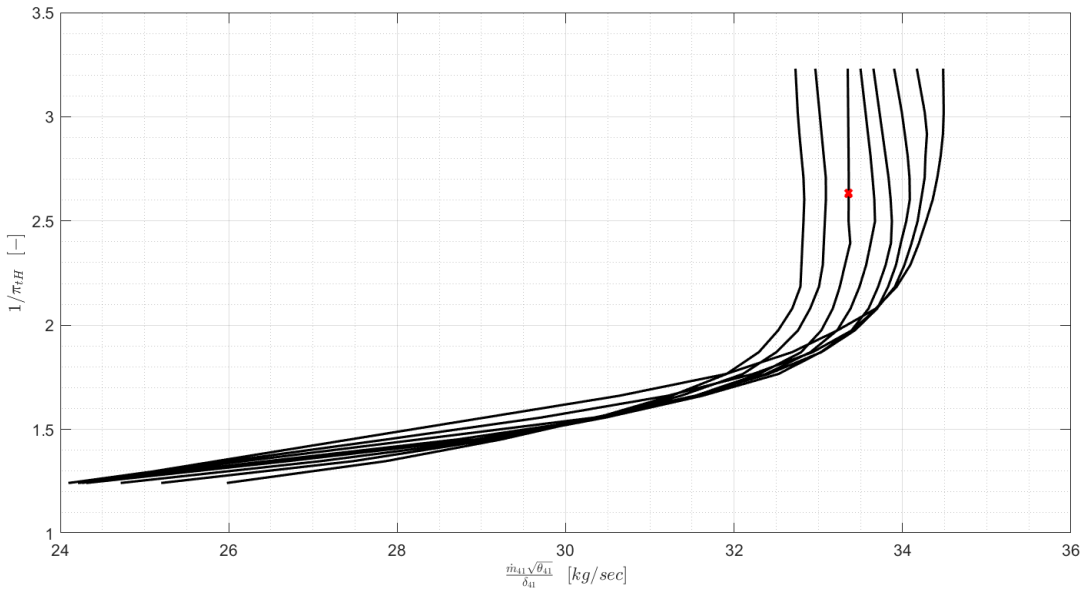

Figure 5.23: Scaled HP Turbine map

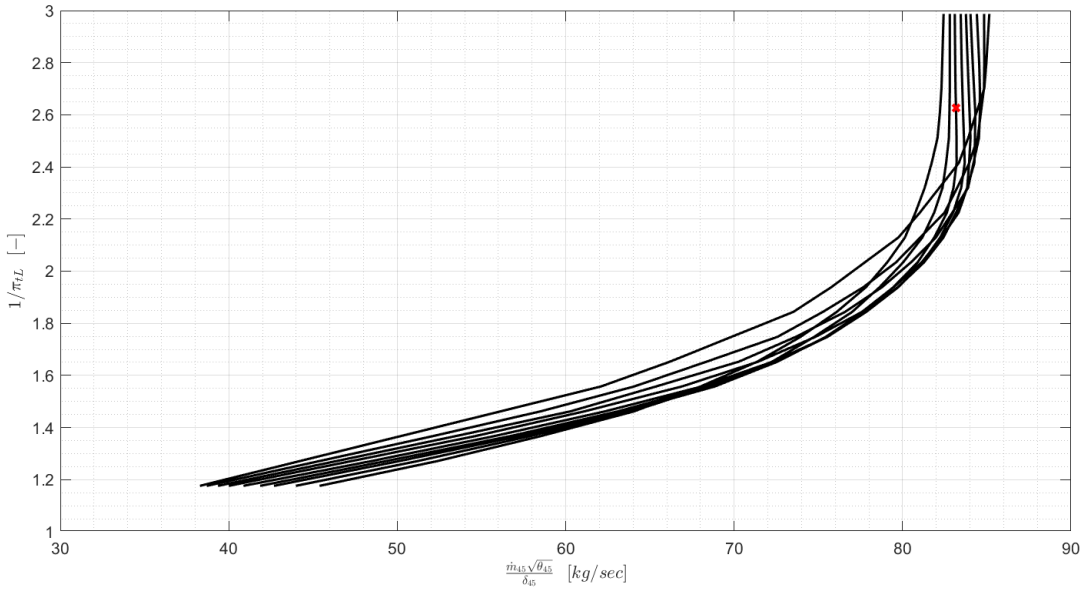

Figure 5.24: Scaled LP Turbine map

5.7.1.4 Nozzle Map Scaling

As mentioned earlier, the corrected mass flow rate is calculated through interpolation using the nozzle map, which is approximated to a conic function. To generate this curve, the critical pressure ratio of the nozzle and the critical mass flow rate are required as the primary inputs. Assuming that $\dot{m}_{c8,M=1}$ and $(P_t/P)_{M=1}$ are known, the corrected mass flow rate is given by

$$\frac{P_t}{P}(n) = 1.0 + \frac{n-1}{N-1} \cdot \left[\left(\frac{P_t}{P} \right)_{M=1} - 1 \right] \tag{5.129}$$

$$\dot{m}_{c8}(n) = \dot{m}_{c8,M=1} \cdot \sqrt{1 - \frac{\left[\frac{n-1}{N-1} \cdot \left[\left(\frac{P_t}{P} \right)_{M=1} - 1 \right] - \left[\left(\frac{P_t}{P} \right)_{M=1} - 1 \right] \right]^2}{\left[\left(\frac{P_t}{P} \right)_{M=1} - 1 \right]^2}} \tag{5.130}$$

Both valid forthe condition $\forall n = 1 \ldots (N-1)$
The last point is calculated as follows

$$\frac{P_t}{P}(N) = 10 \cdot \frac{P_t}{P}(N-1) \tag{5.131}$$

$$\dot{m}_{c8}(N) = \dot{m}_{c8}(N-1) \tag{5.132}$$

The nozzle map is essentially a combination of two series in which the index n change from 1 to a predefined value N.

Once the nozzle map is generated, it is possible to calculate the corrected mass flow rate at the desired pressure ratio using simple linear interpolation.

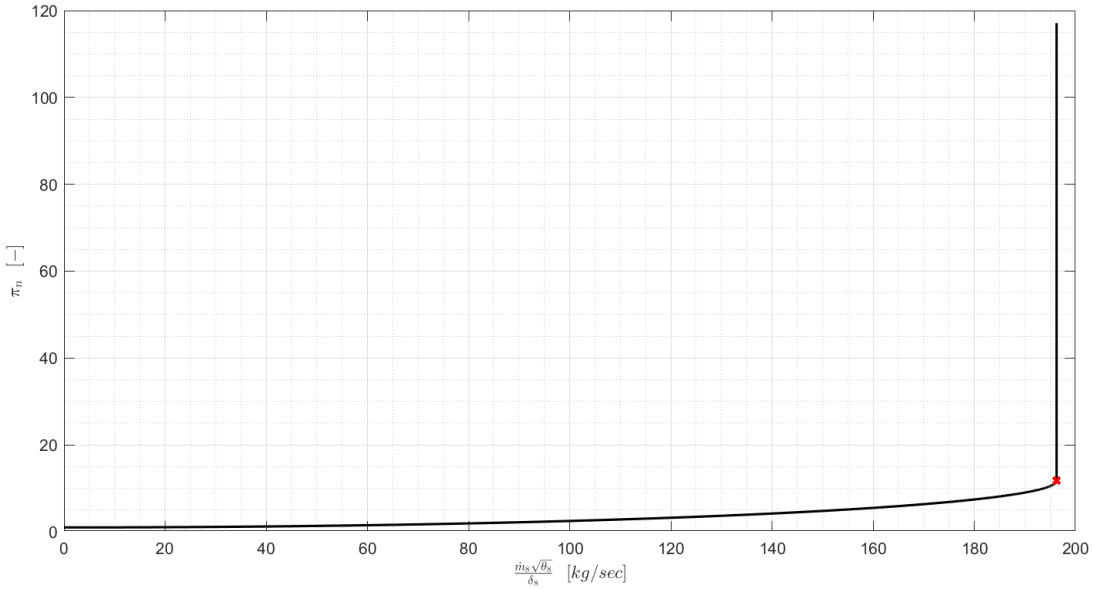

Figure 5.25: Scaled Nozzle map

5.7.2 Matrix Iteration Method Assumptions

The following assumptions are involved:

- The flow is on average steady;
- The flow is one-dimensional at the entry of each component and at each axial station;
- The working fluid is modeled as a "half-ideal gas" using variable specific heat;
- The inlet is modeled according to MIL-E-5008B;
- The low-pressure turbine drives the low-pressure compressor and provides mechanical power for accessories (P_{TOL});
- The high-pressure turbine drives the high-pressure compressor and provides mechanical power for accessories (P_{TOH});
- The turbines are cooled.

For off-design simulations, additional assumption are required:

- The exit area of the nozzle (A_9) is adjustable to maintain the exit pressure ratio of the exhaust equal to the external one ($P_9 = P_0$) or to selected ratio (P_9/P_0);
- The area of station 8 remains constant to its reference value;
- The map scaling procedure is adopted;
- The off-design non-linear system is solved using the Newton-Raphson algorithm;

5.7.3 Matrix Iteration Method Equations

The **Matrix Iteration Method** also known as **Components Matching Method** is used for off-design simulations, which employs the balancing equation of power and corrected mass flow rate. In the case of dual-spool turbojet the vector state chosen, as reported in Ref. [13]

$$\overline{X} = \{\beta_{cL}, \beta_{cH}, \beta_{tL}, \beta_{tH}, \%N_{cL,corr}, \%N_{cH,corr}\}^T \tag{5.133}$$

Then it's necessary to formulate the function vector. We need six balancing equations.
The first equation is the power balance of the low-pressure spool ($P_{tL} = P_{cL}$), considering the the LP turbine drives the LP compressor. The equation is write as follow

$$\dot{m}_{25}(h_{t25} - h_{t2}) + P_{TOL}/\eta_{mPL} = \dot{m}_{45}(h_{t45} - h_{t5})\eta_{mL} \tag{5.134}$$

The second equation involves power balance at the high-pressure spool, also accounting (like before) for mechanical power extraction

$$\dot{m}_{25}(h_{t3} - h_{t25}) + P_{TOH}/\eta_{mPH} = \dot{m}_{41}(h_{t41} - h_{t44})\eta_{mH} \tag{5.135}$$

In order to ensure continuity between the flow rate passing through the low-pressure compressor and that passing through the high-pressure compressor, it is necessary to have a correct balance between the correct flow rates at the inlet to the two components mentioned above.

$$\frac{\dot{m}_{25}\sqrt{T_{t25}}}{P_{t25}} = \frac{\dot{m}_{25}\sqrt{T_{t2}}}{p_{t2}} \frac{P_{t2}}{P_{t25}} \sqrt{\frac{T_{t25}}{T_{t2}}} \tag{5.136}$$

Then we need a congruence of the corrected mass flow rate between the high-pressure compressor and the high-pressure turbine

$$\dot{m}_{c41} = \dot{m}_{c25}[(1 - \beta - \epsilon_1 - \epsilon_2)(1 + f) + \epsilon_1] \frac{P_{t25}}{P_{t41}} \sqrt{\frac{T_{t41}}{T_{t25}}} \tag{5.137}$$

The fifth equation involves the conservation of the corrected mass flow rate between the high-pressure compressor and the low-pressure turbine

$$\dot{m}_{c45} = \dot{m}_{c2}[(1-\beta-\epsilon_1-\epsilon_2)(1+f)+\epsilon_1+\epsilon_2]\frac{P_{t2}}{P_{t45}}\sqrt{\frac{T_{t45}}{T_{t2}}} \tag{5.138}$$

The sixth equation pertains to nozzle-engine matching and addresses the congruence of the corrected mass flow between the mass flow rate at the inlet of the nozzle and the low-pressure compressor

$$\dot{m}_{c8} = \dot{m}_{c2}[(1-\beta-\epsilon_1-\epsilon_2)(1+f)+\epsilon_1+\epsilon_2]\frac{P_{t2}}{P_{t8}}\sqrt{\frac{T_{t8}}{T_{t2}}} \tag{5.139}$$

Each equation represents a function of the vector state, resulting in a nonlinear system.

$$\vec{F}(\vec{X}) = \begin{Bmatrix} P_{cL} + P_{TOL}/\eta_{mPL} - P_{tL}\eta_{mL} \\ P_{cH} + P_{TOH}/\eta_{mPH} - P_{tH}\eta_{mH} \\ \frac{\dot{m}_{25}\sqrt{T_{t25}}}{P_{t25}} - \frac{\dot{m}_{25}\sqrt{T_{t2}}}{p_{t2}}\frac{P_{t2}}{P_{t25}}\sqrt{\frac{T_{t25}}{T_{t2}}} \\ \dot{m}_{c41} - \dot{m}_{c25}[...]\frac{P_{t25}}{P_{t41}}\sqrt{\frac{T_{t41}}{T_{t25}}} \\ \dot{m}_{c45} - \dot{m}_{c2}[...]\frac{P_{t2}}{P_{t45}}\sqrt{\frac{T_{t45}}{T_{t2}}} \\ \dot{m}_{c8} - \dot{m}_{c2}[...]\frac{P_{t2}}{P_{t8}}\sqrt{\frac{T_{t8}}{T_{t2}}} \end{Bmatrix} = \vec{0} \tag{5.140}$$

Each equation represents a function of the vector state, resulting in a nonlinear system.

$$\vec{F}(\vec{X}) = \begin{Bmatrix} f_1(\{\pi_{cL}, \pi_{cH}, \pi_{tL}, \pi_{tH}, (\%N_{cL}), (\%N_{cH})\}^T) \\ f_2(\{\pi_{cL}, \pi_{cH}, \pi_{tL}, \pi_{tH}, (\%N_{cL}), (\%N_{cH})\}^T) \\ f_3(\{\pi_{cL}, \pi_{cH}, \pi_{tL}, \pi_{tH}, (\%N_{cL}), (\%N_{cH})\}^T) \\ f_4(\{\pi_{cL}, \pi_{cH}, \pi_{tL}, \pi_{tH}, (\%N_{cL}), (\%N_{cH})\}^T) \\ f_5(\{\pi_{cL}, \pi_{cH}, \pi_{tL}, \pi_{tH}, (\%N_{cL}), (\%N_{cH})\}^T) \\ f_6(\{\pi_{cL}, \pi_{cH}, \pi_{tL}, \pi_{tH}, (\%N_{cL}), (\%N_{cH})\}^T) \end{Bmatrix} \tag{5.141}$$

To solve this nonlinear system of equations, the **Newton-Raphson method** is implemented in conjunction with the component models presented before. During the Off-design phase, the state vector essentially represents the list of dependent variables of the engine. In order to obtain a solution, the independent variables must be specified. These include:

- The flight Mach Number M_0
- The external pressure P_0 and temperature T_0
- The burner exit temperature T_{t4}

Variable	Nomenclature	Designation Group
Flight Mach Number	M_0	Flight conditions
Flight Altitude	Alt	Flight conditions
Turbine Inlet Temperature	T_{t4}	Throttle Settings
Mechanical Power extraction	P_{TOL} and P_{TOH}	Engine System Interface
Air leakage	β	Engine System Interface

Table 5.6: Engine dipendent and indipendent varaibles

By using the International Standard Atmosphere (ISA) model, it is possible to relate the external pressure and temperature to the flight altitude. Furthermore, the mechanical power extraction and bleed air may vary during the flight. Hence P_{TOL}, P_{TOH}, and β are also indipendent.

The parameters listed in Tab.5.6 are provided by the user to simulate specific flight conditions and throttle settings. Deviations of the independent parameters from the reference point introduce imbalances in the equations. Consequently, the state vector must be computed to satisfy each parameter. In other words, the operating conditions of the compressor and turbine must be regulated to achieve a new engine operating condition (if applicable) while meeting also nozzle constraints. To compute this new state vector, the Newton-Raphson Method is employed.

5.7.4 Newton-Raphson Method

The numerical method that is used in the following pages to estimate the various operating points at which the propulsion system operates is called the tangent method, or **Newton-Raphson method**. This method allows, with a purely iterative approach, to arrive at a solution with high precision and in a very rapid way. It is also called the tangent method because it is based on the geometric idea of approximating the function, at each step, through the tangent line. Therefore, the Newton-Raphson method is used to calculate the zeros of a function. The primary objective is to find a solution for the state vector that satisfies all equilibrium equations.As per Refs. [13] and [25], the mathematical formulation of the Off-design engine regulation involves finding the state vector such that

$$\vec{F}(\vec{X}) = \vec{F}(\vec{X_0}) + \left[\frac{\partial F}{\partial X}\right] \cdot (\vec{X} - \vec{X_0}) = \vec{0} \tag{5.142}$$

In Eq.5.142, the function vector $\vec{F}$ is equal as formulated in Eq.5.140 and 5.143, $\vec{X_0}$, is the state vector in the previous iteration, of course if the first is considered,

it will be equal to the reference one, and $\vec{F_0}$ is the function vector computed in $\vec{X_0}$. The Jacobian Matrix is calculated as

$$\vec{F}(\vec{X}) = \begin{Bmatrix} \frac{\partial f1}{\partial \pi_{cL}} & \frac{\partial f1}{\partial \pi_{cH}} & \frac{\partial f1}{\partial \pi_{tL}} & \frac{\partial f1}{\partial \pi_{tH}} & \frac{\partial f1}{\partial (\%N_{cL})} & \frac{\partial f1}{\partial (\%N_{cH})} \\ \frac{\partial f2}{\partial \pi_{cL}} & \frac{\partial f2}{\partial \pi_{cH}} & \frac{\partial f2}{\partial \pi_{tL}} & \frac{\partial f2}{\partial \pi_{tH}} & \frac{\partial f2}{\partial (\%N_{cL})} & \frac{\partial f2}{\partial (\%N_{cH})} \\ \frac{\partial f3}{\partial \pi_{cL}} & \frac{\partial f3}{\partial \pi_{cH}} & \frac{\partial f3}{\partial \pi_{tL}} & \frac{\partial f3}{\partial \pi_{tH}} & \frac{\partial f3}{\partial (\%N_{cL})} & \frac{\partial f3}{\partial (\%N_{cH})} \\ \frac{\partial f4}{\partial \pi_{cL}} & \frac{\partial f4}{\partial \pi_{cH}} & \frac{\partial f4}{\partial \pi_{tL}} & \frac{\partial f4}{\partial \pi_{tH}} & \frac{\partial f4}{\partial (\%N_{cL})} & \frac{\partial f4}{\partial (\%N_{cH})} \\ \frac{\partial f5}{\partial \pi_{cL}} & \frac{\partial f5}{\partial \pi_{cH}} & \frac{\partial f5}{\partial \pi_{tL}} & \frac{\partial f5}{\partial \pi_{tH}} & \frac{\partial f5}{\partial (\%N_{cL})} & \frac{\partial f5}{\partial (\%N_{cH})} \\ \frac{\partial f6}{\partial \pi_{cL}} & \frac{\partial f6}{\partial \pi_{cH}} & \frac{\partial f6}{\partial \pi_{tL}} & \frac{\partial f6}{\partial \pi_{tH}} & \frac{\partial f6}{\partial (\%N_{cL})} & \frac{\partial f6}{\partial (\%N_{cH})} \end{Bmatrix} \tag{5.143}$$

In practice the Jacobian Matrix is computed numerically by considering a small increment ε, therefore it is possible to use the following expression for the computation

$$\frac{\partial F_{i,j}}{\partial X_j} = \frac{F_{i,j} - F_{0,i,j}}{X_j - X_{0,j}} = \frac{F_{i,j} - F_{0,i,j}}{\varepsilon 0, j} \tag{5.144}$$

As for Ref.[13], the Eq.5.142 can be formulated as a linear system of equations

$$[A]\vec{X} = \vec{b} \tag{5.145}$$

In Eq.5.145 the matrix $[A]$ is equivalent to the Jacobian Matrix and $\vec{b}$ is given by

$$\vec{b}\left[\frac{\partial F}{\partial X}\right] \cdot \vec{X_0} - \vec{F_0} \tag{5.146}$$

The solution of the system is obtained by multiplying the inverse of the Jacobian with the known vector. This operation is carried out using the lower-upper (LU) decomposition, employing the MATLAB function "lu". The state vector is iterative and requires a convergence criterion, which is determined by a residual defined as

$$res = \frac{||\vec{R}|| - ||\vec{R_0}||}{||\vec{R_0}||} \tag{5.147}$$

Where

$$\vec{R} = \left[\frac{\pi_{cL}}{\pi_{cL,r}}, \frac{\pi_{cH}}{\pi_{cH,r}}, \frac{\pi_{tL}}{\pi_{tL,r}}, \frac{\pi_{tH}}{\pi_{tH,r}}, \frac{(\%N_{cL})}{(\%N^r_{cL})}, \frac{(\%N_{cH})}{(\%N^r_{cH})}\right]^T \tag{5.148}$$

$$\vec{R_0} = \left[\frac{\pi_{cL,0}}{\pi_{cL,r}}, \frac{\pi_{cH,0}}{\pi_{cH,r}}, \frac{\pi_{tL,0}}{\pi_{tL,r}}, \frac{\pi_{tH,0}}{\pi_{tH,r}}, \frac{(\%N_{cL,0})}{(\%N^r_{cL})}, \frac{(\%N_{cH,0})}{(\%N^r_{cH})}\right]^T \tag{5.149}$$

In Eq. 5.148 and 5.149, all parameters with "r" subscript refer to reference conditions (On-design). The entire procedure is implemented using the MATLAB environment, as previously described. The chosen values for the residual and increment are

$$\varepsilon = 10^{-12} \tag{5.150}$$

$$res = 10^{-13} \tag{5.151}$$

It is important to note that choosing a very small increment and residual is essential to achieve an accurate solution. However, reducing the increment below 10^{-14} leads to numerical instabilities due to the machine precision of the MATLAB environment. Additionally, an excessively small tolerance increases simulation time. Therefore, the specified parameters offer a balance between accuracy and computational efficiency.

5.7.5 Engine Components Off-design

5.7.5.1 Compressor Off-design

The compressor must be regulated in order to satisfy all new throttle settings and flight conditions. Bleed air and power extraction could change as well.
As already discussed the compressor pressure ratio π_c and the shaft number of speed are known, as the new variables of the Newton-Raphson method iteration. From the map it is possible, with π_c and corrected number of speed as input, to abtain the corrected mass flow rate $\dot{m}_c$ and the adiabatic efficiency η_c. Then we take P_{t2}, P_{rt2} and T_{t2} from inlet model and taking into account the case of Variable Specific Heat gas model. The FAIR routine is needed to resolve the equations. By knowing P_{t2} and P_{rt2} it is possible to compute the compressor output reduced pressure in the ideal case. Then, by calling FAIR routine and by giving the new value as input, the total ideal output compressor enthalpy is computed. Since η_c is obtained from map interpolation, it is possible to calculate the output enthalpy knowing the ideal enthalpy h_{3i} from FAIR

$$h_{t3} = h_{t2} + \frac{1}{\eta_c}(h_{t3i} - h_{t2}) \tag{5.152}$$

It is possible to solve the t3 state completely by recalling the FAIR and giving h_{t3} as input.
After all the necessary calculations it is possible to obtain the complete compressor maps for low and high pressure as shown in Fig.5.26 and 5.27

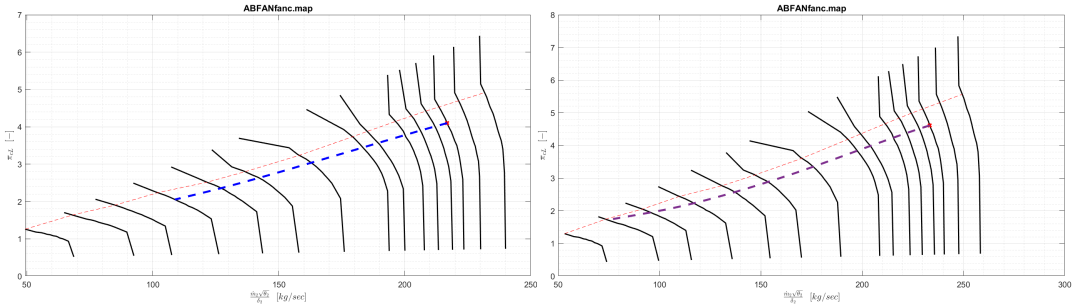

Figure 5.26: LP Compressor Off-design maps for Cruise and Take-off

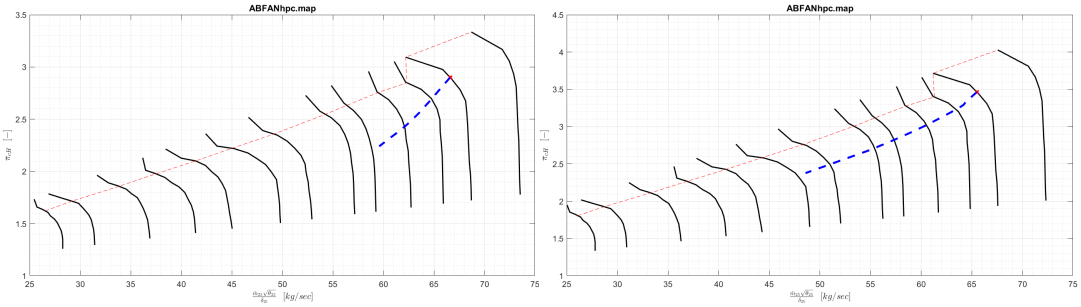

Figure 5.27: HP Compressor Off-design maps for Cruise and Take-off

5.7.5.2 Combustion Chamber Off-design

Off-design analysis of the chamber is similar to the On-design one. The primary difference leads to combustor map interpolation, which adjusts the efficiency value. Subsequent calculations for the fuel-air are replied and the chamber exit pressure is computed using Eq.5.47. In summary, given the temperature variation ΔT_t and the relatice pressure P_{t3}/P_{ref}, it is possible to evaluate the combustor efficiency η_b by linear interpolation of the scaled map. Following there are the combustion chamber maps for cruise and take-off.

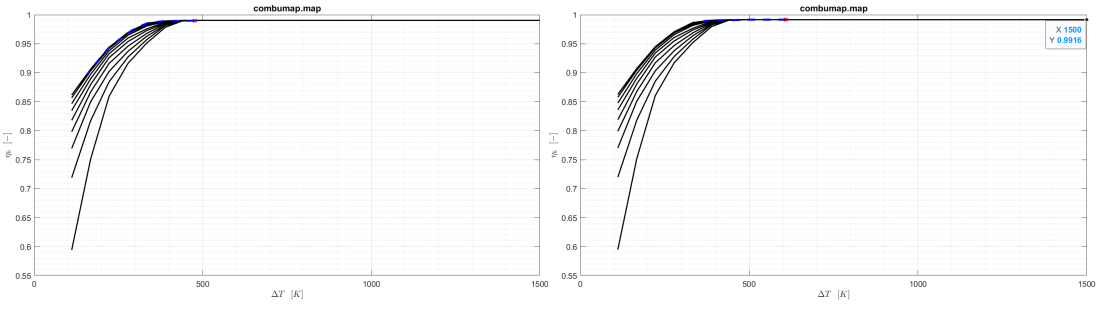

Figure 5.28: Combustion Chamber Off-design maps for Cruise and Take-off

5.7.5.3 Turbine Off-design

The turbine during the regulation, has a constraint related to the congruence of the shaft number of speed ($N_t = N_c$). This relation involves the turbine map interpolation because is one of the two inputs of the map. Particularly, considering the shaft in which a compressor and a turbine are installed, it is possible to write

$$N_t = N_c$$

$$\frac{N_t}{\sqrt{T_{t4}}} = \frac{N_c}{\sqrt{T_{t2}}} \cdot \sqrt{\frac{T_{t2}}{T_{t4}}}$$

$$N_{c,t} = N_{c,c} \cdot \sqrt{\frac{T_{t2}}{T_{t4}}}$$

Generally in the compressor's and turbine's maps, the corrected number of speed is scaled about the reference point, so defining N_c the corrected number of speed, it is possible to derive

$$\frac{N_t}{\sqrt{T_{t4}}} = \frac{N_c}{\sqrt{T_{t2}}} \cdot \sqrt{\frac{T_{t2}}{T_{t4}}}$$

$$\frac{N_{c,t}}{N^r_{c,t}} = \frac{N_{c,c}}{N^r_{c,c}} \cdot \sqrt{\frac{T_{t2}}{T_{t4}}} \frac{N^r_{c,c}}{N^r_{c,t}}$$

$$(N_{c,t})_{\%} = (N_{c,c})_{\%} \cdot \sqrt{\frac{T_{t2}}{T_{t4}}} \frac{N^r_{c,c}}{N^r_{c,t}} \tag{5.153}$$

By knowing efficiency and pressure ratio, it is possible to solve the gas state output of the turbine, considering the general case of the Variable Specific Heat Model

$$P_{rt5,i} = \pi_t \cdot P_{rt4} \tag{5.154}$$

Calling the "FAIR" routine the gas state in ideal condition at turbine exit t5 is solved, so it is possible to use the definition of adiabatic efficiency, to calculate the real enthalpy at turbine exit

$$h_{t5} = h_{t4} - \eta_t \cdot (h_{t4} - h_{t5i}) \tag{5.155}$$

The output pressure is calculated using π_t

$$P_{t5} = \pi_t \cdot P_{t4} \tag{5.156}$$

Concluding the calculations, the power and work both in ideal and real conditions are evaluated

$$W_{t,i} = h_{t4} - h_{t5i} \tag{5.157}$$

$$P_{t,i} = \dot{m}_4 \cdot (h_{t4} - h_{t5i}) \tag{5.158}$$

$$W_t = h_{t4} - h_{t5} \tag{5.159}$$

$$P_t = \dot{m}_4 \cdot (h_{t4} - h_{t5}) \tag{5.160}$$

The complete turbine maps for low and high pressure as shown in Fig.5.29 and 5.30

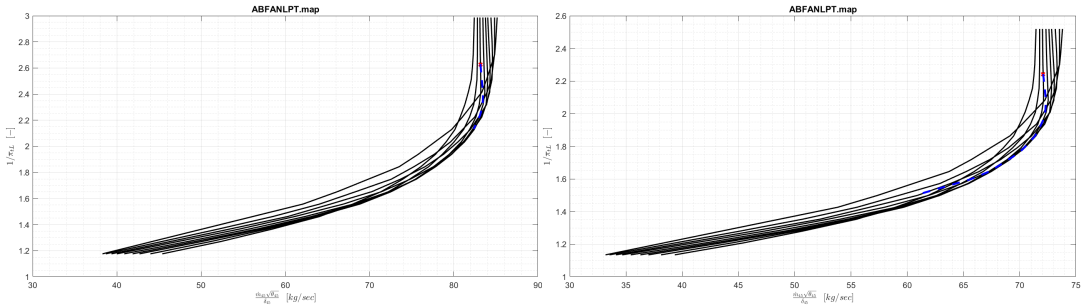

Figure 5.29: LP Turbine Off-design maps for Cruise and Take-off

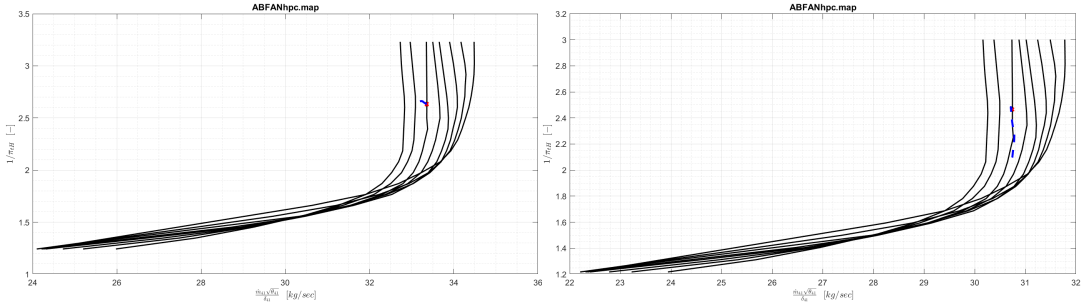

Figure 5.30: HP Turbine Off-design maps for Cruise and Take-off

5.7.5.4 Nozzle Off-design

As already said in Sec.5.7.1.4, the corrected mass flow rate is calculated through interpolation using the nozzle map, which is approximated to a conic function. To generate this curve, the critical pressure ratio of the nozzle and the critical mass flow rate are required as the primary inputs.
Once the nozzle map is generated, it is possible to calculate the corrected mass flow rate at the desired pressure ratio using simple linear interpolation.

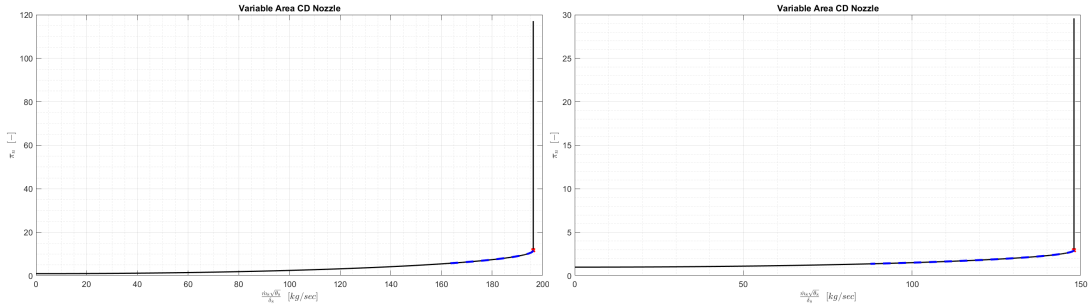

Figure 5.31: Nozzle Off-design maps for Cruise and Take-off

Chapter 6

Emission evaluation

Pollutant Emissions from combustion processes have become of great public concern due to their impact on health and the environment.
The material presented in this chapter is divided into the following main sections:

- A general overview of emissions we need to analyze, NO_x, UHC and CO
- The mechanism of formation of these pollutant emissions
- The prediction techniques to estimate emissions, including the Lefebrve and Munthy semi-empirical relations used for calculations
- The mathematical calculations using the semi-empirical relations

6.1 General Overview on Pollutant emissions

The exhaust from an aircraft gas turbine is composed of carbon monoxide (CO), carbon dioxide (CO_2), water vapor (H_2O), unburned hydrocarbon (UHC), particulate matter (Mostly carbon) and Oxides of Nitrogen (NO_x). CO_2 and H_2O have not alwaysbeen regarded as pollutant because they are the natural consequence of complete combustion of hydrocarbon fuel. However, they both contribute to global warming and can only be reduced by burning less fuel. The principal pollutants are listed in Tab.6.1.

CO reduces the capacity of the blood to absorb oxygen and, in high concentrations, can cause asphyxiation and even death. UHC are not only toxic, but they also combine with NO_x to form photochemical smog. **Particulate Matter** (generally called **soot** or **smoke**) creates problems of exhaust visibility and soiling of the atmosphere. It is not normally considered to be toxic at the levels emitted, but studies by Seaton et al. [27] indicate a strong association between asthma and other respiratory diseases and atmospheric pollution by concentrations of small

Pollutant	Effect
Carbon Monoxide (CO)	Toxic
Unburned Hydrocarbons (UHC)	Toxic
Particulate Matter (C)	Visible
Oxides of Nitrogen (NO_x)	Toxic, precursor of chemical smog, depletion of ozone in stratosphere
Oxides of Sulfur (SO_x)	Toxic, corrosive

Table 6.1: Principal Pollutants Emitted by Gas Turbines [26]

particles in the microgram range. NO_x not only contribute to the production of photchemical smog at groud level, but also cause damage to plant life and add to the problem of acid rain.

6.1.1 Aircraft Engine regulation

The **ICAO (International Civil Aviation Organization)** has promulgated regulations for civil subsonic and supersonic turbojet/turbofan engines with rated thrust levels above 26.7 kN for defined **LTO cycle** (all the aircraft operations around the airport). ICAO standards are represented in Tab.6.2, where π_{00} is the engine pressure ratio at take-off. The quantity in the table are expressed in

Emissions (g/kN)	Subsonic Turbojet/-Turbofan Engines	Supersonic Turbojet/Turbofan Engines
HC	19.6	$140 \cdot (0.92)^{\pi_{00}}$
CO	118.0	$4550 \cdot (\pi_{00})^{-1.03}$
NO_x	$32 + 1.6\pi_{00}$	$36 + 2.4\pi_{00}$

Table 6.2: ICAO Gaseous Emissions Standards. Souce: www.icao.org

terms of a parameter that consists of the total mass in grams of any given gaseous pollutant emitted during LTO cycle per kN of thrust.
Current ICAO regulations are restricted to operations at low altitudes in and around airports, but growing concerns reguarding ozone depletion at high altitudes could lead to them being extended to other flight regimes, such as altitude cruise, where the bulk of NO_x emissions occur.
The emissions in Tab.6.2 for supersonic turbojet engines were set to ensure that the Olympus engine would be in compliance. For future supersonic transport (SST) engines, NASA has proposed a cruise NO_x EI of 5g/kg fuel [28]. Due to the large

pressure rise across the sonic wave generated by SST Aircraft, combustor inlet temperatures will be exceptionally high and the application of current combustor technology would yield EI NO_x levels around 45, so the NASA's standard is a little be complicated to reach today. Meaby in the future would be possible to create an ultralow NO_x supersonic combustor design.

6.2 Mechanism of Pollutant formation

The concentration levels of pollutants in gas turbine exhausts can be related directly to the temperature, time, and concentration histories of the combustion process. These vary from one combustor to another and, for any given combustor, with changes in operating conditions. The nature of pollutant formation is such that the concentrations of CO and UHC are highest at lowpower conditions and diminish with an increase in power. By contrast, NO_x and *smoke* are fairly insignificant at low-power settings and attain maximum values at the highest power condition.

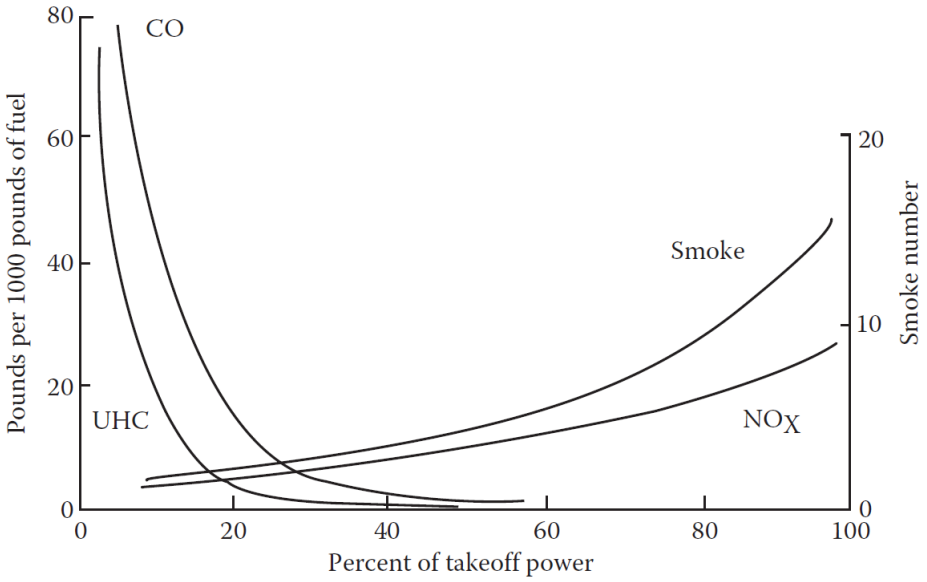

Figure 6.1: Emissions characteristic of gas turbine engines [26]

6.2.1 Oxides of Nitrogen

Four different routes are now identified in the formation of NO_x. These are the **Thermal Route**, the **Prompt Route**, the N_2O **Route** and the **Fuel-Bound Nitrogen Route**. Each of these wil be discussed.

6.2.1.1 Thermal NO

Thermal NO or **Zeldovich NO** (after Y.B. Zeldovich who postulated the mechanism in 1946) is formed by elementary reactions

$$O + N_2 \xrightarrow{k_1} NO + N \tag{6.1}$$

$$N + O_2 \xrightarrow{k_2} NO + O \tag{6.2}$$

$$N + OH \xrightarrow{k_3} NO + H \tag{6.3}$$

Where

$$k_1 = 1.8 \cdot 10^{14}\, exp(-318\, kJ^{-1}/(RT))\, cm^3/(mol \cdot s) \tag{6.4}$$

$$k_2 = 6.4 \cdot 10^{9} T\, exp(-26\, kJ^{-1}/(RT))\, cm^3/(mol \cdot s) \tag{6.5}$$

$$k_3 = 3.8 \cdot 10^{13}\, cm^3/(mol \cdot s) \tag{6.6}$$

The name "thermal" is used because reaction number 1 has a very high activation energy due to the strong triple bond in the N_2 molecule, and is thus sufficiently fast only at high temperatures. The key points regarding thermal NO may be summarized as follow [26], [29]:

- Thermal NO formation is controlled largely by flame temperature
- Little NO is formed at temperature below 1850K
- For conditions typical of those encountered in conventional gas turbine combustors (high temperatures for only a few milliseconds), NO increases linearly with time, but does not attain its equilibrium value
- For very lean-premixed combustors ($\phi < 0.5$), NO formation is largely indipendent of residence time.

6.2.1.2 Prompt NO

The mechanism of **Prompt** or **Fenimore** NO was postulated by C.P. Fenimore (1979), who mesured NO above a hydrocarbon flat flame and noted the the NO did not approach zero as the probe approached the flame from the downstream side, as the thermal mechanism. The additional mechanism that is promptly producting NO at the flame front is more complicated than the thermal one, because the prompt NO results from the radical CH, which was previously considered to be unimportant transient species that is generated through a complex reaction scheme shown in Fig.6.2. The CH, which is formed as an intermediate at the flame front only, reacts with nitrogen forming **Hydrocyanic Acid (HCN)**, which reacts further to NO

$$CH + N_2 \rightarrow HCN + N \tag{6.7}$$

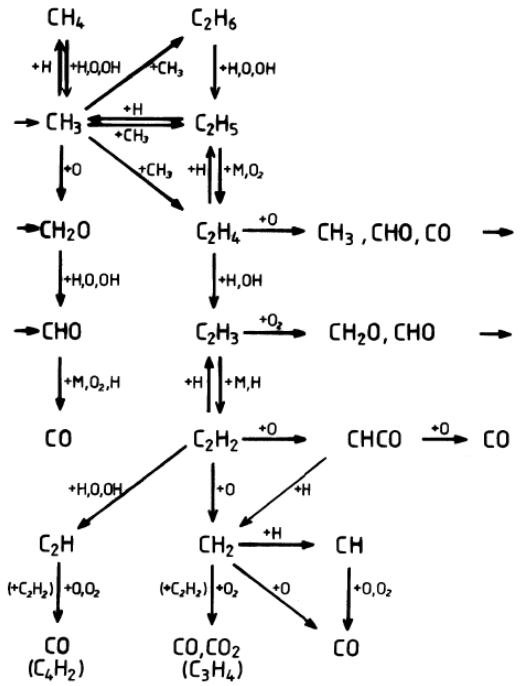

Figure 6.2: Mechanism of oxidation of C_{1-} and C_{2-} hydrocarbons [29]

6.2.1.3 NO Generated via Nitrous Oxide

The **Nitrous Oxide** (N_2O) mechanism is analogous to the thermal one where O atoms attack molecular nitrogen. However, with the presence of a third molecule M, the outcome of this reaction is N_2O

$$N_2 + O + M \rightarrow N_2O + M \tag{6.8}$$

The N_2O may subsequently react with O atoms to form NO

$$N_2O + O \rightarrow NO + NO \qquad E_a = 97kJ/mol \tag{6.9}$$

This reaction has been often overlooked since it usually is an insignificant contributor to the total NO. However, lean conditions can suppress formation of CH and lead to less Prompt NO, and low temperatures can suppress the thermal NO formation. What remains is NO generated via N_2O, which is promoted at high pressures because fo the three body reaction.

6.2.1.4 Conversion of Fuel Nitrogen in NO

Light distillate fuels contain less than 0.06% of organically bonded nitrogen,usually known as **Fuel-Bound Nitrogen (FBN)**, but the heavy distillates may contain

as much as 1.8%. During combustion, some of this nitrogen reacts to form the so-called "**Fuel-NO**". The mechanism scheme is shown in Fig.6.3. The fraction

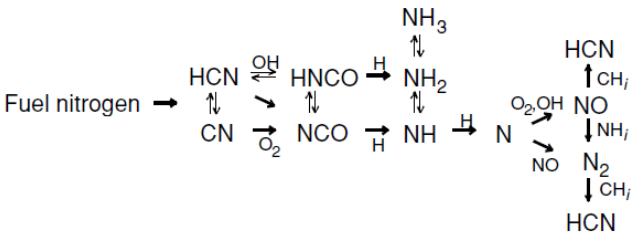

Figure 6.3: Reaction scheme for the NO production from fuel nitrogen [29]

of nitrogen undergoing this change increases only slowly with increasing flame temperature. As far as gaseous fuels are concerned, natural gases contain little or no FBN, but some is found in certain processes and low-Btu gases. Depending on the degree of nitrogen conversion, fuel NO can represent a considerable portion of the total NO.

6.2.2 Unburnt Hydrocarbons

In general, **Unburnt Hydrocarbons** are consequence of **Local Flame Extinction**. There are two effects: flame extinction by strain and flame extinction at walls and in gaps.

6.2.2.1 Flame Extinction Due to Strain

Flame Extinction due to Strain is a phenomenon, which depends only on the processes in the gas mixture. High strain of flame fronts leads to local flame extinction. If the mixture does not reignite, the fuel leaves the reaction zone without being burnt. This effect is increasingly important for rich and lean mixtures, where temperatures are lower and thus reaction times may become larger than the mixing times

6.2.2.2 Flame extinction at Walls and in Gaps

Flame Extinctions at Walls and in Gaps are caused by the interaction of the flame with the walls of the combustion chamber. Heat transfer, as well as the removal of reactive intermediates by surface reactions, are the reason for extinction. From geometrical way, extinction to a parallel wall, perpendicular wall and gaps can be distinguished.

6.2.2.3 Formation of Polycyclic Aromatic Hydrocarbons

If there's no extinction, the fuel seems to be complete broken down to C_1- and C_2- **Hydrocarbons**. From these smaller hydrocarbon fragments new higher hydrocarbons are formed. A class of these new hydrocarbons are **Polyciclic Aromatic Hydrocarbons (PAH)**. These compounds are usually formed under fuel-rich conditions and can be carcinogenic. Acetylene formed in high amounts under rich conditions is the most important precursor of PAH's.
PAH formation is started by C_3H_4 decomposition reaction of CH or CH_2 with C_2H_2 to C_3H_3, which can from the first ring (benzene C_6H_6)(Fig.). The reason is the competing oxidation reactions of C_3H_3 are very slow.

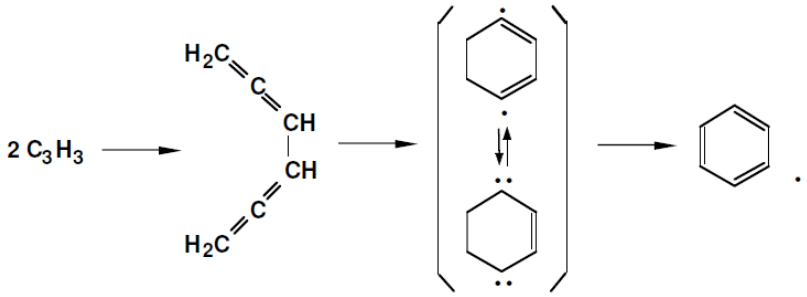

Figure 6.4: Mechanism of PAH formation [29]

In addition PAH are precursors of soot formation.

6.2.3 Carbon Monoxide

When a combustion zone is operating fuel-rich, large amounts of CO are formed owing to the lack of sufficient oxygen to complete the reaction to CO_2. If, however, the combustion zone mixture strength is stoichiometric or moderately fuel-lean, significant amounts of CO will also be present due to the dissociation of CO_2. In practice, CO emissions are found to be much higher than predicted from equilibrium calculations and to be highest at low power conditions, where burning peak temperatures are relatively low. This is in conflict with the predictions of equilibrium theory, and it suggests that much of the CO arises from incomplete combustion of the fuel, caused by various reason: inadequate burning rates in the primary zone due to low fuel/air ratio or insufficient residence time; inadequate mixing of fuel and air, which produces regions with not enough power to support combustion; Quenching of the postflame products by entrainment into the liner wall-cooling air.
CO, once formed, is relatively resistant to oxidation, and in many practical system

its oxidation is rate determining with respect to the attainment of complete combustion. At high temperatures, the major reaction removing CO is

$$CO + OH \rightarrow CO_2 + H \tag{6.10}$$

At lower temperatures the reaction become

$$CO + H_2O \rightarrow CO_2 + H_2 \tag{6.11}$$

The main factors influencing combustion efficiency, and hence CO emissions, are engine and combustor inlet temperatures, combustion pressure, primary zone equivalence ratio and, with liquid fuels, the mean drop size of the spray. All these aspects have been investigated by many workers, including Lefebvre [26] [30].

6.3 Prediction techniques for emissions

The prediction of pollutant emission is a complex and it is still beyond today's physical understanding and modeling capabilities. The detailed prediction of emission involves, depending on the accuracy of the results and the available inputs, various modeling approaches along with different complexity.
It is possible to summarize and categorize the main methods present in the open literature in the following five families, in order of growing complexity

- $P_3 - T_3$ method.
- The Boeing Fuel Flow Method (BFFM2) and Its extension, the Sustainable Supersonic Fuel FLow Method (S2F2) [4].
- High fidelity simulations.
- Semi-Empirical Emissions Correlations.

6.3.1 P3-T3 Method

The $P_3 - T_3$ **Method** is one of the simplest prediction methods present in open literature, and for its simpleness and effectiveness is largely used in the conceptual design phase. The core of the method, expressed in Eq.6.12, is based on the correction of the EI at sea level by using two variables taken from the combustion chamber: **pressure at the ignition** [31] [32] and **fuel-to-air ratio (FAR)** at the ignition both at sea level and at flight level; the correction also depends on the effects of the **atmospheric humidity**, considered via the exponential H explicited in Eq.6.13 in which h represents the specific humidity at the relative altitude in

$$EI_{fl} = EI_{sl} \left(\frac{p_{3,fl}}{p_{3,sl}} \right)^n \left(\frac{FAR_{fl}}{FAR_{sl}} \right)^m e^H \tag{6.12}$$

$$H = 19(h_{sl} - h_{fl}) \tag{6.13}$$

The exponents showing in the equation are variable depending on the engine, but the majority of aeronautic engines fueled by conventional hydrocarbons could be considered $n = 0.4$ and $m = 0$.
Despite the simplicity of the method, it is still possible to observe some issues to its application: $P_3 - T_3$ method need proprietary and punctual data of the engine, such as pressure and temperature in the combustion, and the fuel-to-air ratio. Another relevant detail is that $P_3 - T_3$ is applicable to every engine by changing n and m indeed, but there is not a literature about, complicating the application to unconventional engine architecture. In addition, this method does not take into account most of the variables needed to obtain a very accurate emissions analysis like informations about evaporation and reaction rate, but only the variables entering the combustion chamber.

6.3.2 Boeing Fuel Flow Method and Sustainable Supersonic Fuel Flow Method

With the purpose of avoiding the necessity of proprietary data for $P_3 - T_3$ application, two similar methods are proposed: the **BFFM2** and the **S2F2 Method**, with the purpose to predict the emission indexes in subsonic and supersonic condition, also using sustainable aviation fuels.
Talking about BFFM 2, rather than using proprietary data, the method is based on public information present in the **ICAO Databank** after an engine is certified, such as the Emission Indexes and the fuel flow during the four main phases of the flight, corrected with factors accounting installation losses. Based on these data, the fuel flow in-flight is correlated with the fuel flow at sea-level; than the emission at sea level are correlated with the fuel flow, obtaining the Emission Indexes in generic flight conditions [32].
For BFFM2 the correlation between fuel flow at FL and SL is reported in Eq.6.14,while the correlation between the emissions is expressed in Eq.6.15 and Eq.6.16

$$W_{f,fl} = W_{f,sl} \left(\frac{\theta_{amb}^{3.8}}{\delta_{amb}} \right) e^{0.2M^2} \tag{6.14}$$

$$EI_{NO_{x_{fl}}} = EI_{NO_{x_{sl}}} \left(\frac{\delta_{amb}^{1.02}}{\theta_{amb}^{3.3}} \right) e^{H} \tag{6.15}$$

$$EI_{CO_{fl}} = EI_{CO_{sl}} \left(\frac{\theta_{amb}^{3.3}}{\delta_{amb}^{1.02}} \right) \tag{6.16}$$

Where $\theta = T_{amb}/T_{ref}$ ($T_{ref} = 288.15$), $\delta = p_{amb}/p_{ref}$ ($p_{ref} = 101325Pa$) and $H = 19(h_{sl} - h_{fl})$.

Differently from BFFM2, which is perfect for subsonic flight conditions, the S2F2 is better suitable for supersonic flight, so in this case the process between freestream and combustor inlet cannot be considered isentropic. In addition changes in the fuel lower heating value due to the kerosene blend with a biofuel are considered. The compression process can be split intuitively in two parts: the first part is the non-isentropic compression from the freestream to the compressor inlet, and the second part goes from the compressor inlet to the combustor inlet and can be considered a classic isentropic compression [4].
These considerations leads to three **Correction Factors**: k_p for the pressure ratio, k_t for the temperature ratio and k_b to consider the fuel blend. These factors are expressed in the following equations:

$$k_p = 0.08M_0^2 + 0.06M_0 + 0.86 \tag{6.17}$$

$$k_t = 0.055M_0^2 - 0.395M_0 + 1.34 \tag{6.18}$$

$$k_b = \frac{LHV_{kerosene}}{LHV_{blend\ z\%}} \tag{6.19}$$

The reformulation is reported in the next equation:

$$EI_{NO_{x_{fl}}} = EI_{NO_{x_{sl}}} \left[\frac{\delta_{amb}^{1.02}}{\theta_{amb}^{3.3}} \left(k_p \frac{p_{2,fl}}{p_{1,fl}} \right) \left(\frac{1}{k_t \frac{T_{2,fl}}{T_{1,fl}}} \right)^{3.3} \right]^y e^H k_b \tag{6.20}$$

$$EI_{CO_{fl}} = EI_{CO_{sl}} \left[\frac{\theta_{amb}^{3.3}}{\delta_{amb}^{1.02}} \left(\frac{1}{k_p \frac{p_{2,fl}}{p_{1,fl}}} \right) \left(k_t \frac{T_{2,fl}}{T_{1,fl}} \right)^{3.3} \right]^x k_b \tag{6.21}$$

The structure for EI_{UHC} is the same of EI_{CO}.

6.3.3 High fidelity simulations

Following this path, the numerical modeling of the flow is coupled to the **Advanced Combustion and Mixing Physics Modeling**. These methods bring together all the complication of the computational problems: the complete geometry of the combustor is required for the application of the **Reynolds-averaged Navier-Stokes equations** in terms of boundary conditions.
Due to the different timescales and the physical phenomena involved, trying to maintain the accuracy of the modeling, direct numerical simulation for realistic combustion processes are non practical at the moment, with an excessive CPU-time for a fully 3D CFD simulation. Implementing **Large-Eddy Simulation (LES)** and cutting away the deep modeling of the small-scale turbulence, yet results in a lack of accuracy, a not suitable condition for an emission prediction tool.

6.3.4 Semi-Empirical Emisison correlations

The **Emission Correlation Methods** are based on the defining of characteristics parameters, that can be directly or indirectly correlated with the **Emission Indexes (EI)**. The correlation methods are further subdivided in two types of models: **direct prediction** and **relative correlation**, both based on engine data in term of performances and emissions obtained via combustor rig tests or engine tests at different flight conditions. The direct methods consist of a formula which directly correlates $EINO_x$ to a set of engine parameters. The relative correlation methods overcome the restrictions of the direct methods, and rely on publicly available data from, for example, ICAO database. These models are the simplest to, but face some critical issues and have well noted disadvantages: the number of input is larger and they are difficult to obtain, especially for unconventional propulsive configurations, and the mathematical expression is sensitive to errors, also amplifying any of them if present in input data.
These correlations are the ones chosen for this work and are discussed in detail in the next section.

6.4 Lefebrve and Murthy Correlations for CO, UHC and NOX Emission Indexes calculation

In this chapter, the estimation of emissions using **Lefebrve and Munthy semi-empirical relations** is explored in detail.
In the literature exist different correlations for the calculation of the CO, UHC and NO_x emissions of the Jet-A and a lot of methodology based on different entities. The equations for the calculations of the emission indexes for CO, UHC and NO_x are respectively [33], [34], [30]

$$EI_{CO} = \frac{86\,\dot{m}_a T_{pz}\, exp(-0.00345\,T_{pz})}{(V_c - V_e)(\Delta P/P)^{0.5} P^{1.5}} \tag{6.22}$$

$$EI_{UHC} = \frac{11764\,\dot{m}_a T_{pz}\, exp(-0.00345\,T_{pz})}{(V_c - V_e)(\Delta P/P_3)^{0.5} P_3^{2.5}} \tag{6.23}$$

$$EI_{NO_x} = \frac{9x10^{-8}(P)^{1.25} V_c\, exp(0.01\,T_{st})}{\dot{m}_a\, T_{pz}} \tag{6.24}$$

The first and the third one by Lefebrve, the second by Murthy.
For all the analyzed it may be assumed that their exhaust concentration is proportional to the product of three terms which are selected to represent the following:

- **mean residence time** in the combustion zone

- **chemical reaction rates**
- **mixing rates**

In particular the relations are structured as follow

$$EI_{NO_x} = f(residence\ time)(reaction\ rate)(mixing\ rate) \tag{6.25}$$

$$EI_{CO,UHC} = f(residence\ time)^{-1}(reaction\ rate)(mixing\ rate) \tag{6.26}$$

Expressions for the three foundamental parameters may be derived in simplified form as is now shown

$$residence\ time = \frac{L}{U} = \frac{L\rho A}{\dot{m}_a} = \frac{PV}{\dot{m}_a RT} \tag{6.27}$$

It is assumed that reaction rates are a function of pressure and temperature only. For NO_x

$$reaction\ rate \propto P^m exp(zT) \tag{6.28}$$

For CO and UHC

$$reaction\ rate \propto P^n exp(cT) \tag{6.29}$$

It is assumed that mixing rates are a function of liner pressure drop. Specifically we have

$$mixing\ rate \propto \left(\frac{\Delta P}{P}\right)^{\chi} \tag{6.30}$$

So the Eq.6.25 and 6.26 become

$$EI_{NO_x} = A\left(\frac{PV}{\dot{m}_a T}\right)\left(\frac{\Delta P}{P}\right)^{\chi} P^m exp(zT) = \frac{AV_c(\Delta P/P)^{\chi} P^y exp(zT)}{\dot{m}_a T} \tag{6.31}$$

Where $y = 1 + m$

$$EI_{CO,UHC} = C\left(\frac{\dot{m}_a T}{V_c - V_e}\right)\left(\frac{\Delta P}{P}\right)^{\chi} P^b exp - (cT) \tag{6.32}$$

Where $b = n - 1$.
In the following table all the coefficients of the equations are listed By replacing the coefficients with the correct values we can obtain the relations in Eq.6.22,6.23,6.24. In these equations it may be noted that there's influence of the fuel type in three terms: T_{pz} in all equations, T_{st} in only EI_{NO_x} equation and V_e in the EI_{CO} and EI_{UHC} ones. The former, T_{pz}, is the **termperature in the primary zone** of the liner of the combustor. It is calculated as [30]

$$T_{pz} = T_3 + \Delta T_{pz} \tag{6.33}$$

Coefficient	Tubo-annular	Through flow annular	Reverse flow annular
C_{CO}	18.17	86	26928
C_{UHC}	5288	11764	19606
A_{NO_x}	$9x10^{-8}$	$9x10^{-8}$	$9x10^{-8}$
c_{CO}	0.0023	0.00345	0.00345
c_{UHC}	0.0025	0.00345	0.00345
z_{NO_x}	0.01	0.01	0.01
n_{CO}	1.5	1.5	2.5
n_{UHC}	2.5	2.5	2.5
m_{NO_x}	0.25	0.25	0.25
χ	0.5	0.5	0.5

Table 6.3: Semi-empirical relations coefficients [33], [34], [30]

Where T_3 is the **inlet temperature of the combustion chamber**, while ΔT_{pz} is the rise temperature due to the combustion in primary zone, obtained as $T_3\left(\frac{f_{0v}}{q_{pz}}\right)$, where f_{0v} is the **combustor overall fuel/air ratio** and q_{pz} is **fraction of total combustor air imployed in primary zone combustion**. T_{st}, only present in the EI_{NO_x} relation, is **stoichiometric flame temperature** of the gas mixture corresponding to the inlet temperature T_3. So Eq.6.24 suggests is the stoichiometric flame temperature that determines the formation of NO_x, however, for the residence time in the combustion zone, which is also significant to NO_x formation, the appropriate temperature term is the bulk value T_{pz}.
The formation of CO and UHC in the primary combustion zone takes appreciably longer than the time required to produce NO_x. In consequence the relevant temperature is not the local peak value adjacent to the evaporating fuel drops but the **average value throughout the primary zone** namely T_{pz}. Also because CO and UHC emissions are most important at low pressure conditions, where evaporation rates are relatively slow, it is necessary to reduce the **combustion volume** V_c by the **volume occupied in fuel evaporation** V_e. This was evaluated as [30]

$$V_e = 0.55\,\dot{m}_{pz}D_0^2/\rho_{pz}\lambda_{eff} = 0.55\,q_{pz}\dot{m}_a D_0^2/\rho_{pz}\lambda_{eff} \tag{6.34}$$

All values already known from previous discussion aside from ρ_{pz}, that is the **density of gas mixture in the primary zone**, D_0, the **initial diameter of the fuel droplet** before combustion and the **effective evaporation constant** λ_{eff}.
To find these last two values the approach used it is to assume a **spherically symmetric model** of a vaporizing drop in which the rate-controlling process is

that of molecular diffusion [35]. Consider the hypothetical case of a pure fuel drop that is suddenly immersed into gas at high temperature. At normal fuel injection temperatures the concentration of fuel vapor at the liquid surface is low, and there is little mass transfer from the drop in this initial stage. Under these conditions the fuel drop heats up exactly like any other cold body when placed in a hot environment. Due to the limited heat conductivity of the fuel, the temperature inside the drop is not uniform, but is cooler at the center of the drop than at the liquid surface.
As the liquid temperature rises so also does the partial pressure and concentration of fuel vapor at the surface. This increases the rate of dispersion of fuel vapor away from the droplet which has two effects:

- a larger proportion of the heat transferred to the drop is needed to furnish the heat of vaporization of the liquid
- the outward flow of fuel vapor impedes the rate of heat transfer to the drop

This tends to diminish the rate of increase of the surface temperature so that the level of temperature within the droplet becomes more uniform. Eventually, a stage is reached where all of the heat transferred to the droplet is used as heat of vaporization and the droplet temperature stabilizes at its "**steady-state**" or "**wet bulb**" temperature.
This state allows mass evaporation rates and drop lifetimes to be estimated to a reasonable level of accuracy. During its lifetime the diameter D of an evaporating drop may be related to its initial diameter D_0 by the equation [35]

$$D_0^2 - D^2 = \lambda t \tag{6.35}$$

Where λ, as already said, is the evaporation constant. This definition of λ allows to express the rate of fuel evaporation as [35]

$$\dot{m}_F = (\pi/4)\rho_F \lambda D \tag{6.36}$$

We can also write the steady state evaporation of a single fuel drop

$$\dot{m}_F = 2\pi D(k/c_p)_g ln(1+B) \tag{6.37}$$

Equating Eq.6.36 and 6.37 we obtain

$$\lambda_{st} = \frac{8ln(1+B)}{\rho_F(c_p/k)_g} \tag{6.38}$$

This equation allows to calculate λ_{st} from a knowledge of the fluid properties ρ_F, $c_{p,g}$ (average c_p in combustion chamber) and k_g (average themal conductivity of

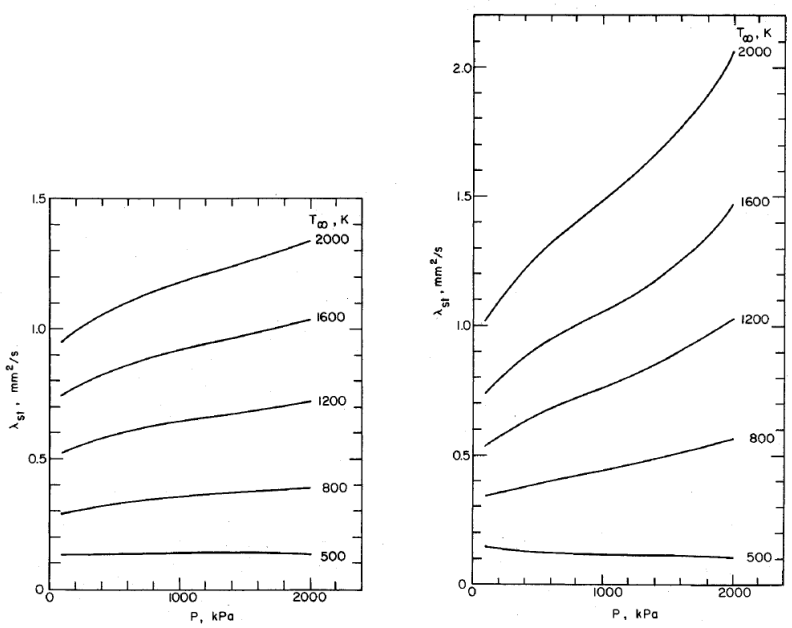

Figure 6.5: Influence of ambient pressure and temperature on steady-state evaporation constant for avaition gasoline and n-heptane [35]

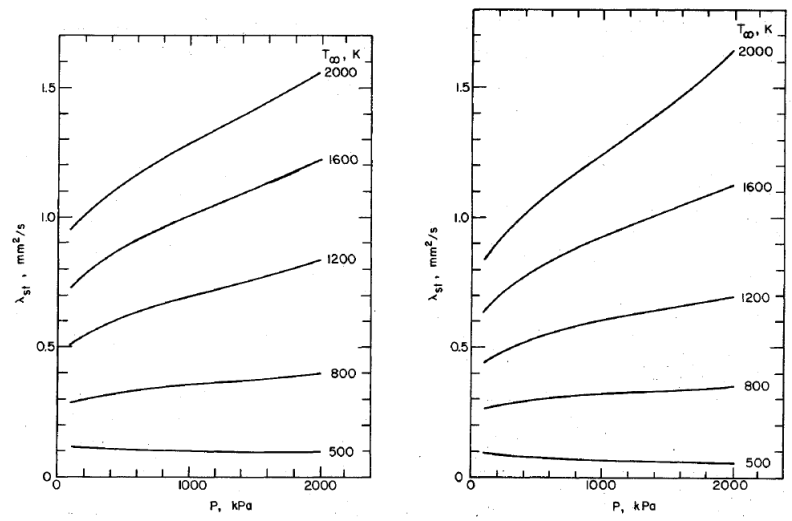

Figure 6.6: Influence of ambient pressure and temperature on steady-state evaporation constant for JP4 and JP5 [35]

gas mixture) and the transfer number B, value linked to the gas mix pressure and mass fractions and to the fuel vapor pressure at the drop surface.
Calculated value of λ_{st} for some fuels, over wide ranges of pressure and ambient

temperature, are shown in Fig.6.5 and 6.6 The graphs show clearly that evaporation rates increase markedly with increase in ambient temperature. The effect of pressure on evaporation rates is more complex. The figures show that λ_{st} increases with pressure when the ambient temperature is high ($> 800K$) and declines with increase in pressure when the ambient temperature is low ($< 600K$). Between 600 and $800K$ evaporation rates are sensibly independent of pressure. If the pressure dependence of λ_{st} is expressed in the form

$$\lambda_{st} \propto P^k \tag{6.39}$$

It is found that, over the range of pressures and temperatures considered, the value of k can varies between ± 0.25 and depends also from the type of fuel considered. From these graphs it is possible to extract the λ_{eff} usefull for EI_{CO} and EI_{UHC} relations. Unfortunately, no graphs were found in the literature for the fuels used, and the calculation of the B value are too complex with the informations we have. In the Sec.7.2 an alternative way of calculation is proposed.

Chapter 7

Results and discussions

In this chapter the exposed models and procedures to size the propulsion system, generate the **Propulsive Datbase** and **Evaluate Emissions** are applied. As discussed, the first step is to perform the **On-design analysis** to obtain the **reference point**. After that, set the conditions vector for *Altitude*, M_0 and T_{t4} to solve the thermodynamic cicle for all **Off-design conditions** to obtain the propulsive database. At last, use the combustion chamber and fuels characteristic values to calculate the **emission indexes** for all the examined fuels and for various engine power settings.

7.1 Propulsive Database Generation

One of the main goals of this thesis work is to generate the propulsive database for the Olympus 593. After the On-design calculations, many Off-design iterations might be run by varying the **throttle**, the **flight Mach number** and the **altitude**. Of course, in real operative conditions, other parameters may change during the flight, such as the power request by other systems and the bleed air of the aircraftHowever, it is reasonable to consider these two parameters in the worst-case scenario and constants, since they have no significant impact on engine performance. To conclude, it is possible to summarise the database generation in the following subsections

7.1.1 Propulsion system requirements analysis

The requirements are always the starting point of the entire procedure. Without them, it is impossible to size an engine that is configured for the aircraft. These are derived from the previous analyses of the aircraft and from the initial sizing of its systems.

Having a clear idea of which engine type is more appropriate for the reference study and considering different configurations such as turbofan mixed, turbofan separated, turbojet with a single spool or dual spools.
For this work of thesis, as already said, we choose the Olympus 593 as propulsive system, a well known engine with well known characteristics.
The reference aircraft is obviously the Concorde (Fig.7.1).

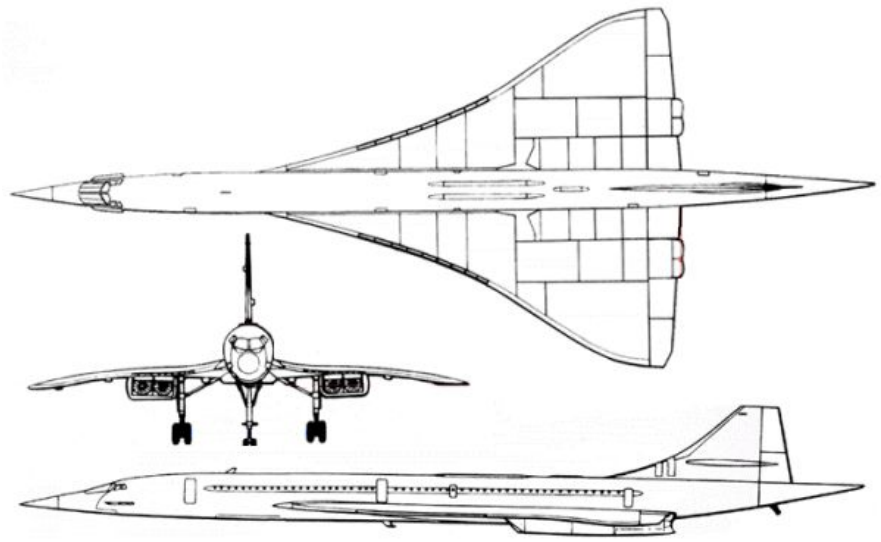

Figure 7.1: Concorde schematic

Using the **ASTOS** software, knowing all the necessary aircraft informations, it is possible to obtain the mission profile and the **Propulsive System Requirements**, in therms of **Thrust**, **Mach number** and **Altitude**, which will be inputs of the engine sizing procedure and object of validation for the propulsive database. ASTOS results are reported in Fig.7.2, Fig.7.3 and Tab.7.1

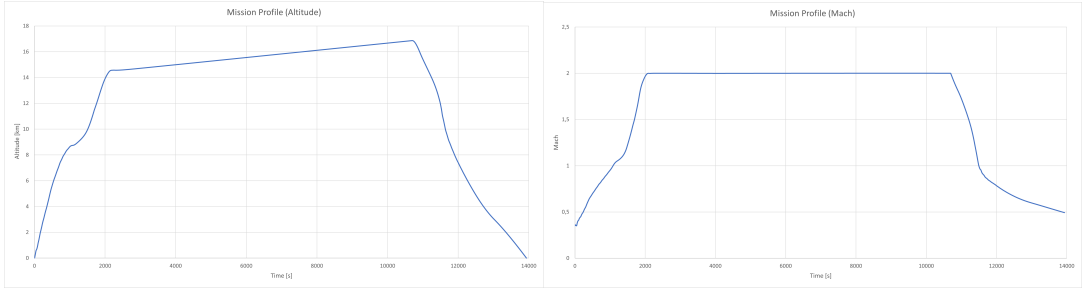

Figure 7.2: Mission altitude and Mach

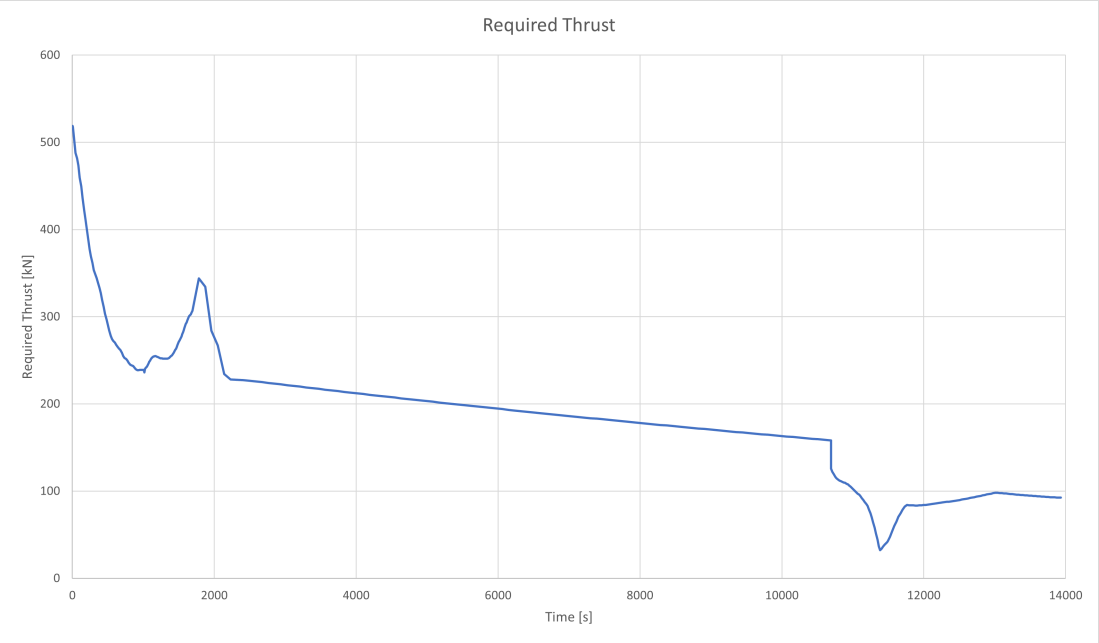

Figure 7.3: Required Thrust for Concorde (four engines)

Propulsion System Requirements		
Number of Engine	4	$[-]$
Supercruise Altitude	16.154	$[km]$
Flight Mach Number	2	$[-]$
Inlet Diameter	1.077675	$[m]$
Supercruise Thrust (1 engine)	≥ 44.6	$[kN]$
Take-off Thrust (1 engine)	≥ 140	$[kN]$
Total Power Extraction (1 engine)	240	$[kW]$
Bleed Air	0	$[kg/s]$

Table 7.1: Concorde propulsion system requirements

7.1.2 On-design Results

Considering a **level of technology** equal to 2 (because Olympus 593 is an enigne from the 60s/70s), it is possible to perform the On-Design during the **Supercruise** to begin a preliminary size of the system. In the Tab.7.2 there are all the engine values that respect the requirements, and are necessary to evaluate the on-design conditions. For this work of thesis supercruise, at $16154m$ and $M = 2$, have

been choesn as design point. In addition, the **end of runway during take-off**, at altitude $0m$ and $M = 0.35$, have been chosen as critical point to modify the on-design parameters to confirm that the engine can provide sufficient thrust during take-off. For the calculations of S and $TSFC$ the following formulas were used

Engine On-design results			
Parameter	Symbol	Value	Unit
Altitude	Alt	16154	$[m]$
Flight Mach	M_0	2	$[-]$
Overall Pressure Ratio (OPR)	π_c	7	$[-]$
LP Compressor Pressure Ratio	π_{cL}	4.1	$[-]$
HP Compressor Pressure Ratio	π_{cH}	2.9	$[-]$
Temperature Inlet Turbine (TIT)	T_{t4}	1350	$[K]$
Air Mass Flow Rate	$\dot{m}_0$	131	$[kg/s]$
Cooling fractions	$\varepsilon_{1,2}$	5	$[\%]$
Bleed fraction	β	1	$[\%]$
Intake Pressure Ratio	ε_d	0.937	$[-]$
LP Spool Mechanical Efficiency	η_{mL}	0.99	$[-]$
HP Spool Mechanical Efficiency	η_{mL}	0.99	$[-]$
Adiabatic LP Compressor Efficiency	η_{cL}	0.853	$[-]$
Adiabatic HP Compressor Efficiency	η_{cH}	0.817	$[-]$
Adiabatic LP Turbine Efficiency	η_{tL}	0.890	$[-]$
Adiabatic LP Turbine Efficiency	η_{tH}	0.900	$[-]$
Burner Design Efficiency	η_b	0.990	$[-]$
Burner Pressure Ratio	ε_b	0.960	$[-]$
Installed Supercruise Thrust	S	47.49	$[kN]$
Installed Thrust Specific Fuel Consumption	$TSFC$	34.5961	$mg/(Ns)$

Table 7.2: Propulsion system: On-design results

$$S = \dot{m}_9 V_9 - \dot{m}_0 V_0 + A_9(P_9 - P_0) \tag{7.1}$$

$$TSFC = \frac{\dot{m}_b}{S} \tag{7.2}$$

Where "V" is the velocity calculated as $M \cdot a$ (where "a" is the local speed of sound) and $\dot{m}_b$ is the mass flow rate of fuel.

7.1.3 Off-design Results

As already said, for off-design analysis, the **Matrix Iteration method** uses the **Newton-Raphson algorithm** in concert with the **Models of the components** installed in the engine to solve the Off-design problem. Have already been generated and seen the maps of each component to study the behaviour of every engine part. Now performances are analyzed.
The **Thrust (S)** and **Specific-Thrust Fuel Consumption (TSFC)** are calculated by using the solution of the thermodynamics cycle. The results are shown in Fig.7.4, 7.5

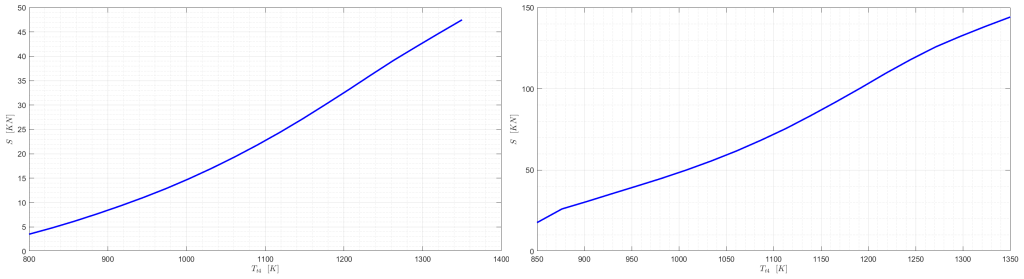

Figure 7.4: Thrust behavior off-design: Supercruise And Take-Off Conditions

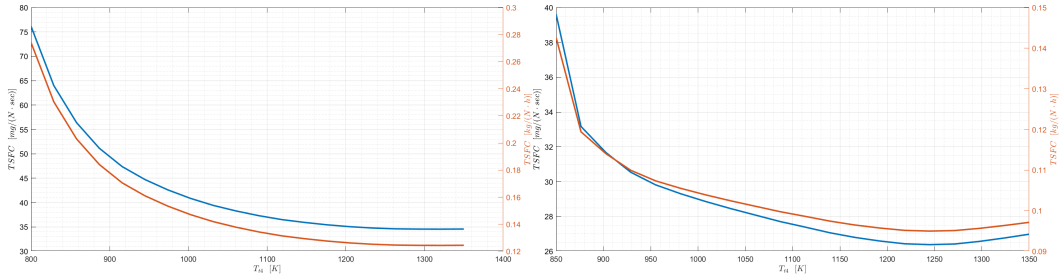

Figure 7.5: TSFC behavior off-design: Supercruise And Take-Off Conditions

The thrust, as the T_{t4} drops, decreases up to $\sim 4kN$ for supercruise conditions and $\sim 18kN$ for take-off. The behavior is what expected because thrust decreses as the T_{t4} decreases. However, this extreme low conditions is very difficult to realize in operative conditions, they are just theoretical. Lastly, the TSFC in Fig.7.5 increases in perfect agreement with its definition. In fact, TSFC is an indicator of how efficiently the engine generates thrust: the lower it is, the more efficiently thrust is produced. Therefore, as conditions shift towards lower temperatures and lower thrust, the engine is working less efficiently, thus increasing the TSFC value. The TSFC results are also supported by flow rate results in Fig.7.6

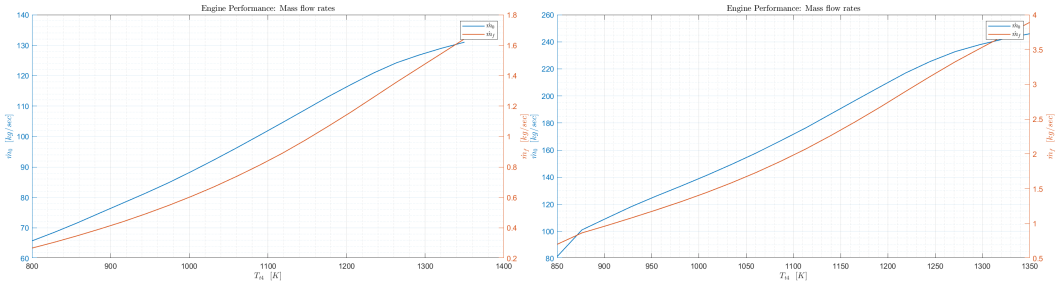

Figure 7.6: Mass Flow Rate behavior off-design: Supercruise And Take-Off Conditions

Finally, the results just discussed are compared for all fuels considered in this thesis in Fig.7.7, 7.8

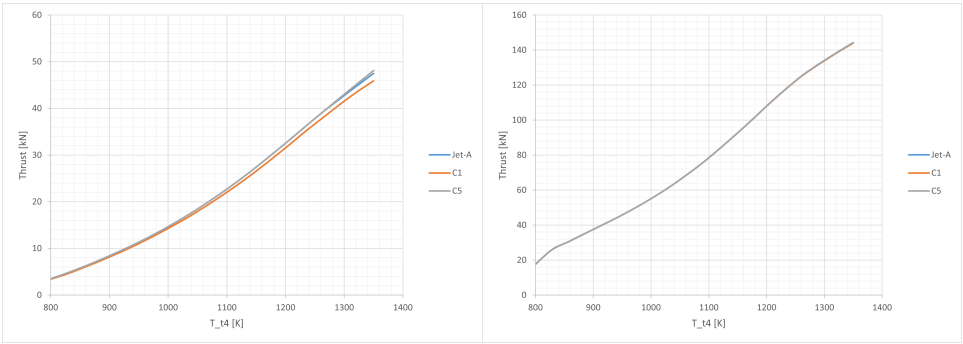

Figure 7.7: Thrust for Jet-A, C1 and C5: Supercruise And Take-Off Conditions

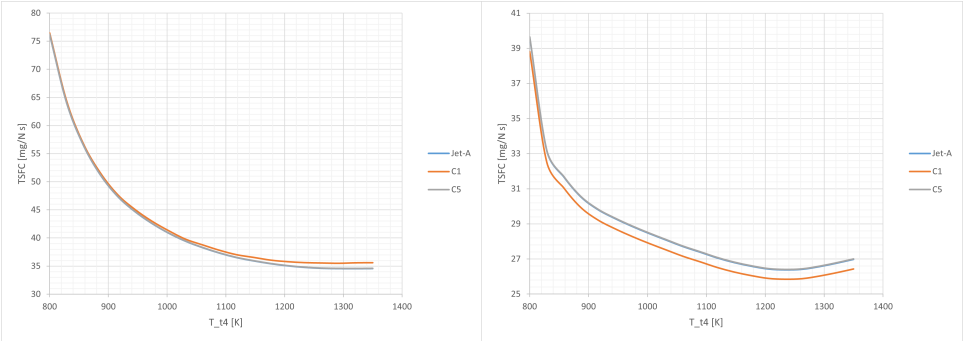

Figure 7.8: TSFC for Jet-A, C1 and C5: Supercruise And Take-Off Conditions

The values are very similar between all fuels.

7.1.4 Database Generation - Throttle variation at differnt Mach numbers and Altitudes

The **propulsive database generation** requires the performance's computation at different altitudes and flight Mach numbers aiming to cover the entire mission profile or its greatest part. The procedure is very hard to automatise, since different flight conditions require an appropriate selection of the throttle τ in concert with the nozzle throat area variation. Variable τ is defined as

$$\tau = \frac{T_{t4}}{T_{t4}^*} \tag{7.3}$$

Where T_{t4}^* is the **Temperature Inlet Turbine (TIT)** in On-design conditions. For a complete study it is necessary to vary the throttle from its design value, which in this case corresponds to maximum thrust conditions, to the value that determines the **IDLE condition**. Therefore, it is necessary to know the thrust value that determines the IDLE condition. This value is conventionally defined as 5% of the maximum thrust:

$$S_{idle} = 0.05\, S_{max} \tag{7.4}$$

In most cases, selecting the throttle close to 1 protects the engine and avoids the related simulation divergence. However, selecting the maximum value for τ leads to the maximum thrust generation, therefore a minimum value must be set manually, by checking if the low-pressure components are working with a sufficient surge margin.
Two databases were generated for this work: one (not reported here) that shows all performances with the variation of Mach and Altitude and max throttle; the second one mission related. The former is attached to this work as excell file and analyze the convergence of the off-design solutions for the Altitude vary from 0 to $17000m$ and Mach from 0 to 2 for max throttle ($T_{t4} = 1350K$). The last one, more useful, show the performance data relating to the various points of the mission extracted from ASTOS. Mach and altitude values are taken from ASTOS and for each of these pairs of values the throttle is varied from maximum to Idle condition value, in this way the entire mission is covered with the relative performance values. At last, selecting the right throttle setting for each condition, considering the correct throttle percentage for a typical Concorde mission (taken from a Concorde Flight Tutorial [36]), it is possible to obtain the available thrust and available TSFC for the whole mission, and compare them with the required values extracted from ASTOS. Avaliable Thrust, available TSFC and fuel mass flow rate ($\dot{m}_b$) for the mission and for all three fuels considered are shown in Fig.7.9, 7.10 and 7.11

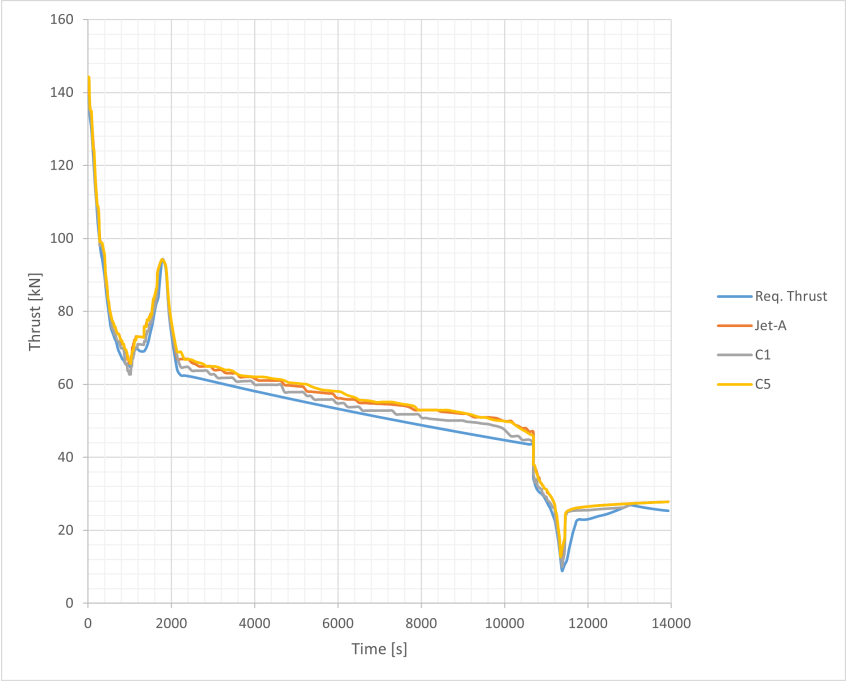

Figure 7.9: Available Thrust for Concorde mission for Jet-A, C1 and C5

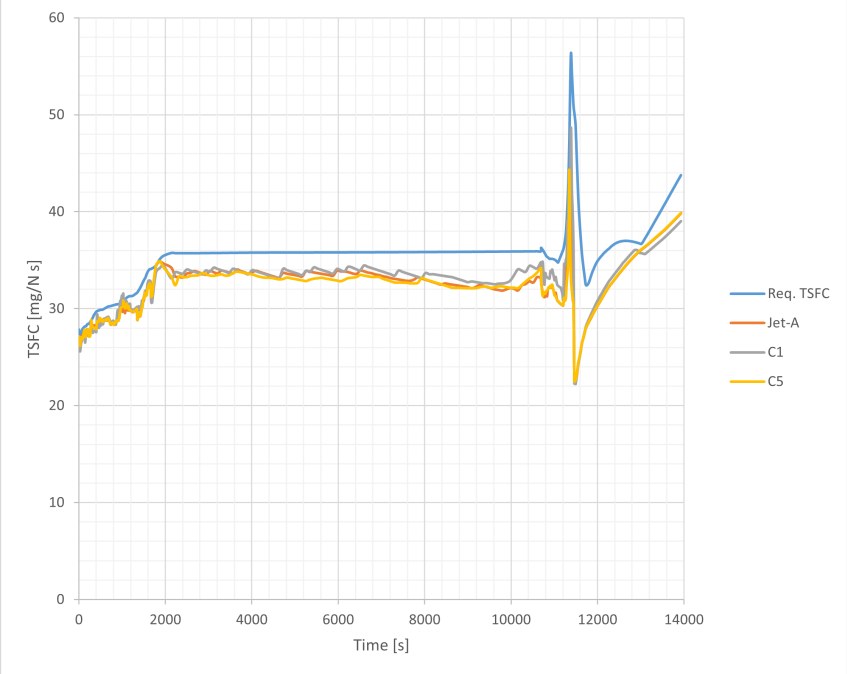

Figure 7.10: Available TSFC for Concorde mission for Jet-A, C1 and C5

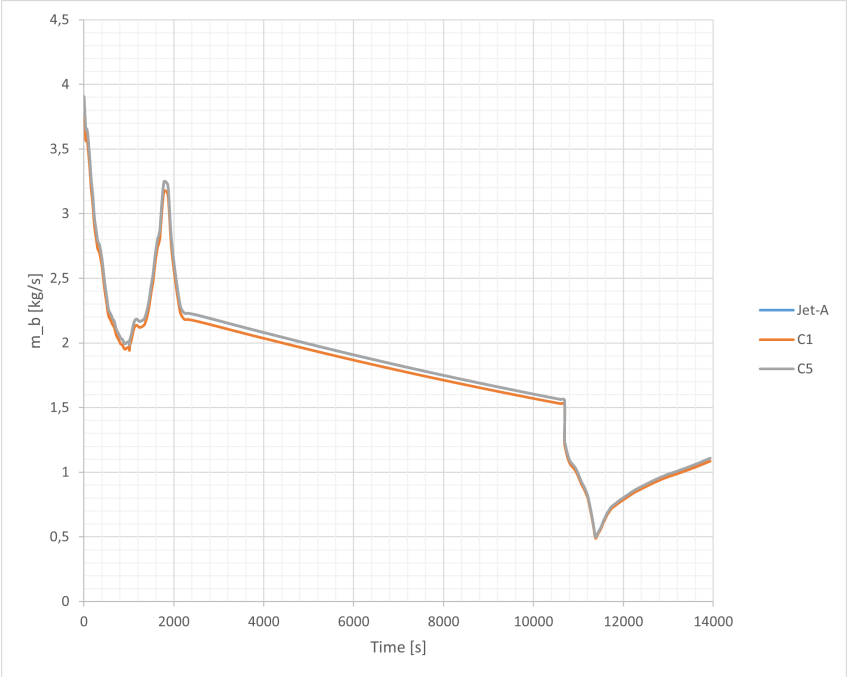

Figure 7.11: Fuel Mass Flow rate for Concorde mission for Jet-A, C1 and C5

7.2 Emission indexes

Following the development of the propulsive database of the case of study, it is possible to use the engine variable and values to calculate the emissions for various flight conditions. As already discussed in Sec.6.4 the **Murthy and Lefebvre semi-empirical relations** have been used

$$EI_{CO} = \frac{86\,\dot{m}_a T_{pz}\,exp(-0.00345\,T_{pz})}{(V_c - V_e)(\Delta P/P)^{0.5} P^{1.5}} \tag{7.5}$$

$$EI_{UHC} = \frac{11764\,\dot{m}_a T_{pz}\,exp(-0.00345\,T_{pz})}{(V_c - V_e)(\Delta P/P_3)^{0.5} P_3^{2.5}} \tag{7.6}$$

$$EI_{NO_x} = \frac{9x10^{-8}(P)^{1.25} V_c\,exp(0.01\,T_{st})}{\dot{m}_a\,T_{pz}} \tag{7.7}$$

The conditions chosen for the emissions study are three: **Supercruise**, **Take-off** and **Idle**. The first two most representative for NO_x emissions, the last one for UHC and CO emissions.
Now we need to discuss how to find all the values linked to the semi-empirical relations, starting from the **Combustion volume** (V_c). The numerical value for

V_c is constant and correspond to the volume inside the liner of the combusiton chamber. The value of V_c is taken from literature, but it is possible to evaluate it following a simplified approach for a combustion chamber design like the works of Conrado A.C. et al. [37] and Priyant Mark C. [38], very handy and useful for conceptual design or preliminary design work, or follow a more complex and deep approaches, like the Lefebvre's one [26].
The other volume, the **Evaporation volume** (V_e), is a bit more complicated to evaluate. As already said V_e is defined as

$$V_e = 0.55\, \dot{m}_{pz} D_0^2 / \rho_{pz} \lambda_{eff} \tag{7.8}$$

All values require a different methodology to be found. Starting from the easiest one, **Mass Flow Rate in the Primary zone** ($\dot{m}_{pz}$) is obtained from a table of typical airflow appotioning in a generic annular combustor (the design of the Olympus 593 combustor) as shown in Fig.7.12

Table 2 Air mass flow rate distribution.

Air mass flow rates	Symbol	Percentage/%
Inlet	$\dot{m}_3$	100
Recirculation zone/snout	$\dot{m}_{RZ}$	20
Swirler	$\dot{m}_{SW}$	12
Dome cooling	$\dot{m}_{Dcool}$	8
Annulus	$\dot{m}_{an}$	80
Primary zone	$\dot{m}_{PZ}$	20
Secondary zone	$\dot{m}_{SZ}$	10
Dilution zone	$\dot{m}_{DZ}$	10
Cooling air	$\dot{m}_{cool}$	40

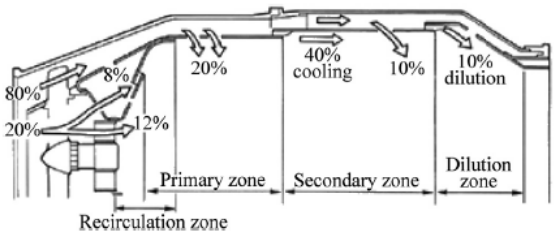

Figure 7.12: Typical Airflow Apportioning for generic annular combustor

As reguard the **Initial Fuel Drop Diameter** (D_0) and the **Effective Evaporation Constant** (λ_{eff}), things become more complicated. For Fuel Drop Diameter we can simply consider various studies and take an average value of D_0 around $15\mu m$ because the evaluation of the diameter require a deep knoledge of velocity of the gas mixture, type of atomization process and nozzles used in this process, all concepts that go beyond this thesis work. For λ_{eff}, instead, we can use the

method of calculation exposed in Sec.6.4, but as already said is too complex with the amout of informations we have about the alternatives fuels C1 and C5, and we can't even use the λ_{st} graphs, because are fuel related. Thanks to Lefebvre [30] it is possible to find another formula with the same values ratio: the **Pattern Factor** definition. The pattern factor is a parameter that describe the temperature distribution at the combustor exit section and it is defined as

$$PF = (T_{t,max} - T_{t4})/(T_{t4} - T_{t3}) \tag{7.9}$$

Where $T_{t,max}$ is the maximum temperature found in the traverse and it's a design parameter for the durability of the combustion chamber. All the parameters that define the pattern factor are known from the engine model. Two parameters of crucial importance to pattern factor are liner length, which controls the time and distance that are available for mixing, and the pressure drop across the liner which governs the penetration of the dilution jets and their rate of mixing with the products of combustion. In particular

$$PF = (T_{t,max} - T_{t4})/(T_{t4} - T_{t3}) = \int (L_L/D_L)(\Delta P_L/q_{ref}) \tag{7.10}$$

Where the subscript "L" indicates the liner values (lenght, diameter and pressure drop) and q_{ref} is the reference dynamic head. For annular combustor the relation become

$$(T_{t,max} - T_{t4})/(T_{t4} - T_{t3}) = 1 - exp(-[0.050(L_L/D_L)(\Delta P_L/q_{ref})]^{-1}) \tag{7.11}$$

Considering now the length of the liner used in mixing and combustion (L_e)

$$(T_{t,max} - T_{t4})/(T_{t4} - T_{t3}) = 1 - exp(-[0.050((L_L - L_e)/D_L)(\Delta P_L/q_{ref})]^{-1}) \tag{7.12}$$

L_e is the liner length required to evaporate the fuel spray. It is obtained as the product of the average predilution liner velocity and the evaporation time as shown in Eq.7.13

$$L_e = U_g t_e = \left(\frac{0.6\,\dot{m}_a}{\rho_g A_L}\right)\left(\frac{D_0^2}{\lambda_{eff}}\right) \tag{7.13}$$

The constant of 0.6 stems from the assumption that 60% of the total combustor airflow enters the liner upstream of the dilution zone. So the Eq.7.12 may be rewritten as

$$\frac{T_{t,max} - T_{t4}}{T_{t4} - T_{t3}} = 1 - exp\left(-\left[0.050\left(\frac{\Delta P_L}{q_{ref}}\right)\left(\frac{L_L}{D_L} - \frac{0.33\,\dot{m}_a D_0^2}{\rho_g A_L D_L \lambda_{eff}}\right)\right]^{-1}\right) \tag{7.14}$$

Now all the parameters in the pattern factor equation are known: all the T_t are known from the engine model, same for $\dot{m}_a$; the liner geometry from literature; ρ_g

is the average density in the liner, easily calculated by knowing temperatures and pressures; the ratio $\Delta P_L/q_{ref}$ is linked to the combustor type as shown in Fig.7.13

Combustor	$\Delta P_{3-4}/P_3$ (%)	$\Delta P_{3-4}/q_{ref}$	$\dot{m}_3\sqrt{T_3}/A_{ref}P_3$
Multi-can	5,3	40	$3{,}0\times10^{-3}$
Can-annular	5,4	30	$3{,}5\times10^{-3}$
Annular	6,0	20	$4{,}5\times10^{-3}$

Figure 7.13: Representative values of pressure-loss terms for Combustors [37]

So by inverting the equation, we can obtain the $\frac{D_0^2}{\lambda_{eff}}$ ratio useful for the V_e calculation.
The last term is ρ_{pz}. To find the quantities relating to the primary zone, not only ρ_{pz}, but also T_{pz}, CANTERA was used. At first the **Adiabatic Flame Temperature** (T_{st}) corresponding to the inlet tempertature T_3 is calculated. This value is also useful for the EI_{NO_x} relation. From this value it is possible to find T_{pz} as

$$T_{pz} = T_3 + \Delta T_{pz} \tag{7.15}$$

Where

$$\Delta T_{pz} = \eta \cdot \Delta T \tag{7.16}$$

Where ΔT is the temperature rise from T_3 to adiabatic flame temperature already calculated and η is the combustion efficiency in the ricirculation zone, calculated as [37]

$$\eta = 0.71 + 0.29\, tanh[1.5475 \cdot 10^{-3}(T_3 + 108\, ln(p_3) - 1863)] \tag{7.17}$$

Then, still using CANTERA, pressure and density (ρ_{pz}) in the primary zone is obtained with a simple function.
With this last consideration we found all the parameters for the Emisison Indexes calculation, the only thing to do is to adapt and recalculate the values described for all three fuels and as the equivalence ratio varies.

7.2.1 Results

Entering all values discussed in an Excel file as the equivalence ratio changes, it is possible to obtain the graphs of the Emission Indexes through semi-empirical relation for Jet-A, C1 and C5. For this work three flight conditions have been chosen: superruise, take-off and idle.
The results for EI_{NO_x} for the three fuels in all three flight conditions are shown in Fig.7.14,7.15 and 7.16

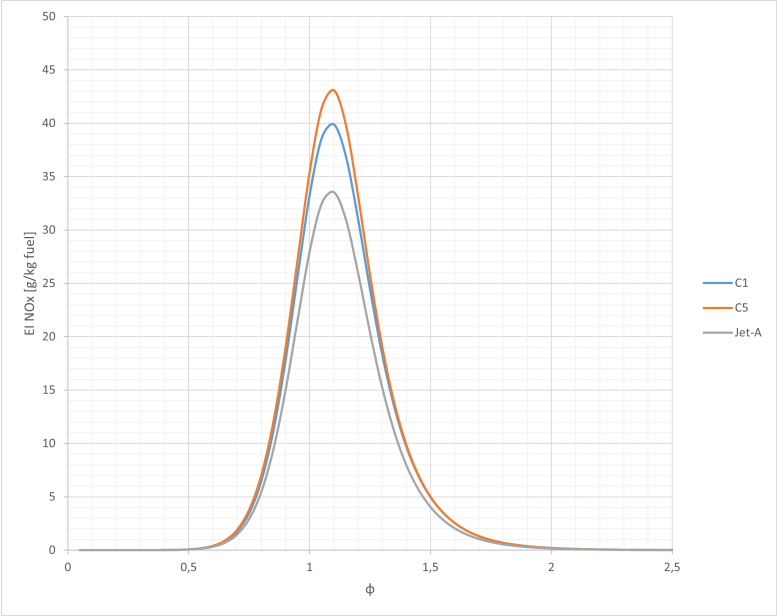

Figure 7.14: EI_{NO_x} vs Equivalence ratio for $Jet - A$, $C1$ and $C5$ in supercruise conditions

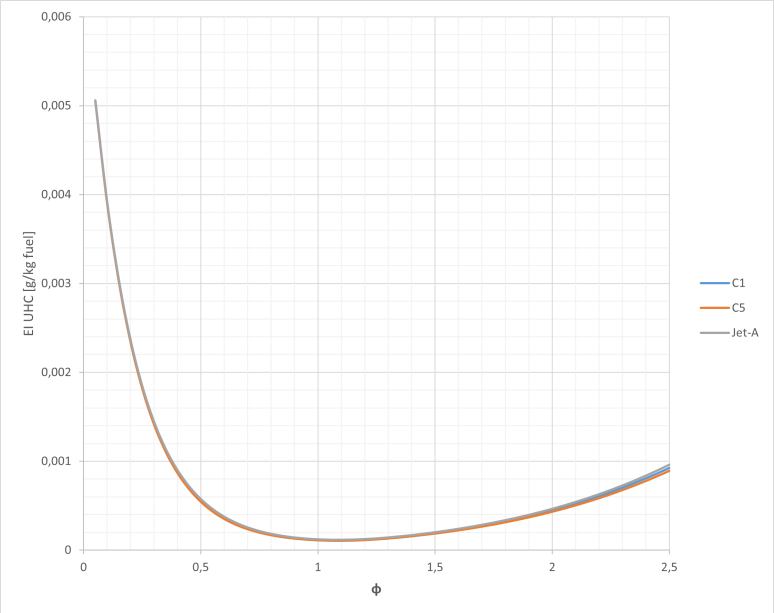

Figure 7.15: EI_{UHC} vs Equivalence ratio for $Jet - A$, $C1$ and $C5$ in supercruise conditions

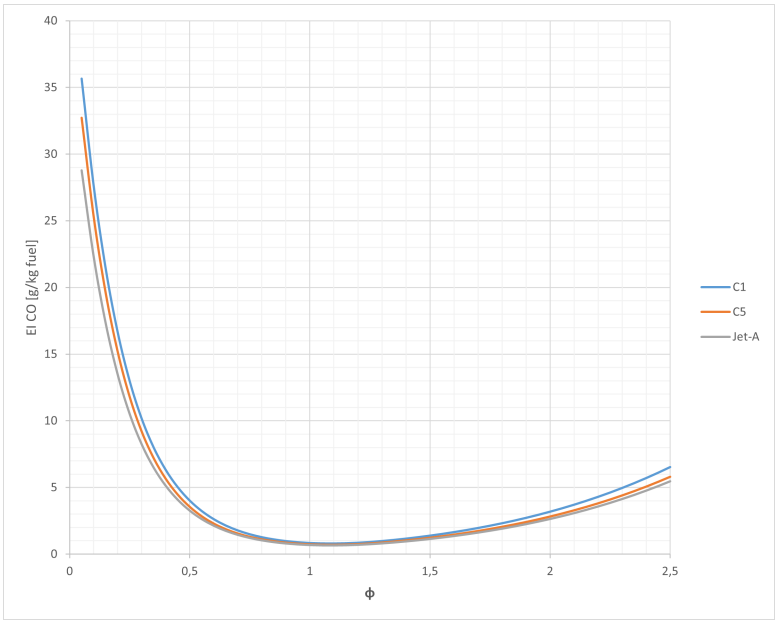

Figure 7.16: EI_{CO} vs Equivalence ratio for $Jet - A$, $C1$ and $C5$ in supercruise conditions

It is possible to see that C1, and even more C5, generates more NO_x emissions. This is linked to the fact that the numerator of the Lefebvre equation contains the adiabatic flame temperature exponent. As shown in Fig.7.17 the Adiabatic Flame Temperature (in standard conditions) is higher for C1 and C5 (This trend is even more pronounced for the adiabatic flame temperature relative to the combustion chamber inlet). For CO and UHC there are not big differences between the three fuels: slightly lower UHC emissions for C1 and C5 and slightly higher for CO. However this emissions are in very low and short range of values, due to the flight condition, not very representative for this type of emission, as already discussed in Sec.6.2. We exclude the values before $\Phi = 0.4$ because outside operative conditions and with combustion inefficiencies too high to be representative for any case of study.
For take-off we have very similar results, since supercruise and take-off are very similar in terms of enigne power settings. Results for take-off are shown in Fig.7.18,7.19 and 7.20

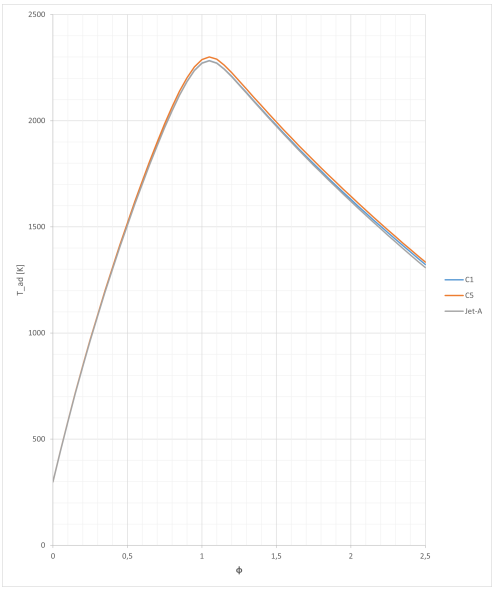

Figure 7.17: Adiabatic Flame Temperature vs Equivalence ratio for Jet-A, C1 and C5

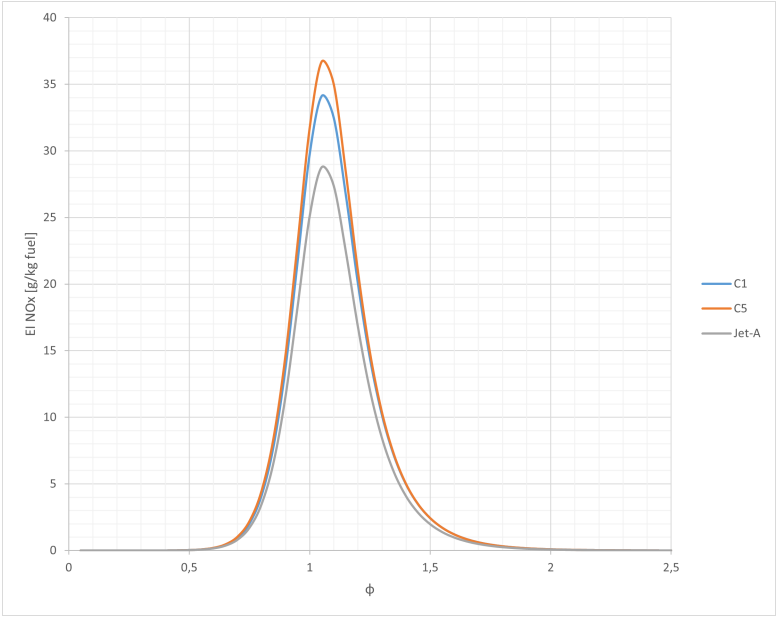

Figure 7.18: EI_{NO_x} vs Equivalence ratio for $Jet - A$, $C1$ and $C5$ in take-off conditions

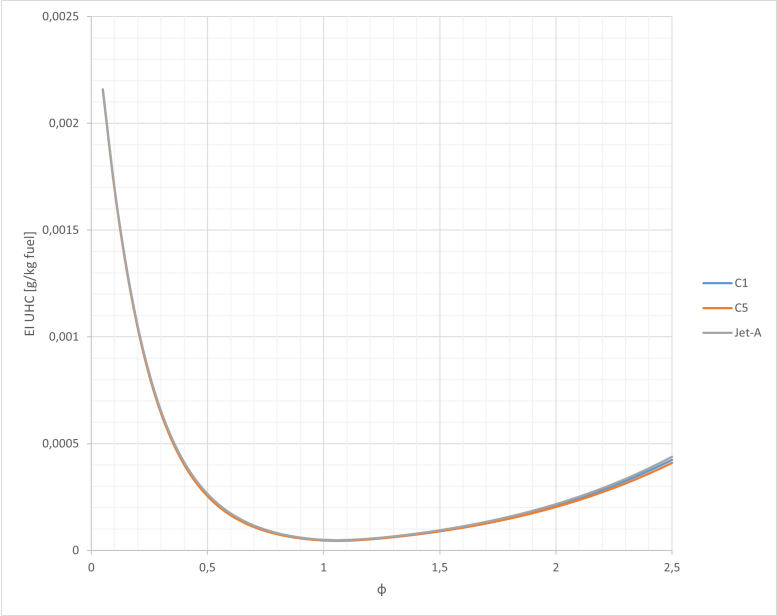

Figure 7.19: EI_{UHC} vs Equivalence ratio for $Jet - A$, $C1$ and $C5$ in take-off conditions

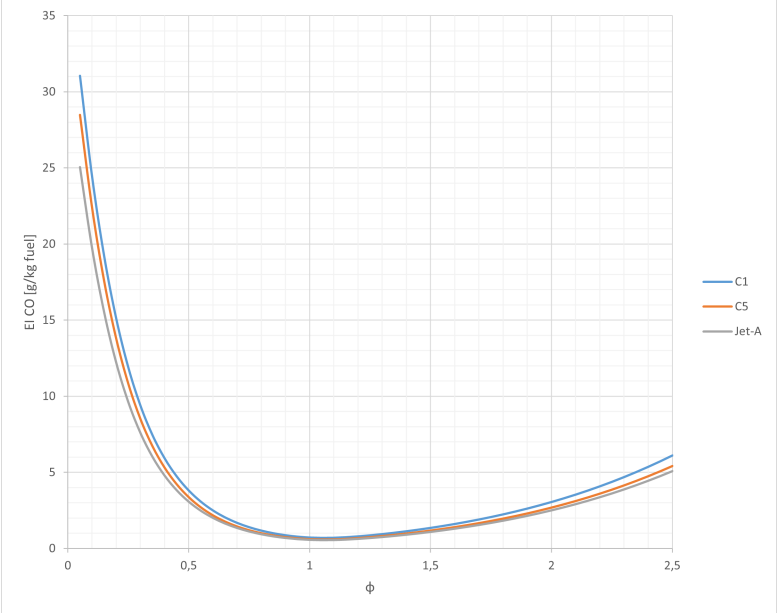

Figure 7.20: EI_{CO} vs Equivalence ratio for $Jet - A$, $C1$ and $C5$ in take-off conditions

Very different is the situation in Idle conditions Fig.7.21,7.22 and 7.23

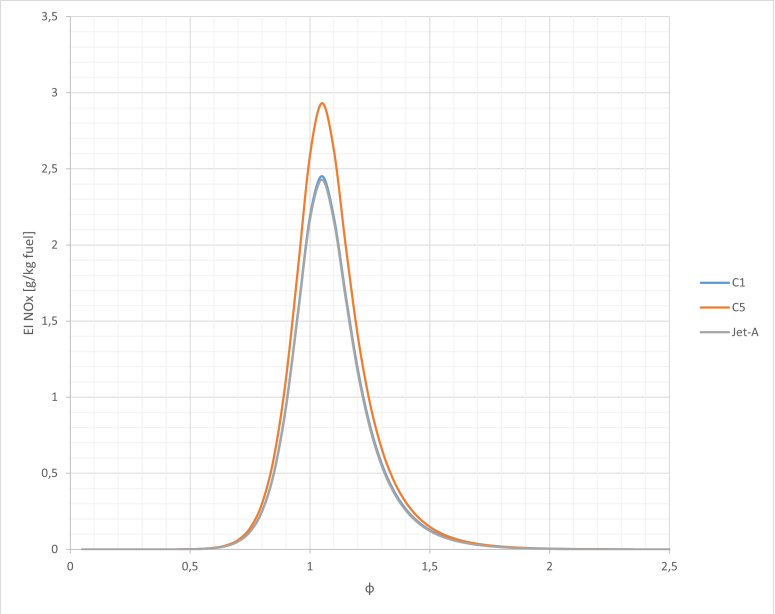

Figure 7.21: EI_{NO_x} vs Equivalence ratio for $Jet-A$, $C1$ and $C5$ in idle conditions

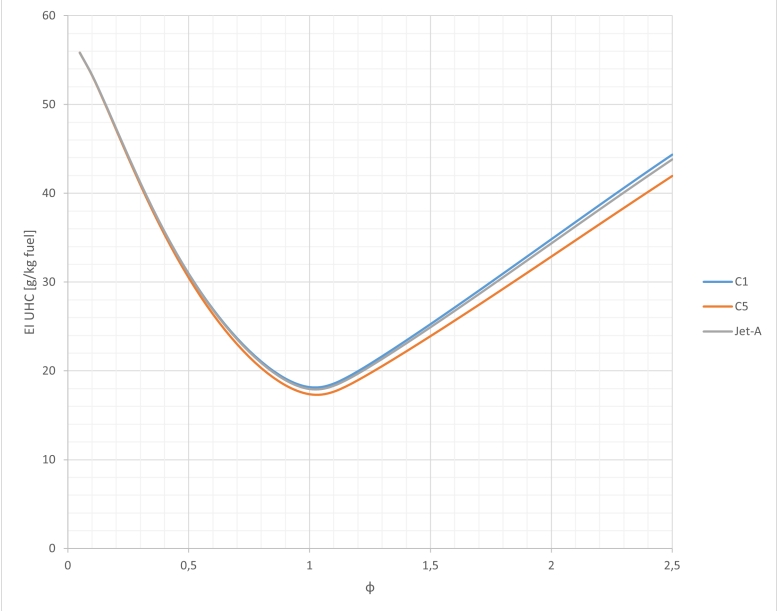

Figure 7.22: EI_{UHC} vs Equivalence ratio for $Jet-A$, $C1$ and $C5$ in idle conditions

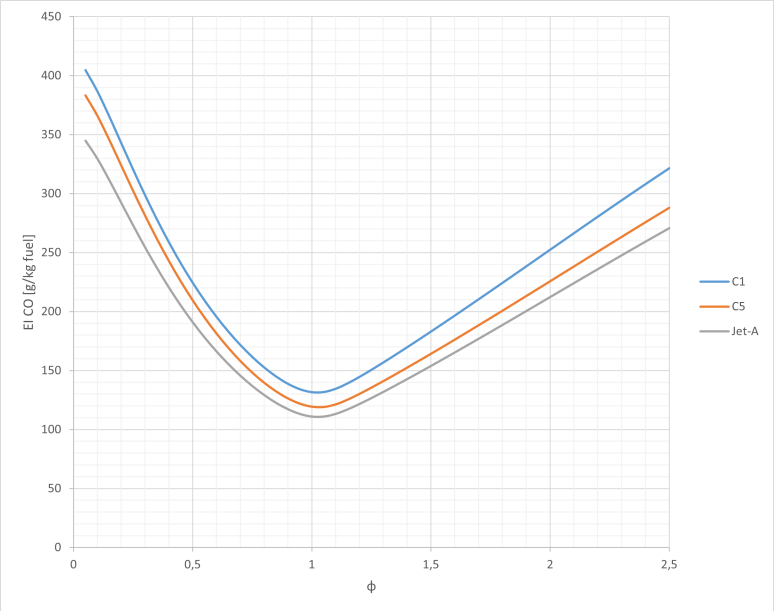

Figure 7.23: EI_{CO} vs Equivalence ratio for $Jet-A$, $C1$ and $C5$ in idle conditions

As expected the NO_x emissoins are much lower, due to the lower temperatures in combustion chamber of this flight condition. For the same reason, due to the negative value of the exponential, and the much higher V_e at denominator, the emission indexes for UHC and CO are much higher. Due to the lower temperatures the gas mixture needs a higher evaporation volume to evaporate.

7.2.2 Discussions and Validation

The **results** obtained, as outlined in the previous section, make one thing clear: C1 and C5 fuels generate **more emissions** than Jet-A, at least in terms of NO_x and CO, and slightly lower emissions for UHC, probably due to the absence of certain compounds in the kinetic scheme and the lower molecular weight of these two fuels, both factors responsible for poorer atomization. However, the semi-empirical relationships used take into account a limited number of thermodynamic and chemical factors for emission analysis, an extremely complex process that is still poorly understood.
All in all, the trends found are consistent with the theoretical trends described in the literature. The biggest difference lies in the position of the maxima (for NO_x) and minima (for CO and UHC) straddling equivalence ratio values of 1.05/1.1 rather than 0.8/0.85/0.9 as described in the literature [26]. This deviation is undoubtedly due to the predominant role of temperatures (both adiabatic flame temperature and primary zone temperature) in semi-empirical relationships, which

have maximum values precisely at those equivalence ratios (around 1.1).
It is possible to perform validations on numerical values. On the one hand, we can use CANTERA and, in particular, a **zero-dimensional reactor model** to obtain the emission index results for the three fuels, a simulation model that is much more accurate than simple mathematical relationships. Secondly, there are values in the literature given by experimental and operating conditions, which can be used as a comparison for those few cases that represent.
Let's start from the CANTERA validation. Cantera opens up many possibilities. In fact, it was possible to use a zero-dimensional reactor model to calculate the **ignition delay time** of the fuel in the combustion chamber. Usually, this time is very short, but it is possible to extend the simulation further to obtain results for the entire residence time of the fuel in the combustion chamber. The model returns a time history of the combustion process as a result, based on the kinetic scheme (set of all elements and chemical reactions involved in the combustion process) of each individual fuel. The time histories file presents the results showing the evolution over time of the mass of air and fuel, the temperature, and the mass fractions of each individual chemical component involved in the combustion process (including the pollutant emissions that are the subject of this study) as shown in Fig.7.24 The inputs of the model are: pressure and temperature of the reactor

	A	B	C	D	E	F	G	H	I	J	K	L	M	N	O	P
1		mass	volume	emperatur	POSF10325	C2H4	CH4	C3H6	iC4H8	C4H81	H2	C2H6	CO	C6H6	C2H2	C6H5CH3
2	7,91E-13	1,468854	1	780,1898	0,14547	2,72E-16	4,38E-17	1,92E-16	2,72E-17	8,16E-17	7,82E-24	1,18E-35	9,76E-43	1,17E-16	4,21E-43	1,33E-16
3	3,31E-09	1,468854	1	780,1898	0,14547	1,14E-12	1,84E-13	8,04E-13	1,14E-13	3,42E-13	1,35E-16	8,65E-25	1,25E-28	4,9E-13	4,11E-31	5,56E-13
4	1,19E-08	1,468854	1	780,1898	0,14547	4,12E-12	6,64E-13	2,9E-12	4,12E-13	1,24E-12	1,08E-15	2,12E-23	4,82E-27	1,77E-12	1,63E-29	2,01E-12
5	2,05E-08	1,468854	1	780,1898	0,14547	7,12E-12	1,15E-12	5,02E-12	7,12E-13	2,14E-12	2,81E-15	8,66E-23	2,4E-26	3,06E-12	8,17E-29	3,47E-12
6	2,91E-08	1,468854	1	780,1898	0,14547	1,01E-11	1,63E-12	7,15E-12	1,01E-12	3,04E-12	5,36E-15	2,27E-22	7,74E-26	4,36E-12	2,54E-28	4,94E-12
7	4,56E-08	1,468854	1	780,1898	0,14547	1,6E-11	2,57E-12	1,13E-11	1,6E-12	4,79E-12	1,25E-14	8,61E-22	4,39E-25	6,87E-12	1,31E-27	7,79E-12
8	7,9E-08	1,468854	1	780,1898	0,14547	2,8E-11	4,5E-12	1,97E-11	2,8E-12	8,39E-12	3,53E-14	4,64E-21	4,18E-24	1,2E-11	1,03E-26	1,36E-11
9	1,12E-07	1,468854	1	780,1898	0,14547	4,02E-11	6,47E-12	2,83E-11	4,02E-12	1,2E-11	6,83E-14	1,31E-20	1,57E-23	1,73E-11	3,45E-26	1,96E-11
10	1,46E-07	1,468854	1	780,1898	0,14547	5,26E-11	8,47E-12	3,71E-11	5,26E-12	1,58E-11	1,1E-13	2,83E-20	4,19E-23	2,26E-11	8,35E-26	2,56E-11
11	2E-07	1,468854	1	780,1898	0,14547	7,34E-11	1,18E-11	5,18E-11	7,34E-12	2,2E-11	1,97E-13	7,38E-20	1,41E-22	3,16E-11	2,48E-25	3,58E-11
12	2,55E-07	1,468854	1	780,1898	0,14547	9,47E-11	1,53E-11	6,67E-11	9,47E-12	2,84E-11	3,01E-13	1,53E-19	3,48E-22	4,07E-11	5,59E-25	4,62E-11
13	3,1E-07	1,468854	1	780,1898	0,14547	1,16E-10	1,87E-11	8,2E-11	1,16E-11	3,49E-11	4,2E-13	2,77E-19	7,16E-22	5E-11	1,07E-24	5,67E-11
14	3,8E-07	1,468854	1	780,1898	0,14547	1,44E-10	2,32E-11	1,02E-10	1,44E-11	4,33E-11	5,88E-13	5,15E-19	1,51E-21	6,2E-11	2,11E-24	7,03E-11
15	4,5E-07	1,468854	1	780,1898	0,14547	1,72E-10	2,78E-11	1,22E-10	1,72E-11	5,17E-11	7,7E-13	8,68E-19	2,76E-21	7,42E-11	3,67E-24	8,41E-11
16	5,19E-07	1,468854	1	780,1898	0,14547	2,01E-10	3,24E-11	1,42E-10	2,01E-11	6,03E-11	9,64E-13	1,36E-18	4,57E-21	8,64E-11	5,85E-24	9,8E-11
17	5,89E-07	1,468854	1	780,1898	0,14547	2,3E-10	3,7E-11	1,62E-10	2,3E-11	6,89E-11	1,17E-12	2,01E-18	7,02E-21	9,88E-11	8,73E-24	1,12E-10
18	6,59E-07	1,468854	1	780,1898	0,14547	2,59E-10	4,17E-11	1,82E-10	2,59E-11	7,76E-11	1,37E-12	2,85E-18	1,02E-20	1,11E-10	1,24E-23	1,26E-10
19	7,28E-07	1,468854	1	780,1898	0,14547	2,88E-10	4,64E-11	2,03E-10	2,88E-11	8,63E-11	1,59E-12	3,89E-18	1,41E-20	1,24E-10	1,69E-23	1,4E-10
20	7,98E-07	1,468854	1	780,1898	0,14547	3,17E-10	5,11E-11	2,23E-10	3,17E-11	9,51E-11	1,81E-12	5,17E-18	1,89E-20	1,36E-10	2,23E-23	1,55E-10
21	8,68E-07	1,468854	1	780,1898	0,14547	3,46E-10	5,59E-11	2,44E-10	3,46E-11	1,04E-10	2,03E-12	6,72E-18	2,44E-20	1,49E-10	2,86E-23	1,69E-10
22	9,38E-07	1,468854	1	780,1898	0,14547	3,76E-10	6,06E-11	2,65E-10	3,76E-11	1,13E-10	2,25E-12	8,54E-18	3,09E-20	1,62E-10	3,59E-23	1,83E-10
23	1,01E-06	1,468854	1	780,1898	0,14547	4,05E-10	6,54E-11	2,86E-10	4,05E-11	1,22E-10	2,47E-12	1,07E-17	3,82E-20	1,74E-10	4,41E-23	1,97E-10
24	1,08E-06	1,468854	1	780,1898	0,14547	4,35E-10	7,01E-11	3,06E-10	4,35E-11	1,3E-10	2,7E-12	1,31E-17	4,65E-20	1,87E-10	5,34E-23	2,12E-10
25	1,19E-06	1,468854	1	780,1898	0,14547	4,83E-10	7,8E-11	3,41E-10	4,83E-11	1,45E-10	3,08E-12	1,8E-17	6,2E-20	2,08E-10	7,11E-23	2,36E-10
26	1,31E-06	1,468854	1	780,1898	0,14547	5,32E-10	8,59E-11	3,75E-10	5,32E-11	1,6E-10	3,46E-12	2,4E-17	8,01E-20	2,29E-10	9,17E-23	2,6E-10
27	1,42E-06	1,468854	1	780,1898	0,14547	5,81E-10	9,39E-11	4,1E-10	5,81E-11	1,74E-10	3,84E-12	3,11E-17	1,01E-19	2,5E-10	1,15E-22	2,83E-10
28	1,54E-06	1,468854	1	780,1898	0,14547	6,31E-10	1,02E-10	4,45E-10	6,31E-11	1,89E-10	4,22E-12	3,96E-17	1,24E-19	2,71E-10	1,42E-22	3,07E-10
29	1,72E-06	1,468854	1	780,1898	0,14547	7,07E-10	1,14E-10	4,98E-10	7,07E-11	2,12E-10	4,81E-12	5,56E-17	1,64E-19	3,04E-10	1,9E-22	3,44E-10
30	1,96E-06	1,468854	1	780,1898	0,14547	8,13E-10	1,31E-10	5,73E-10	8,13E-11	2,44E-10	5,64E-12	8,43E-17	2,31E-19	3,5E-10	2,71E-22	3,96E-10
31	2,15E-06	1,468854	1	780,1898	0,14547	8,92E-10	1,44E-10	6,29E-10	8,92E-11	2,68E-10	6,26E-12	1,11E-16	2,89E-19	3,84E-10	3,42E-22	4,35E-10
32	2,33E-06	1,468854	1	780,1898	0,14547	9,71E-10	1,57E-10	6,85E-10	9,71E-11	2,91E-10	6,88E-12	1,43E-16	3,54E-19	4,18E-10	4,22E-22	4,73E-10
33	2,51E-06	1,468854	1	780,1898	0,14547	1,05E-09	1,7E-10	7,41E-10	1,05E-10	3,15E-10	7,5E-12	1,81E-16	4,25E-19	4,52E-10	5,13E-22	5,12E-10
34	2,7E-06	1,468854	1	780,1898	0,14547	1,13E-09	1,83E-10	7,97E-10	1,13E-10	3,39E-10	8,12E-12	2,24E-16	5,04E-19	4,86E-10	6,14E-22	5,51E-10

Figure 7.24: Time history file example

(combustor) taken from the engine model, the type of fuel and oxidizer (air) and the equivalence ratio. So it is possible to obtain the mass fraction of pollutant

emissions at the residence time for each equivakence ratio and, with some easy calculation, to obtain the Emission Indexes for the considered pollutant. Therefore, by running the code for an equivalence ratio between 0 and 2.5, exactly as for semi-empirical correlations, it was possible to obtain the desired results as shown in following figures.

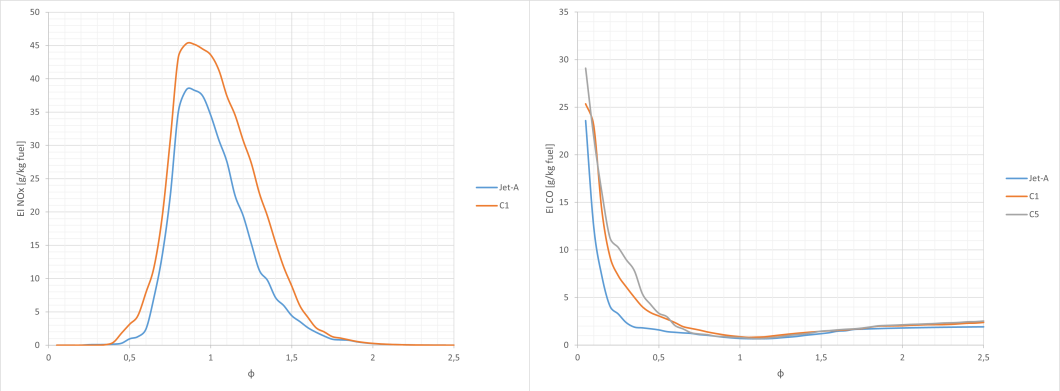

Figure 7.25: EI_{NO_x} and EI_{CO} obtained with CANTERA for Cruise conditions

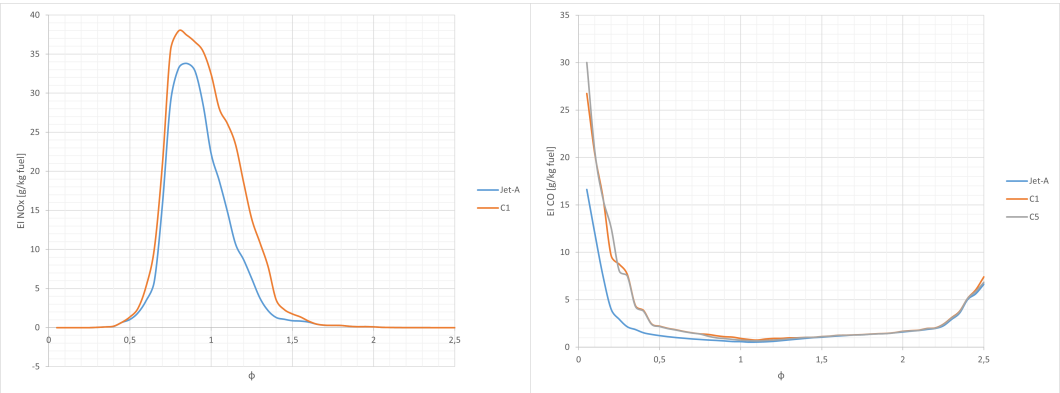

Figure 7.26: EI_{NO_x} and EI_{CO} obtained with CANTERA for Take-off conditions

Validations were only possible for NO_x and CO (for C5 only for CO) due to the structure of the kinetic schemes used, provided by the **HyChem (Hybrid Chemestry) Project**, the only Kinetic schemes available about $C1$ and $C5$. To obtain accurate results for UHC emissions more detailed mechanisma are required. More info about the HyChem project and the Kinetic schemes in Appendix B.
The trends are more in line with the theoretical ones. As for the numerical values, however, it is immediately apparent how similar they are to those found with semi-empirical relationships. The figures are of the same order of magnitude, even

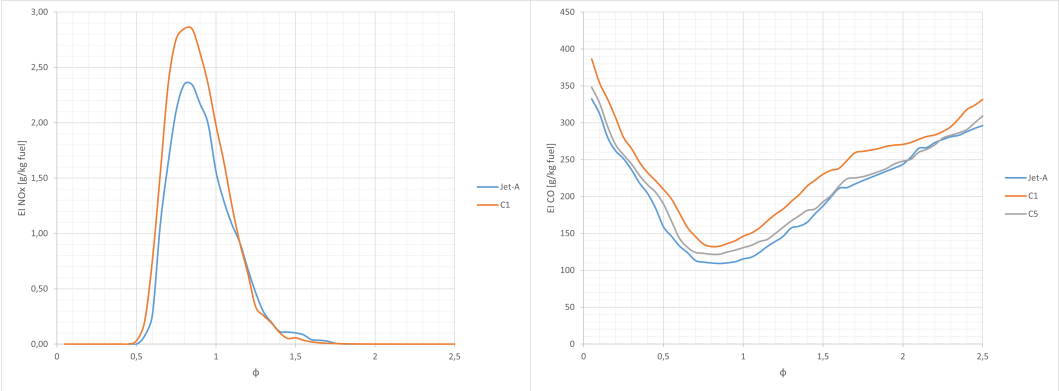

Figure 7.27: EI_{NO_x} and EI_{CO} obtained with CANTERA for Idle conditions

if they differ. This difference is justifiable, however.
The semi-empirical correlations only consider thermal NO_x, so for CANTERA the values are slightly higher because also other formation mechanisms are considered. In addition, numerical coefficients in Lefebvre and Murthy correlations are derived from experimental data relating to their own case studies. In fact, these coefficients vary depending on the propulsion model and the type of fuel used to power it [39]. Consequently, these coefficients, or even the quantities present in these correlations, should be adapted to the specific case study by using experimental data on which to adapt the formulations. Unfortunately, there are no data sets on which to base this adaptation, in fact there are very few data on the Concorde emissions during mission or LTO cycle, fewer data about combustion and emissions of $C1$ and $C5$ and no data at all on the use of these fuels to power the Olympus. So the adaptation of this relations is an impossible task at the moment.
We report the few data available in the literature as an additional validation tool (Fig.7.28 and 7.29)

Production	P_3 (atm)	T_3 (°R)	M_a (Kg/S)	M_f (Kg/hr)	f/a	Comb. Ineff.	EI HC	EI CO	EI NOx	Sk
Idle				1140		.0584	36	118	2.5	
Descent				2360		.0380	22	82	4.0	
Approach				4550		.0201	8.5	55	6.5	
Climbout				9100		.0059	1.5	20	12.5	
Takeoff*	15.5			12700		.0003	0	1.1	22.3	
Afterburner**				10000		.0207	6.6	64.5	0	
						EPAP	129	530	70.1	

Figure 7.28: Concorde LTO-cycle emissions [40]

Parameter	Jet A	C1	C5	Influenced by
Vaporizability	Low	Medium	High	Composition
CN	48.3	17.1	39.6	Ignition
Modeled H/C	2	2.15	1.9	Composition
Premixed flame size	High	High	Low	Flame temperature[a]
Premixed fluctuations	High	Low	Medium	CN
Spray length	High	Medium	Low	Vaporizability
Droplet size	High	Medium	Low	Vaporizability
Droplet velocity	Medium	Medium	Medium	Independent
Droplet temperature	High	Medium	Low	Vaporizability
Flame lift (idle)	Medium	Medium	Medium	Strong premixing
Flame lift (cruise)	High	Low	Low	Vaporizability
$EINO_x$ [g/kg] (idle)	2.4	2.3	1.4	Spray length, H/C
$EINO_x$ [g/kg] (cruise)	15	27	24	Flame lift, H/C
Thermoacoustics	Low	High	High	CN/Vaporizability[b]

Figure 7.29: Jet-A, C1 and C5 observed trends and the parameters these trend are mainly influenced by [41]

All the data in Fig.7.28 refer to usage of conventional aviation fuel and main burner only with the exception of the Afterburner data, related to takeoff with reheat. The Idle and Take-off sets of data confirm the results found with the usage of Jet-A.
In the table of Fig.7.29 the results of a combustion high fidelity study conduct at Lund University [41] are reported. The analysis is limited to the major species and focus on how these are affected by composition, liquid properties, and flame shape. The UHC are excluded because, as already said, require more complex studies and models.
This work confirm that CO is heavily influenced by the temperature in the emissions, which in turn is determined by the LHV and global Φ of each fuel, which also ultimately stem from the H/C ratio. In the HyChem mechanisms we used, C1 has the highest LHV, in fact EI_{CO} are the highest. Unlike CO, which mainly depend on the emission temperature, NO_x is heavily dependent on the local flame temperature. Another information that this study [41] add is that NO_x is therefore the most sensitive to the flame shape, particularly important to determines the local temperature. Fig.7.29 shows emissions at idle and cruise conditions of a generic Turboengine model in each simulation. In this work the values are those that deviate the most, but nevertheless confirm once again the order of magnitude of emissions indexes and the trends that these indixes assume when switching from one fuel to another. To summarize: higher emissions in the case of C1 and C5.

Chapter 8

Conclusions

The main goals of this work were two:

- to discuss an approach to size an engine, new or already known, for a supersonic aircraft (like the Concorde), in order to generate a propulsive database to know all the operrative conditions of the engine
- evaluate the applicability and the effectiveness of the Lefebvre and Murthy semi-empirical correlations to estimate engine pollutant emissions, taking into account factors more closely related to combustion, unlike other methods such as $P_3 - T_3$ or $BFFM2$.

The process of the engine analysis and generation of propulsive database replicates the one developed by Francesco Piccionello [12], inspired by the Mattingly Engine Design Process [16] and widely validated. In this work the model was upgraded and modified to allow the analysis of a different propulsion system than Piccionello's and, above all, to use fuels other than conventional ones. As seen in Sec.4, this was done by modifying the gas model and the FAIR routine using CANTERA.
The main engine's components are modeled following the Mattingly approach, and the entire engine performances are evaluated using the Matrix Iteration Method. All the process is applied to the Olympus-593 (Concorde engine). All main engine parameters are chose from literature and to satisfy all requirements, in terms of cruise thrust and take-off thrust.
The Matrix Iteration method, solved with the Newton-Raphson aprroach, is used to generate the propulsive database. It si important to underline the high constraint of the GPS maps use: it must be assuemd a map of an existing engine for a future one. In addition, the method is very complex, because differnt routines must be set for a single simulation, so a great quantity of data and a great knowledge of the propulsive system are required. However with the expansion of the gas model there's no more the limitation on the SAFs and Alternative Jet Fuels: previously, these

fuels were associated with a chemical structure identical to that of conventional fuels ($C_{12}H_{23}$), because in the Engine Model code data relating to these fuels was missing.
The Second part of the work was all about the emissions evaluation. As shown in this work, other calculation methods were rejected in favor of Lefebvre's and Murthy's semi-empirical relationships, because they take into account more variables related to combustion and the combustion chamber itself, rather than just those related to the thermodynamic cycle. After the research and the calculations about all the quantities involved in these equations, an emission database (with relative graphs) was generated for three main flight conditions, particularly representative for NO_x and CO emissions: Supercruise, Take-off and Idle. Subsequently the results was validated through CANTERA and literature values. The methodology adopted presents acceptable results, but not completely in line with those of CANTERA and present in the literature. This, as analyzed, is due to the fact that semi-empirical relationships require a large set of experimental data to be adapted to the specific case study.

8.1 Future works

About the Engine Model, it significantly improves and expand the previous, especially with the changes made to the gas model, which allow new types of fuel to be introduced in addition to conventional ones. However more updates could be implemented: for example, the addition of further fuels, more common than C1 and C5, and also the study of fuel blends; in addition, the addition of an afterburner to the engine components is necessary in order to obtain a more accurate study of the Concorde's mission performance. Furthermore, given the complexity of the Concorde's air intake, more detailed modeling of the latter would be necessary to obtain more reliable results regarding the internal flows within the engine.
Regarding the Emission Evaluation the results are near what we want and expected, but a broader set of data is needed to obtain ad hoc relationships for each individual case study, given the complexity and limited understanding of the phenomenon of emissions production within the scientific community.

Appendix A

Jet-A properties

The **Category A jet fuels**, which includes **Jet-A**, were defined by selecting important combustion-related properties and attempting to find production fuels that would represent the range of properties of jet fuels in use today. In particular **A-2** or Jet-A is the fuel with "**average**" properties among those in its category. Fig.A.1 shows the desider properties for this type of fuel Instead in Fig.A.2 a

Fuel	Flash Point, °C		Viscosity, mm^2s^{-1} (cSt) (at -20 °C)		Aromatics, % (vol)	
	Desired	Actual	Desired	Actual	Desired	Actual
A-1, POSF 10264	≤40	42	≤3.4	3.5	≤14	11.2
A-2, POSF 10325	50±3	48	4.5±0.5	4.5	17±1	17.0
A-3, POSF 10289	≥66	60	≥6.5	6.5	≥21	18.0

Figure A.1: Desidered properties of Category A conventional fuels [9]

summary of key properties of the fuels is given, which shows that the three fuels do indeed encompass a wide range of properties within the jet fuel “experience base". At last, the combustion-related specification properties are shown in Fig.

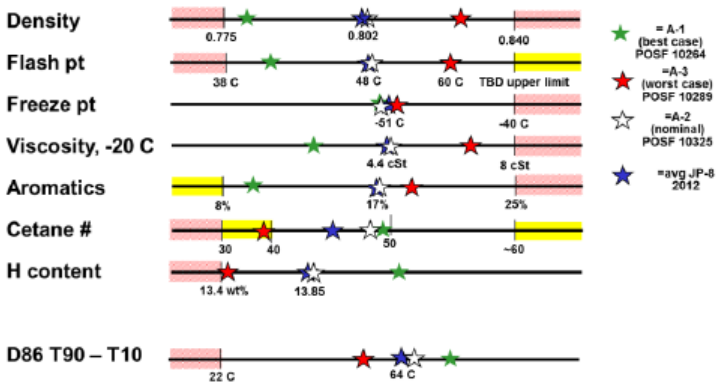

Figure A.2: Properties Range of Category A conventional fuels [9]

			Category A Fuels			
Property	Test Method	Spec limits	A-1, 10264	A-2, 10325	A-3, 10289	PQIS 2012 wt mean
Density	D4052	0.775-0.84	0.780	0.803	0.827	0.8022
Flash point, C	D93	>38	42	48	60	47.6
Viscosity, -20 C (cSt)	D445	<8	3.5	4.5	6.5	4.399
Aromatics, vol%	D1319	<25	11.2	17.0	18.0	17.1
Heat of Combustion, MJ/kg	D4809	>42.8	43.2	43.1	43.0	43.2
Heat of Combustion, MJ/kg	D4809 (SwRI[32])		43.24	43.06	42.88	
H content, mass% (meas) SwRI	D3701	>13.4	14.26	13.84	13.68	n/a
H content, mass % (meas)	D7171	>13.4	14.4	13.7, 13.9	13.4	n/a
H content, mass %	GCxGC (UDRI)	>13.4	14.4, 14.5	14.0	13.7	n/a
H/C ratio (based on D3701)	calculation	n/a	1.99	1.91	1.89	n/a
Molecular formula	GCxGC	n/a	$C_{10.8}H_{21.8}$	$C_{11.4}H_{22.1}$	$C_{11.9}H_{22.6}$	n/a
Derived cetane #, SwRI	D6890	n/a	48.8	48.3	39.2	n/a
Distillation, C	D86					
IBP			145	159	174	160*
10%		<205	164	176	192	176*
20%			171	184	199	183*
50%			189	205	218	201*
90%			234	244	244	238*
FBP		<300	256	269	258	254*
Engine cetane, SwRI	D613	n/a	48.0	47.9	40.4	n/a
Smoke pt, mm	D1322	>18	28.5	23	20	22.8
Freeze pt, C	D5972	>-47 (JP-8)	-51	-51	-50	-51.3

Figure A.3: Specification Test Results for Category A conventional fuels [9]

Appendix B

HyChem Reaction Mechanism

A **Reaction Mechanism** explains the step-by-step sequence of elementary reactions that occur during a chemical reaction. It details the individual events, like the breaking and forming of bonds, that lead from reactants to products and includes any intermediates that are formed and consumed. The sum of these elementary steps must equal the overall balanced chemical equation. If one assumes that the chemical reactions are fast compared to the other processes like diffusion, heat conduction, and flow, thermodynamics alone allow the description of the system locally. In most cases, however, chemical reactions occur on tiem scales comparable with that of the flow and of the molecular transport processes. All the reaaction mechanisms used in this work are taken from the HyChem website of the Stanford University (https://web.stanford.edu/group/haiwanglab/HyChem/pages/download.html).
The first part of a reaction mechanism presents a list of all of the elements and the species involved in reactions and some generic charateristic of the mixture. In Fig.B.1, B.2 and B.3, as example, fragments of the C1 reaction mechanism are shown

```
45
46  generator: ck2yaml
47  input-files: [C1_nox_ignite.inp, therm.dat.inp, tran.dat.inp]
48  cantera-version: 3.1.0
49  date: Tue, 23 Sep 2025 13:34:22 +0200
50
51  units: {length: cm, time: s, quantity: mol, activation-energy: cal/mol}
52
53  phases:
54  - name: gas
55    thermo: ideal-gas
56    elements: [O, H, C, N, Ar, He]
57    species: [POSF11498, C2H4, CH4, C3H6, iC4H8, H2, C2H6, CO, C2H2,
58        pC3H4, aC3H4, CH3, O2, H, OH, HO2, O, H2O, H2O2, C, CH, CH2,
59        CH2*, HCO, CH2O, CH3O, CH2OH, CO2, C2O, C2H, C2H3, C2H5, HCCO,
60        CH2CO, CH3CO, CH2CHO, C3H3, aC3H5, CH3CCH2, iC3H7, C2H3CHO,
61        iC4H7, C5H5, C6H5, C6H5O, iC4H7-1, NO, NO2, HCN, NH3, NH2, NH, N,
62      NNH, HNO, N2O, HNC, CN, HNCO, HCNO, NCO, NCN, HNCN, CH2NH, H2CN,
63        N2]
64    kinetics: gas
65    transport: mixture-averaged
66    state: {T: 300.0, P: 1 atm}
```

Figure B.1: Elements and species of C1 reaction mechanism

After this there's a part where are listed all the thermal and transport characteristic of every species, properties shown in form of **NASA7 Polynomials**.

```
68  species:
69  - name: POSF11498
70    composition: {C: 13, H: 28}
71    thermo:
72      model: NASA7
73      temperature-ranges: [298.0, 1000.0, 3000.0]
74      data:
75      - [4.2177753, 0.093084201, 8.0710743e-05, -1.7453084e-07,
76          7.9970509e-11, -4.7017836e+04, 18.436749]
77      - [33.64304, 0.067928091, -2.0546e-05, 2.4969564e-09,
78          -6.9632051e-14, -5.8361672e+04, -148.04048]
79      note: S07/15
80    transport:
81      model: gas
82      geometry: nonlinear
83      well-depth: 179.321
84      diameter: 10.607
85      rotational-relaxation: 1.0
86      note: C13H28; sigma and epsilon derived from NC13H28-N2
```

Figure B.2: Thermochemical properties defined by NASA7 polynomials

These Polynomials are used to compute the species standard-state thermodynamic properties $\frac{c_{p,t}(T)}{R}$, $\frac{h_t(T)}{R}$ and $\frac{s_t(T)}{R}$ as follow

$$\frac{c_{p,t}(T)}{R} = a_1 + a_2 T + a_3 T^2 + a_4 T^3 + a^5 T^4 \tag{B.1}$$

$$\frac{h_t(T)}{R} = a_1 + \frac{a_2}{2}T + \frac{a_3}{3}T^2 + \frac{a_4}{4}T^3 + \frac{a_5}{5}T^4 + \frac{a_6}{T} \tag{B.2}$$

$$\frac{s_t(T)}{R} = a_1 ln(T) + a_2 T + \frac{a_3}{2}T^2 + \frac{a_4}{3}T^3 + \frac{a_5}{4}T^4 + a_7 \tag{B.3}$$

The coefficients are the ones reported in Fig.B.2: the first set of seven values is the one relative to the temperature range from 298 K and 1000 K, the second one from 1000 K and 3000 K. The temperature ranges are reported above the coefficients and change for every species. After the coefficients there are some geometrical and rotational values relative to the species molecule.
At last there's the set of **Elementary Reactions** that describe the chemical reaction.

```
902
903  reactions:
904  - equation: POSF11498 => 2.4625807 iC4H8 + 0.5710129 C3H6 + 0.2461822 C2H4 + 1.055726
905      H + 0.944274 CH3
906    rate-constant: {A: 2.83e+26, b: -2.58, Ea: 8.0197e+04 cal/mol}
907  - equation: POSF11498 + H => H2 + 2.6513789 iC4H8 + 0.6147906 C3H6 + 0.2650562 C2H4
908      + 0.98 H + 0.02 CH3
909    rate-constant: {A: 872.0, b: 2.4, Ea: 2580.0 cal/mol}
910  - equation: POSF11498 + CH3 => CH4 + 2.6513789 iC4H8 + 0.6147906 C3H6 + 0.2650562
911      C2H4 + 0.98 H + 0.02 CH3
912    rate-constant: {A: 4.64e-03, b: 3.46, Ea: 4600.0 cal/mol}
913  - equation: POSF11498 + OH => H2O + 2.6513789 iC4H8 + 0.6147906 C3H6 + 0.2650562 C2H4
914      + 0.98 H + 0.02 CH3
915    rate-constant: {A: 4.88e+07, b: 0.51, Ea: 64.0 cal/mol}
916  - equation: POSF11498 + O2 => HO2 + 2.6513789 iC4H8 + 0.6147906 C3H6 + 0.2650562 C2H4
917      + 0.98 H + 0.02 CH3
918    rate-constant: {A: 1.49e+12, b: 0.0, Ea: 4.3e+04 cal/mol}
919  - equation: POSF11498 + HO2 => H2O2 + 2.6513789 iC4H8 + 0.6147906 C3H6 + 0.2650562
920      C2H4 + 0.98 H + 0.02 CH3
921    rate-constant: {A: 9.03, b: 2.77, Ea: 1.05e+04 cal/mol}
922  - equation: POSF11498 + O => OH + 2.6513789 iC4H8 + 0.6147906 C3H6 + 0.2650562 C2H4
923      + 0.98 H + 0.02 CH3
```

Figure B.3: Reactions from R1 to R7 for C1, the most important ones in the combustion process

In addition to the balance equations, there are values relating to the Arrhenius law, that describes how the rate constant of a chemical reaction depends on temperature

$$k = A\, e^{-\frac{E_a}{RT}} \tag{B.4}$$

Where k is the rate constant of the reaction, that determines the reaction speed, A is the pre-exponential or frequency factor (accounts for collision frequency and orientation) and E_a is activation energy (the minimum energy needed for a reaction). The rates of the elementary reactions in combustion processes differ greatly. Sensitivity analyses show that only a few reactions (like the first seven shown above) are rate-limiting. Other reactions are so fast, that the accuracy of

the rate coefficints has a minor influnce on the simulation of the overall combustion process. This knowledge has important consequences for applications: the rate coefficients of elementary reactions with high sensitivities have to be well known, because they have a great influence on the results of mathematical modelling. If reactions have low sensitivities, only aproximate values for the rate coefficients have to be known.
As already mentioned, complete mechanism for hydrocarbons may consist of several thousand elementary reactions. Depending on the question posed, many of these reactions can be neglected, to reduce the computational load of simulations, otherwise be impossible to sustain. In addition to the **Sensitivity Analysis** described above, other analysis can be performed: **Reaction Flow ANalysis**, that determines the characteristic reaction paths, **Eigenvector Analysis**, that determines the characteristic time scales and directions of the chemical reactions.In this way it is possible to obtain a **Reduced Mechanism**, like the ones used in this work, based on quasi-stady state and partial-equilibrium assumptions, that provides reliable results only for certain range of temperature and mixture composition.

Bibliography

[1] Air Transport Action Group. *Beginner's Guide to Sustainable Aviation Fuel - Edition 4*. 2023 (cit. on pp. 1, 8, 10).

[2] International Civil Aviation Organization. *Aviation and Environmental Report*. 2019 (cit. on p. 2).

[3] European Union Aviation Safety Agency. *European Aviation Environmental Report*. 2022 (cit. on p. 2).

[4] Fusaro R. Viola N. Galassini D. «Sustainable Supersonic Fuel Flow Method: an evolution of the 2 Boeing Fuel Flow Method for supersonic aircraft using sustainable aviation fuels». In: *Aerospace* 331.8(11) (2021). DOI: https://doi.org/10.3390/aerospace8110331 (cit. on pp. 3, 87, 89).

[5] M. Colket J. Heyne M. Rumizen M. Gupta T. Edwards W.M. Roquemore G. Andac R. Boehm J. Lovett R. Williams. «Overview of the National Jet Fuels Combustion Program». In: *AIAA journal* 54 (2016). DOI: https://doi.org/10.2514/1.J055361 (cit. on pp. 9, 12).

[6] Yang J. Xin Z. Corscadden K. Niu H. «An overview on performance characteristics of bio-jet fuels». In: *Fuel* 237 (2019), pp. 916–936. DOI: https://doi.org/10.1016/j.fuel.2018.10.079 (cit. on p. 10).

[7] IATA. *Sustainable Aviation Fuel: Technical Certification*. 2021 (cit. on p. 10).

[8] Paula Kurzawska. «Overview of Sustainable Aviation Fuels including emission of particulate matter and harmful gaseous exhaust gas compounds». In: *Transportation Research Procedia* 59 (2021), pp. 38–45. DOI: https://doi.org/10.1016/j.trpro.2021.11.095 (cit. on pp. 10, 11).

[9] Edwards T. «Reference Jet Fuels for Combustion Testing». In: *AIAA journal* (2017) (cit. on pp. 12, 13, 120, 121).

[10] Rui Xu, Hai Wang, Med Colket, and Tim Edwards. «Thermochemical Properties of Jet Fuels». In: (2015) (cit. on p. 14).

[11] Kraan at al. «An Energy Transition That Relies Only on Technology Leads to a Bet on Solar Fuels». In: *Joule* (2019) (cit. on p. 16).

[12] Piccionello F. «Modeling of Propulsion Systems for Supersonic Civil Aircraft». In: *MA thesis, Politecnico di Torino* (2023) (cit. on pp. 17, 20, 23, 25, 26, 45, 47, 118).

[13] Stiuso G. «Tecnica di simulazione numerica delle prestazioni stazionarie e transitorie di turbomotori». In: *MA thesis, Politecnico di Torino* (2019) (cit. on pp. 19, 71, 73, 74).

[14] Kurzke J. *GasTurb 12-Design and Off-Design Performance of Gas Turbines Manual*. 2014 (cit. on p. 20).

[15] GSP Development Team. *GSP-11 User Manual*. National Aerospace Laboratory NLR Anthony Fokkerweg 2 1006 BM Amsterdam The Netherlands. 2009 (cit. on p. 20).

[16] J.D. Mattingly. *Aircraft Engine Design*. AIAA Education Sereis. American Institute of Aeronautics and Astronautics. 2002 (cit. on pp. 20, 22, 32, 44, 45, 52, 55, 59, 63, 118).

[17] J.D. Mattingly. *Elements of Gas Turbine Propulsion*. AIAA Education Sereis. American Institute of Aeronautics and Astronautics. 2005 (cit. on pp. 20, 23, 25, 32).

[18] Sanford Gordon and Bonnie J. McBride. *Computer program for calculation of complex chemical equilibrium compositions and applications. Part 1: Analysis*. 1994 (cit. on pp. 22, 23).

[19] AIAA Foundation Student. *Let's Re-engine the Concorde, Design Competition Request for Proposal*. 2020 (cit. on pp. 35, 38, 60).

[20] L. Trainelli. *Lezioni di Meccanica del Volo*. 2011 (cit. on p. 38).

[21] Lewis W.G.E Rettie J.H. «Design and Development of an Air Intake for a Supersonic Transport Aircraft». In: *Journal of Aircraft* 5.6 (1968) (cit. on p. 43).

[22] Claire Soares. *Gas Turbines. A Handbook of Air, Land, and Sea Applications*. 2008 (cit. on pp. 46, 50, 52, 55).

[23] Heritage Concorde group. *Heritage Concorde website*. 2010 (cit. on pp. 49, 56, 57).

[24] I. Halliwell J. Kurzke. *Propulsion and power: An exploration of gas turbine performance modelling*. Springer International Publishing. 2018 (cit. on p. 65).

[25] AJ Fawke and HIH Saravanamuttoo. «Digital computer simulation of the dynamic response of a twin-spool turbofan with mixed exhausts». In: *The Aeronautical Journal* (1973) (cit. on p. 73).

[26] Dilip R. Ballal Arthur H. Lefebvre. *Gas Turbine Combustion, Alternative Fuels and Emissions*. CRC Press. 1994 (cit. on pp. 81–83, 87, 105, 113).

[27] A. Seaton, W. MacNee, K. Donaldson, and E. Godden. *Particulate Air Pollution and Acute Health Effects*. Lancet. 1995 (cit. on p. 80).

[28] Wesocky H.L. and Prather M.J. «Atmospheric Effects of Stratospheric Aircraft: A Status Report from NASA's High Speed Research Program». In: *Tenth International Symposium on Air Breathing Engines, AIAA* (1991) (cit. on p. 81).

[29] R.W. Dibble J. Warnatz U. Maas. *Combustion, Physical and Chemical Foundamentals, Modeling and Simulations, Experiments, Pollutant Formation*. Springer. 2006 (cit. on pp. 83–86).

[30] A.H. Lefebvre. «Fuel effects on gas turbine combustion-liner temperature, pattern factor, and pollutant emissions». In: *Journal of Aircraft* (1984) (cit. on pp. 87, 90–92, 106).

[31] ICAO. «ICAO annex 16: Environmental protection, Volume II - Aircraft Engine Emissions». In: (2008) (cit. on p. 87).

[32] Lorenzo Dal Bo. «Pollutant and GHG emissions predictions of high-speed aircraft LH2». In: *MA thesis, Politecnico di Torino* (2022) (cit. on pp. 87, 88).

[33] Onder Turan Ahmet Topal. «Emission analysis for a new tubular aeroengine combustor in atmospheric test rig conditions». In: *Aircraft Engineering and Aerospace Technology* (2022) (cit. on pp. 90, 92).

[34] J.N. Murthy. «Gas turbine combustor modelling for design». In: *Ph.D Thesis, Cranfield Institute of Technology, School of Mechanical Engineering, Cranfield* (1988) (cit. on pp. 90, 92).

[35] A.H. Lefebvre and J.S. Chin. «Steady-State Evaporation Characteristic of Hydrocarbon Fuel Drops». In: *AIAA Journal* (1983) (cit. on pp. 93, 94).

[36] Flight simulator Aerofly FS. *Concorde Flight Tutorial - https://www.aerofly.com/aircraft-tutorials/concorde-flight-tutorial/* (cit. on p. 102).

[37] A.C. Conrado, P.T. Lacava, A.C. Pereira Filho, and M. de S. Sanches. «Basic Design Principle for Gas Turbine Combustor». In: *10th Brazilian Congress of Thermal Sciences and Engineering* (2004) (cit. on pp. 105, 107).

[38] C. Priyant Mark and A. Selwyn. «Design andanalysisofannularcombustion chamber of a low bypass turbofan engine in a jet trainer aircraft». In: *Propulsion and Power Research* (2016) (cit. on p. 105).

[39] A. Tsalavoutas, M. Kelaidis, N. Thoma, and K. Mathioudakis. «Correlations Adaptation for Optimal Emissions Predictions». In: *ASME Turbo Expo 2007: Power for Land, Sea and Air* (2007) (cit. on p. 116).

[40] R. Munt. «Aircraft Technology Assessment: Progress in Low Emissions Engine». In: *EPA Technical Report* (1981) (cit. on p. 116).

[41] A. Akerblom. «Large Eddy Simulations of Alternative Jet Fuel Combustion». In: *Doctoral Thesis, Department of energy Sciences, Lund University* (2025) (cit. on p. 117).